Electron Interactions with CF_4

L. G. Christophorou,[a] J. K. Olthoff, and M. V. V. S. Rao
National Institute of Standards and Technology, Gaithersburg, Maryland 20899-0001

Received 29 March 1996; revised manuscript received 26 June 1996; accepted for publication 30 July 1996

Carbon tetrafluoride (CF_4) is one of the most widely used components of feed gas mixtures employed for a variety of plasma-assisted material-processing applications. It has no stable excited states and, in a plasma environment, is an ideal source of reactive species, especially F atoms. To assess the behavior of CF_4 in its use in manufacturing semiconductor devices and other applications, it is necessary to have accurate information about its fundamental properties and reactions, particularly its electronic and ionic interactions and its electron collision processes at low energies (<100 eV). In this article we assess and synthesize the available information on the cross sections and/or the rate coefficients for collisional interactions of CF_4 with electrons. Assessed information is presented on: (i) cross sections for electron scattering (total, momentum, elastic differential, elastic integral, inelastic), electron-impact ionization (total, partial, multiple, dissociative), electron-impact dissociation (total, and for dissociative excitation), and electron attachment (total, and for specific anions); (ii) coefficients for electron transport (electron drift velocity, transverse and longitudinal electron diffusion coefficients), electron attachment, and electron-impact ionization; and (iii) cross section sets derived from analyses of electron transport data. The limited ionization data on CF_4 radicals are also presented, and references are made to measurements of electron transport properties of CF_4 gas mixtures. Based upon the assessment of published experimental data, recommended values for various cross sections and coefficients are generated which are presented in graphical and tabular form. © *1996 American Institute of Physics and American Chemical Society.*

Key words: carbon tetrafluoride; CF_4; cross sections; electron interactions; scattering; ionization; attachment; dissociation; fragments; transport.

Contents

[a]Also at the Department of Physics, The University of Tennessee, Knoxville, TN 37996.

List of Tables

List of Figures

1. Introduction

Carbon tetrafluoride (CF_4) is a man-made gas with wide technological applications: plasma etching in the semiconductor industry,[1–4] pulse power switching,[5–7] gaseous dielectrics,[8–10] particle detectors,[11–14] and a host of other applications in plasma and space sciences, gas discharges, and atmospheric physics and chemistry. In non-equilibrium plasmas used for plasma assisted material processing applications, CF_4 is one of the most widely used components of feed gas mixtures.[15–17] It serves as a source of reactive species (ions, neutrals, radicals) which are largely responsible for surface reactions in various etching and deposition applications. The CF_4 molecule is attractive as a feed gas component because it is relatively inert in its electronic ground state and because it has no stable excited states. The CF_4^+ parent ion is also unstable both in its ground and excited electronic states. As a consequence of these properties, in a plasma environment, the CF_4 molecule is an ideal source for a variety of reactive neutral and ionic fragment atoms and molecules formed in either the ground state or excited states and especially neutral F atoms which is a desirable active species in etching processes.

Carbon tetrafluoride is, unfortunately, a greenhouse gas with a high potential of global warming.[18,19] Its half-life in the atmosphere is greater than 50 000 years[18] and its global warming potential over a one-hundred year period is 6300 with reference to the absolute global warming potential[18] for CO_2. The CF_4 molecule is not expected to cause ozone depletion in the stratosphere because the catalytic destruction of stratospheric ozone by free fluorine atoms formed in the photodissociation of CF_4 is negligible.[18,20]

To assess the behavior of this gas in the atmosphere and in its many applications, especially in the semiconductor industry, it is necessary to have accurate basic information on its fundamental properties and reactions, particularly on its electronic and ionic interactions and its electron collision processes at low energies (<100 eV). Most applications, such as those involving the testing of theoretical models for plasma reactors, require knowledge of collision cross sections over a wide energy range. Such knowledge is crucial in attempting to investigate, understand, characterize, and model the gas-phase reactions in a plasma and to estimate the fluxes of species, which are ultimately responsible for the multitude of surface interactions. Recently, it was reported that the effect of electron and ion reactions on the atmospheric lifetimes of fully fluorinated compounds is also of environmental importance.[21]

The collisional interactions of CF_4 with electrons under controlled, single and multiple collision conditions have been studied by many groups, and in this article we assess, synthesize, and present this knowledge comprehensively. We also refer to interactions of CF_4 with photons which are relevant to the present discussion and of interest to applications and to the environment. This work is a part of broader effort to build a database on electronic and ionic collision processes that would: (i) aid in the understanding of the properties of low-temperature plasmas and the role played by collision processes, (ii) help the development of more sophisticated *in situ* non-intrusive plasma diagnostic techniques, (iii) help the development of more sophisticated plasma models, and (iv) impact our ability to provide a scientific underpinning to the existing processing technologies and help, in this way, the development of new plasma-assisted processes.

A number of collision cross sections, coefficients, and rate constants are used in this work to quantify various processes which result from the collisions of low-energy electrons with the CF_4 molecule. These are defined in Table 1 along with their corresponding symbols and units. For a more complete discussion of the various types of collision cross sections and their definitions the reader is referred to Christophorou.[22,23]

One of the goals of this work is to reach a conclusion as to the most reliable available data for the various electron collision processes in CF_4. To reach this goal for each cross section and coefficient, we have attempted to consider and present all published data, even those which have been superseded by subsequent studies. We have done this in order to aid in the understanding of the changes, to assist in the determination of the reliability of the data, and to draw attention to these changes for researchers who may have used earlier data in their work. When possible, data were obtained from published tables. However, for data presented only in graphical form, the published figures were scanned and the data digitized for use in this work.

In order to provide reasonably complete and consistent sets of cross section and transport data for CF_4, we have determined a set of "recommended" values for each type of cross section and coefficient when possible. These recommended values are derived from fits to the most reliable data that are available at the time of preparation of this article. The reliability of each set of data is determined by the following selection criteria:

(i) data are published in peer reviewed literature;

(ii) no evidence of unaddressed errors;

(iii) data are absolute determinations;

(iv) multiple data sets are consistent with one another over ranges of overlap within combined stated uncertainties; and

(v) in regions where both experimentally and theoretically derived data exist, the experimental data are preferred.

In instances where only a single set of data for a given cross section or coefficient satisfies the above-mentioned selection criteria, that data set is designated as our recommended set and is tabulated here as originally published. In cases where two or more data sets satisfy the selection criteria, each selected data set is analyzed by a weighted-least-squares (WLS) fit, with the resulting data having an equal spacing of data points. This is done in order to ensure that each selected data set is equally weighted in the final fit regardless of the number of points in the original data. The recommended data set is then derived by a combined WLS fit to all of the fitted data, and is presented in tabular and graphical format.

TABLE 1. Definition of symbols.

Symbol	Definition	Common scale and units
$\sigma_{sc,t}(\epsilon)$	Total electron scattering cross section	10^{-16} cm^2; 10^{-20} m^2
$\sigma_m(\epsilon)$	Momentum transfer cross section	10^{-16} cm^2; 10^{-20} m^2
$\sigma_{e,diff}(\epsilon)$	Differential elastic electron scattering cross section	10^{-16} cm^2 sr^{-1}
$\sigma_{e,int}(\epsilon)$	Integral elastic electron scattering cross section	10^{-16} cm^2; 10^{-20} m^2
$\sigma_{inel,t}(\epsilon)$	Total inelastic electron scattering cross section	10^{-16} cm^2; 10^{-20} m^2
$\sigma_{inel,indir,t}(\epsilon)$	Total indirect inelastic scattering cross section	10^{-16} cm^2; 10^{-20} m^2
$\sigma_{vib,dir,t}(\epsilon)$	Total direct vibrational excitation cross section	10^{-16} cm^2; 10^{-20} m^2
$\sigma_{vib,indir}(\epsilon)$	Cross section for indirect vibrational excitation	10^{-16} cm^2; 10^{-20} m^2
$\sigma_{i,t}(\epsilon)$	Total ionization cross section	10^{-16} cm^2; 10^{-20} m^2
$\sigma_{i,partial}(\epsilon)$	Partial ionization cross section	10^{-16} cm^2; 10^{-20} m^2
$\sigma_{i,pair}(\epsilon)$	Positive ion pair formation cross section	10^{-16} cm^2; 10^{-20} m^2
$\sigma_{i,t,count}(\epsilon)$	Total counting ionization cross section	10^{-16} cm^2; 10^{-20} m^2
$\sigma_{i,mult}(\epsilon)$	Multiple ionization cross section	10^{-16} cm^2; 10^{-20} m^2
$\sigma_{i,diss}(\epsilon)$	Dissociative ionization cross section	10^{-16} cm^2; 10^{-20} m^2
$\sigma_{diss,t}(\epsilon)$	Total dissociation cross section	10^{-16} cm^2; 10^{-20} m^2
$\sigma_{diss,neut,t}(\epsilon)$	Total dissociation cross section into neutral species	10^{-16} cm^2; 10^{-20} m^2
$\sigma_{diss,exc}(\epsilon)$	Dissociative excitation cross section	10^{-16} cm^2; 10^{-20} m^2
$\sigma_{a,t}(\epsilon)$	Total electron attachment cross section	10^{-18} cm^2; 10^{-22} m^2
$\sigma_{i,fragment}(\epsilon)$	Cross section for electron impact ionization of fragments	10^{-16} cm^2; 10^{-20} m^2
$\sigma_{i,diss,fragment}(\epsilon)$	Cross section for electron impact dissociative ionization of fragments	10^{-16} cm^2; 10^{-20} m^2
$\sigma_{F,t}(\epsilon)$	Total cross section for F atom production	10^{-16} cm^2; 10^{-20} m^2
$k_{a,t}$	Total electron attachment rate constant	10^{-11} cm^3 s^{-1}
a/N	Density reduced ionization coefficient	10^{-18} cm^2
η/N	Density reduced electron attachment coefficient	10^{-18} cm^2
$(\alpha-\eta)/N$	Effective ionization coefficient	10^{-18} cm^2
W	Average energy to produce an electron ion pair	eV
w	Electron drift velocity	10^6 cm s^{-1}
D_T/μ	Transverse electron diffusion coefficient to electron mobility ratio	V
D_L/μ	Longitudinal electron diffusion coefficient to electron mobility ratio	V
$\langle\epsilon\rangle$	Mean electron energy	eV

No uncertainty values are assigned to the recommended data sets. While some measure of uncertainty can be obtained from an analysis of the combined relative uncertainties of the original data fitted to derive the recommended set, we do not report this value since we have no means of confirming the experimental uncertainties reported by the original authors. Additionally, any uncertainty value calculated in this way would be strongly affected by the number of data sets used to derive the recommended cross sections, and would vary for each cross section and over each energy range. Individuals who are interested in more information about the uncertainties of these cross sections are referred to the original references and to the discussion in the text of the individual data used to derive the recommended values.

It should be emphasized that the derived data sets which we designate as "recommended" are recommended only in so far as they are the most reliable data that can be currently derived based on the presented selection criteria. A complete summary of our recommended data is given at the end of this article. It is important to note that the recommended cross sections are based on independent experimental measurements and are, thus, different from model dependent cross section sets such as those of Hayashi[24] and Nakamura.[25]

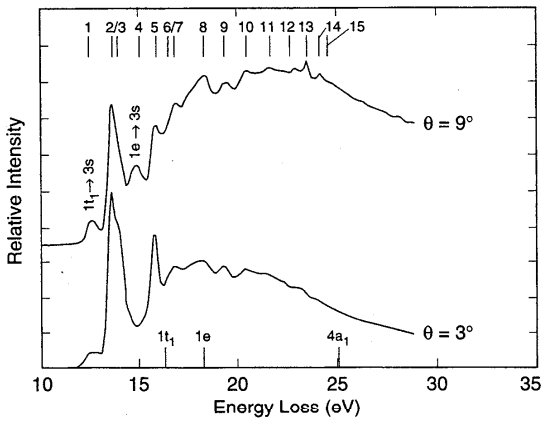

FIG. 1. Electron energy loss spectrum of CF_4 obtained by Kuroki *et al.*(Ref. 28) using 200 eV incident energy electrons and scattering angles θ equal to 3° and 9°. See the text and Table 2 for discussion and explanation of symbols.

2. Electronic and Molecular Structure

The CF_4 molecule is a tetrahedral and has spherical top structure. It does not have a dipole or a quadrupole moment,[26] and its electric dipole polarizability is small (Beran and Kevan[27] listed two values, 27.3×10^{-25} cm^3 and 29.3×10^{-25} cm^3, for the electric dipole polarizability of CF_4). It belongs to the T_d point group and the ground-state configuration[28,29] of its outer valence shell is $[....(4a_1)^2(3t_2)^6(1e)^4(4t_2)^6(1t_1)^6]\,{}^1A_1$.

There have been many studies of the electronic and molecular structure of CF_4 (see, for example, Kuroki *et al.*[28] and Robin[30] and literature cited therein; see, also, a discussion by Boesten *et al.*[31] concerning the symmetries of the various unoccupied orbitals of the CF_4 molecule). A number of energy-loss studies have been published,[28,32,33] and in Fig. 1 is shown the electron energy-loss spectrum from a recent study[28] obtained using incident electrons of 200 eV energy at scattering angles of 3° and 9°. All excitations from the outer valence shell appear to follow a Rydberg pattern and have been so classified.[28] The energy-loss regime shown in Fig. 1 covers the entire range of transitions from the outer valence shell. Excitation energies, type of orbital transitions, and ionization potential values[28,32–34] are given in Table 2. In Fig. 1 the angular dependence exhibited by the peaks labeled 1, 4, and 11 in the electron energy-loss spectrum at 12.56, 14.84, and 21.63 eV, respectively, correspond to optically forbidden transitions[28] (see also Iga, Lopes, and Galdino[35]). The excitation energies determined in the recent electron energy-loss spectroscopy (EELS) study[28] are compared in Table 2 with those obtained from two earlier EELS measurements.[32,33] The energy-loss results are consistent with each other, and with the photoabsorption data.[36,37,39] Figure 2 shows the photoabsorption cross sections of Lee, Phillips, and Judge[39] and others.[36,40]

All electronically excited states of CF_4 seem to dissociate or predissociate with high probability[41,42] and this is consistent with the absence of optical emission from the CF_4 molecule[30] itself. The parent molecular ion CF_4^+ also must be unstable (lifetime <10 μs) since it has not been observed.[43,44] It can be seen from Table 2 that the threshold for electronic excitation is rather high at ~12.6 eV. Conse-

TABLE 2. Excitation energies, types of transition, and ionization potentials (IP) of CF_4 (from Ref. 28).

No.[a]	Excitation energy (eV)[b,c] EELS (Ref. 28)	EELS (Ref. 32)	EELS (Ref. 33)	Orbital transition (Refs. 28, 32, 33)	IP (eV) (Refs. 33, 34)
1	12.56	12.69	12.51	$1t_1\rightarrow3s$	16.20
2	13.60	13.67	13.59	$1t_1\rightarrow3p$	
3	13.94	13.96	13.89	$4t_2\rightarrow3s$	17.40
4	14.84	14.71		$1e\rightarrow3s$	18.50
5	15.82	15.86	15.81	$4t_2\rightarrow4s$, $3d$ $1e\rightarrow3p$	
6	16.56	16.53		$4t_2\rightarrow5s$, $4d$ $1e\rightarrow3d$	
7	16.87	16.88	16.86	$1e\rightarrow4s$, $3d$	
8	18.39	18.0	18.01	$3t_2\rightarrow3s$	22.12
9	19.43	19.45	19.42	$3t_2\rightarrow3p$	
10	20.48	20.45	20.53	$3t_2\rightarrow4s$, $3d$	
11	21.63	(21.55)		$4a_1\rightarrow3s$	25.1
12	22.68	22.78		$4a_1\rightarrow3p$	
13	23.55			$4a_1\rightarrow3d$	
14	24.21			$4a_1\rightarrow4d$	
15	24.7			$4a_1\rightarrow5d$	

[a]Numbers in column 1 identify the transitions in this table and in Fig. 1.
[b]See Refs. 36 and 37 for relevant information obtained from photoabsorption and photoionization studies.
[c]The excitation maxima in the threshold electron spectra of Ref. 38 are consistent with the EELS values.

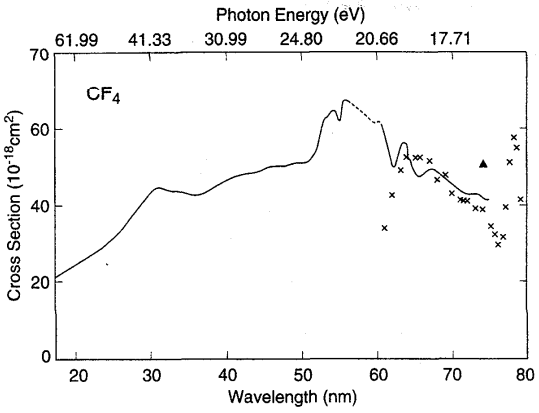

FIG. 2. Photoabsorption cross sections of CF_4 in the range 17.5–80 nm (from Ref. 39) —, ..., Ref. 39; ×, Ref. 36; ▲, Ref. 40.

quently, below this energy, collisions of electrons with the CF_4 molecule lead to elastic scattering, vibrational excitation, and dissociative electron attachment. Above 12.6 eV electronic excitation becomes energetically possible, and the dissociation of the CF_4 molecule into neutral and/or charged fragments becomes significant (see Secs. 4 and 5).

The CF_4 molecule has four fundamental vibrational modes:[45] the symmetric stretch $h\nu_1$ (0.112 eV) (this mode is singly degenerate), the symmetric bend $h\nu_2$ (0.054 eV) (this mode is doubly degenerate), the asymmetric stretch $h\nu_3$ (0.157 eV) (this mode is triply degenerate), and the asymmetric bend $h\nu_4$ (0.078 eV) (this mode is triply degenerate). Most electron collision studies cannot resolve the ν_2 and ν_4 levels and often[24,25,46] (see Sec. 3.6) two vibrational cross sections are obtained σ_v (1, 3) for the stretching modes and σ_v (2, 4) for the bending modes with the former having a statistical weight of 4 and the latter having a statistical weight of 5. The excitation energy of the ν_3 mode almost coincides with the deep Ramsauer–Townsend minimum in the momentum and total electron scattering cross sections at 0.16 eV.[47] Threshold-electron excitation studies have indicated strong vibrational excitation by electron impact below 2.0 eV (Refs. 37 and 48) (see Sec. 3.6). Rotational excitation cross sections are expected to be very small for the CF_4 molecule due to the absence of a dipole and a quadrupole moment.

Carbon tetrafluoride is a weak electronegative gas. Electron attachment to the CF_4 molecule occurs mainly in the 6 to 8 eV range via two negative ion resonances; one, at 6.8 eV, associated with the ground state of CF_4^- producing F^- and CF_3^-, and another, at 7.6 eV, associated with the first electronically excited CF_4^{*-} producing only F^- (see Refs. 49 to 51 and Sec. 6). Besides the electron attachment studies, electron scattering experiments and calculations confirm the locations of these two negative ion resonances and assign the T_2 symmetry to the 6.8 eV resonance[52 62] (see Table 3). A number of other negative ion resonances at higher energies have been identified with various degrees of certainty (see Table 3 and subsequent sections). These negative ion resonances play a crucial role in electron impact induced (indirect) vibrational excitation of CF_4 (Sec. 3.6).

The parent negative ion CF_4^- has not been observed in the gas phase. Two theoretical calculations[63,64] give a value of -0.7 eV for the electron affinity (EA) of the CF_4 molecule. (See Ref. 65 for EA values of the F atom and radicals formed by electron impact on CF_4.) There have been, however, studies[66,67] reporting the observation of the CF_4^- parent anion in van der Waals aggregates (clusters) of CF_4. This does not mean that the EA of CF_4 is positive, but it rather indicates that in CF_4 clusters the CF_4^{-*} transient anion can be in a potential minimum where, due to small Franck–Condon overlap, autodetachment is sufficiently slow (autodetachment lifetime >1 μs) to allow its detection with mass spectrometric techniques. According to Lotter and Illenberger[67] "it is likely that CF_4^- represents a weakly bound $F^- \cdots CF_3$ adduct with one bond significantly weakened, rather than a tetrahedral CF_4^-."

The structure of the CF_4 molecule accounts for its high ionization threshold energy [values of 15.5 eV (Ref. 68); 15.9 eV (Refs. 69 and 70); 16.20 eV (Ref. 34) have been reported]. The dissociation process generating neutral fragments via electron impact has an energy threshold at 12.5 eV.[42] Since all excited electronic states of CF_4 and CF_4^+ are unstable (see Ref. 42 and subsequent discussion), the total electronic excitation cross section of CF_4 is effectively equal to the total dissociation cross section. In view of the energetic thresholds for electron impact dissociation and ionization, the total dissociation cross section is dominated by the dissociation processes producing neutral fragments near the threshold, while the dissociative ionization process (i.e., production of neutral-ion dissociation products) progressively takes over as the electron energy increases above the ionization threshold and dominates above about 30 eV. Furthermore, since no parent CF_4^+ ion has been observed, the total ionization cross section of CF_4 is equal to the total dissociative ionization cross section (see Secs. 4 and 5).

From the preceding discussion and the results summarized in the subsequent sections of this article, it becomes apparent that the CF_4 structure leads to a rather simple picture of the collisional behavior of this molecule with low energy electrons:

- Vibrational excitation is the dominant inelastic process below 12.5 eV, i.e., below the threshold for electronic excitation, and is dominated by the excitation of the infrared active modes ν_3 and ν_4 via direct dipole scattering below the negative ion resonance region 6–8 eV and via indirect scattering in the resonance region.
- All electronic excitations of CF_4 lead to dissociation.
- Dissociation of CF_4 into neutrals begins at ~ 12.5 eV, dominates until ionization sets in, and progressively yields to dissociative ionization which takes over and accounts, at sufficiently high electron impact energies (>35 eV), for the total electronic excitation cross section.

Cross sections for positive ion pair formation, multiple

TABLE 3. Negative ion resonance states of CF_4.

Energy (eV)[a]	Type of resonance	Symmetry	Reference and method of observation
6.8	Shape	T_2	Electron impact
~8.0	Feshbach	T_1	spectroscopy (Ref. 52)
8.0		T_2	Electron scattering (Refs. 53, 54)
~9.0		A_1	
3.6[b]			Time-of-flight electron transmission
~8.9			(Ref. 55)
~9.0			Electron transmission (Ref. 56)
7	Shape	T_2	Electron scattering (Ref. 31)
6.7 (F^- production)			Dissociative attachment
7.1 (CF_3^- production)			(Ref. 57)
6.15 (F^- production)			Dissociative attachment
6.9 (CF_3^- production			(Ref. 58)
~7.5 (F^- production)			
7.3 (total)[c]			Electron swarm (Ref. 59)
7–8			Dissociative attachment (Ref. 60)
6.9 (CF_3^- production)			
~7.0 (F^- production)			Threshold-electron excitation (Ref. 37)[d]
12.0	Core-excited Feshbach		
13.0	Core-excited Feshbach		
6.8 (F^- production)			Dissociative attachment
6.8 (CF_3^- production)			(Refs. 49, 50, 51)[e]
7.6 (F^- production)			
6.6	Shape	T_2	Static-exchange
11.7	Shape	A_1	approximation calculation
27.5	Shape	E	(Ref. 61)[f]
29.1	Shape	T_2	
3.2		T_2	CMS-$X\alpha$ calculation (Ref. 62)[g]
5.2		A_1	

[a]Energy at the cross section maximum.
[b]It was argued in Ref. 53 that this cross section maximum cannot be due to a resonance process.
[c]For the production of both F^- and CF_3^-.
[d]See also Ref. 48.
[e]Electron capture in the 6 to 8 eV range occurs via two negative ion states, the ground state of CF_4^- at 6.8 eV producing both F^- and CF_3^- and an electronically excited state CF_4^{*-} at 7.6 eV producing only F^-.
[f]Mann and Linder (Ref. 54) do not agree with the findings of Huo (Ref. 61); however, the calculated values at 6.6 eV and at 11.7 eV are consistent with the experiment.
[g]Mann and Linder (Ref. 53) argued that the energy positions calculated by Tossell and Davenport (Ref. 62) for the T_2 and A_1 resonances are located at too low energies. In the calculation of Ref. 62 the energy position of the T_2 resonance was rather sensitive to the C–F distance.

ionization, and positive ion–negative ion pair formation are generally smaller than those for single ionization in the low energy range of interest in this article (see Sec. 6).

3. Electron Scattering

3.1 General

In this section information is presented and discussed on the following cross sections used to describe the various electron scattering processes: total electron scattering cross section, momentum transfer cross section, differential elastic electron scattering cross section, integral elastic electron scattering cross section, and inelastic electron scattering cross section for total vibrational excitation and total electronic excitation. The data are first presented in ways that facilitate their comparison and usefulness and they are subsequently assessed and discussed. Recommended cross section values are given when possible. (See also reviews by Morgan[71,72] and Bonham[73] and the model-based cross section sets of Hayashi[24] and Nakamura.[25])

Note added in proof: Since the completion of this work, another model-based cross section set of electron impact

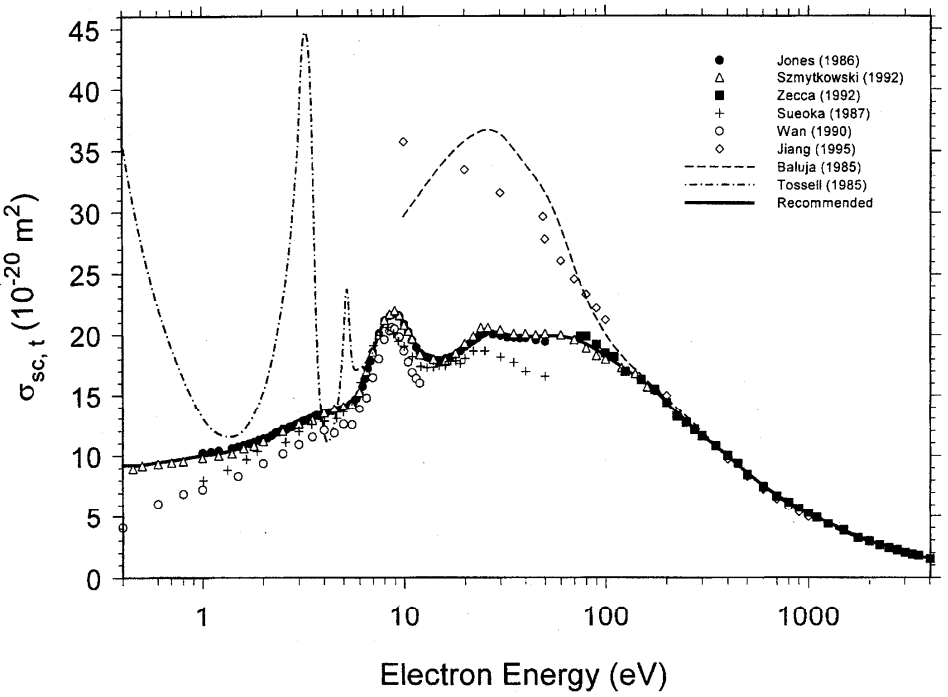

FIG. 3. Total electron scattering cross section $\sigma_{sc,t}(\epsilon)$ as a function of electron energy for CF_4. ●, Ref. 55; △, Ref. 56; ■ Ref. 74; +, Refs. 76, 77, and 78; ○, Ref. 75; ◇, Ref. 79; ----, Ref. 80; –.–.–, Ref. 62; —, Recommended (see Sec. 3.2 and Table 4).

cross sections for CF_4 has been published [M. C. Bordage, P. Ségur, and A. Chouki, J. Appl. Phys. **80**, 1325 (1996)].

3.2 Total Electron Scattering Cross Section, $\sigma_{sc,t}(\epsilon)$

In Fig. 3 are summarized the measured and calculated total electron scattering cross sections as a function of electron energy for CF_4. There are three absolute measurements of the total electron scattering cross section: those measured by Jones[55] using a time-of-flight electron transmission spectrometer in the electron energy range 1.0 eV to 50 eV, those of Szmytkowski *et al.*[56] using the linear transmission technique in the electron energy range 0.5 eV to 200 eV, and those of Zecca, Karwasz, and Brusa[74] using a Ramsauer-type apparatus in the electron energy range 75 eV to 4000 eV. Jones[55] reported that the most probable uncertainty in his measurements was ± 2.3% below 4.0 eV, +3.3% and −3.0% between 4.2 eV and 15.0 eV, +3.4% and −2.1% between 16.0 eV and 25.0 eV, and +7.5% and −2.8% between 26 eV and 50 eV. The direct sum of all potential individual systematic uncertainties in the experiment of Szmytkowski *et al.*[56] was estimated to be ±4% below 1 eV, gradually decreasing to ±3% near 20 eV, and increasing to ±4% at higher energies. Zecca, Karwasz, and Brusa[74] estimated their systematic errors to be $<\pm 3\%$ at all energies. The three sets of absolute cross section measurements are generally in good quantitative agreement in the energy ranges over which they overlap. Another absolute measurement[75] of $\sigma_{sc,t}(\epsilon)$ in the energy range 0.2 to 12 eV gave much lower values than the two other absolute measurements in this energy range (see Fig. 3).

Also shown in Fig. 3 are the normalized measurements of Sueoka and others[76,77] These data differ substantially from those of Jones,[55] Szmytkowski *et al.*,[56] and Zecca, Karwasz, and Brusa.[74] Szmytkowski *et al.*[56] pointed out that a correction the results of Sueoka *et al.* related to the normalization procedure[78] they applied. The results of two calculations, one based on the additivity rule[79] and the other based on a parameter-free spherical complex potential optical potential,[80] are also shown in Fig. 3. The calculated total electron scattering cross sections for energies below ~200 eV are seen to be substantially larger than the experimental values, with agreement at higher energies where the Born approximation is valid. The total cross sections obtained by a multiple scattering X_α calculation[62] in the low energy regime are in disagreement with the measured cross sections both in magnitude and shape.

To arrive at a recommended data set for $\sigma_{sc,t}(\epsilon)$, we considered the experimental measurements of Jones,[55] Szmytkowski *et al.*,[56] and Zecca, Karwasz, and Brusa.[74] Each set of these data was fitted independently and was weighted equally in the averaging process. The resultant average cross section values are indicated by the solid line in Fig. 3 and are listed in Table 4 as our recommended values for the total electron scattering cross section for energies above 0.5 eV

TABLE 4. Recommended total electron scattering cross sections $\sigma_{sc,t}(\epsilon)$.

Electron energy (eV)	$\sigma_{sc,t}(\epsilon)$ (10^{-20} m^2)	Electron energy (eV)	$\sigma_{sc,t}(\epsilon)$ (10^{-20} m^2)
0.003	12.69	8	21.13
0.0035	12.24	8.5	21.60
0.004	11.86	9	21.81
0.0045	11.51	9.5	21.49
0.005	11.19	10	20.82
0.006	10.63	15	17.90
0.007	10.13	20	19.15
0.008	9.69	25	20.39
0.009	9.26	30	20.16
0.010	8.89	35	19.93
0.015	7.40	40	19.91
0.020	6.35	45	19.86
0.025	5.41	50	19.91
0.030	4.67	52.5	19.92
0.035	4.12	55	19.91
0.040	3.63	60	19.86
0.045	3.21	65	19.78
0.050	2.86	70	19.63
0.060	2.30	75	19.45
0.070	1.98	80	19.24
0.080	1.76	85	19.00
0.090	1.62	90	18.76
0.10	1.50	95	18.49
0.125	1.30	100	18.27
0.15	2.17	125	17.17
0.175	4.74	150	16.24
0.20	7.35	175	15.40
0.25	9.12	200	14.40
0.30	9.26	250	12.75
0.35	9.28	300	11.64
0.40	9.25	350	10.75
0.45	9.23	400	9.95
0.5	9.27	450	9.24
0.6	9.45	500	8.60
0.7	9.60	550	8.04
0.8	9.75	600	7.57
0.9	9.89	650	7.15
1.0	10.01	700	6.80
1.5	10.37	750	6.49
2.0	11.29	800	6.21
2.5	12.04	850	5.95
3.0	12.62	900	5.70
3.5	13.00	950	5.49
4.0	13.50	1000	5.28
4.5	13.80	1250	4.43
5.0	14.02	1500	3.79
5.5	14.33	1750	3.33
6.0	15.25	2000	2.95
6.5	16.92	2500	2.42
7.0	18.60	3000	2.05
7.5	20.05	3500	1.75
		4000	1.49

(recommended values at lower energies are determined from the data presented below in Fig. 4).

The overall energy dependence of $\sigma_{sc,t}(\epsilon)$ is rather interesting. Above about 100 eV the usual systematic fall-off of the cross section with increasing electron energy sets in. In this high-energy range the Born-based calculations generally agree with the experimental measurements and can be used to normalize or to check the latter. In the energy range of about 6 eV to about 50 eV there are two broad structureless enhancements in the total electron scattering cross section. The peak at 9 eV is due to indirect electron scattering via short-lived negative ion states (Sec. 2 and Table 3). The second broad maximum in the experimental total electron scattering cross section centered near 24 eV may be due to both direct electron scattering and indirect electron scattering via negative ion resonances (resonant scattering). A very broad resonance has been reported[31] around 21 eV, and the theoretical work of Huo[61] indicated an E-type resonance at 27.5 eV (see Table 3). The predicted[62] resonant effects at about 3 eV are not clearly and unambiguously reflected in the measured data.

Below about 6 eV the cross section $\sigma_{sc,t}(\epsilon)$ decreases smoothly with electron energy. Analysis of electron beam[31,37,48] and electron swarm[24,25,81–84] data indicates that in the lower part of this energy range (below about 2 eV) vibrational excitation of the CF_4 molecule (mainly the ν_3 symmetric mode) contributes appreciably to the scattering.

In order to determine $\sigma_{sc,t}(\epsilon)$ below ~2 eV, it is necessary to consider other types of cross sections which are discussed later in this article. In Fig. 4 are shown measurements of $\sigma_{sc,t}(\epsilon)$, $\sigma_m(\epsilon)$, and $\sigma_{e,int}(\epsilon)$ below about 2 eV. The total scattering cross section,[81] the momentum transfer cross section,[54] and the integral elastic cross section[54] continuously decrease with decreasing electron energy to about 0.2 eV where a deep Ramsauer–Townsend minimum appears,[24,25,53,54,81,82] and increase again as the electron energy decreases to the left of the minimum[53,54,85] [$\sigma_m(\epsilon)$ and $\sigma_{e,int}(\epsilon)$ will be discussed in detail later in Secs. 3.3 and 3.6, respectively]. We have arrived at a recommended set of values for $\sigma_{sc,t}(\epsilon)$ below ~2 eV by considering the available data as follows: (i) We accepted the values of $\sigma_{sc,t}(\epsilon)$ of Jones[55] and Szmytkowski *et al.*[56] (●, △ in Fig. 4), but the data of Curtis, Walker, and Mathieson[81] were not considered because they were indirectly determined. (ii) We accepted the $\sigma_m(\epsilon)$ and $\sigma_{e,int}(\epsilon)$ values of Mann and Linder[54] in the energy range between 0.08 eV and 1 eV because they were deduced from more direct measurements. (iii) Below the lowest vibrational threshold of 0.054 eV, $\sigma_{sc,t}(\epsilon)=\sigma_{e,int}(\epsilon)$. (iv) In the energy range between about 0.08 eV and 1 eV, a value of $\sigma_{sc,t}(\epsilon)$ can be obtained by adding $\sigma_{e,int}(\epsilon)$ and $\sigma_{vib,dir,t}(\epsilon)$, the latter being the total cross section for vibrational excitation (which will be discussed in detail later; see Table 9 in Sec. 3.6), since in this energy range electronic excitation is absent and rotational excitation is negligible (due to the absence of a dipole and a quadrupole moment). Therefore, we assume that in the energy range 0.08 eV to 1 eV $\sigma_{sc,t}(\epsilon)=\sigma_{e,int}(\epsilon)+\sigma_{vib,dir,t}(\epsilon)$, and determine the $\sigma_{sc,t}(\epsilon)$ using the $\sigma_{e,int}(\epsilon)$ of Mann and Linder[54] and the $\sigma_{vib,dir,t}(\epsilon)$ listed in Column 4 of Table 9. The values so obtained are plotted in Fig. 4 (dashed line from 0.08 eV to 2 eV). The values of $\sigma_{sc,t}(\epsilon)$ we determined agree well with the measured $\sigma_{sc,t}(\epsilon)$ for energies near 1 eV and with the $\sigma_{e,int}(\epsilon)$ for energies below about 0.08 eV. Figure 4 provides a direct

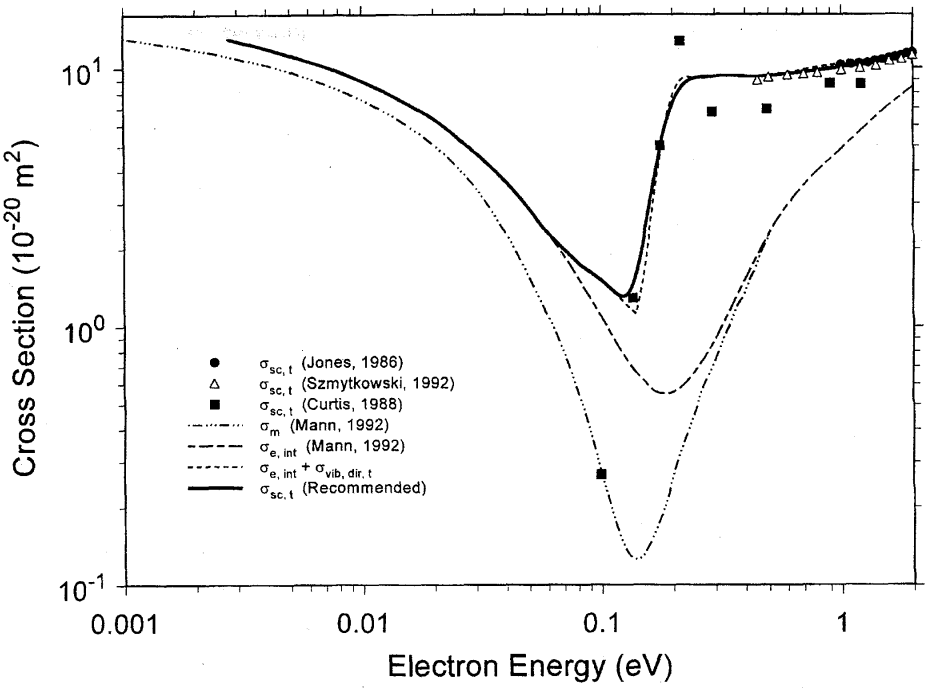

FIG. 4. Electron scattering cross sections for CF_4 in the extreme low energy range (electron impact energies less than about 2 eV). $\sigma_{sc,t}(\epsilon)$: ●, Ref. 55; △, Ref. 56; ■, Ref. 81. $\sigma_m(\epsilon)$: ···–···–, Ref. 54. $\sigma_{e,int}(\epsilon)$: - · -, Ref. 54. -------, Sum of $\sigma_{e,int}(\epsilon)$ and $\sigma_{vib,dir,t}(\epsilon)$ (see the text). —, Recommended, see Sec. 3.2 and Table 4.

comparison of $\sigma_{sc,t}(\epsilon)$, $\sigma_{e,int}(\epsilon)$, and $\sigma_m(\epsilon)$ in the region of the Ramsauer–Townsend cross section minimum. It appears that the minimum is the deepest for $\sigma_m(\epsilon)$. Below ~0.5 eV, $\sigma_m(\epsilon) < \sigma_{e,int}(\epsilon)$ indicating small angle scattering.

The cross section $\sigma_{sc,t}(\epsilon)$ estimated in the manner outlined above from 0.08 eV to 2 eV was used along with the measurements of Mann and Linder[54] for $\sigma_{e,int}(\epsilon)$ below 0.08 eV, and the measurements of Jones[55] and Szmytkowski[56] for $\sigma_{sc,t}(\epsilon)$ above about 0.5 eV to obtain a best estimate of $\sigma_{sc,t}(\epsilon)$ below ~1 eV. The values of this best estimate are shown by the solid line in Fig. 4, and are listed in Table 4 (along with the data for energies above 1 eV from Fig. 3). The data in Table 4 are our recommended $\sigma_{sc,t}(\epsilon)$ from 0.001 eV to 4000 eV and are further discussed later in the article (Figs. 30 and 43).

3.3 Momentum Transfer Cross Section, $\sigma_m(\epsilon)$

There exist three types of data on $\sigma_m(\epsilon)$: experimental determinations,[31,54,86] swarm-unfolded cross sections,[24,25,81,82,84] and calculated cross sections.[61,87,88] These are compared in Fig. 5 from 0.001 eV to 1000 eV. There is a large uncertainty in these cross section values due to the indirect determination of many cross section sets in this region and to the fact that various methods (calculations and experiments) yield different types of cross sections. The experimental and the calculated $\sigma_m(\epsilon)$ are for elastic electron scattering. The swarm-based determinations[24,25,81,82] have employed the Boltzmann code[24,25,82] or the Monte Carlo method.[81] It should be noted that swarm-based cross sections are model-specific and are thus of limited value. (See, also, reviews by Morgan.[71,72] These reviews contain data that have been revised since the review of the subject by Morgan. The present work incorporates these revisions and also new recent information. The present review is broader in scope and aims at a more comprehensive data base for the CF_4 molecule than has previously been attempted.)

The measurements of Sakae *et al.*[86] were made using a crossed-beam method with an estimated uncertainty of about 10%, and are in agreement with the data of Boesten *et al.*,[31] which were also obtained in a crossed-beam experiment. Boesten *et al.* determined their momentum transfer cross sections from their elastic differential cross section measurements which had an uncertainty of 15% to 20%. At lower energies, Mann and Linder[54] determined the momentum transfer cross section using their measurements on the elastic differential cross sections and modified effective range theory (MERT). Their elastic differential cross sections were measured using a crossed-beam apparatus with a quoted uncertainty of 20% to 30%.

The swarm-unfolded cross sections have different degrees of uncertainty and rely heavily on the accuracy of the electron transport measurements and energy range over which they were made. Although none of the cross sections of the five studies[24,25,81,82,84] of this kind agree well with the low-

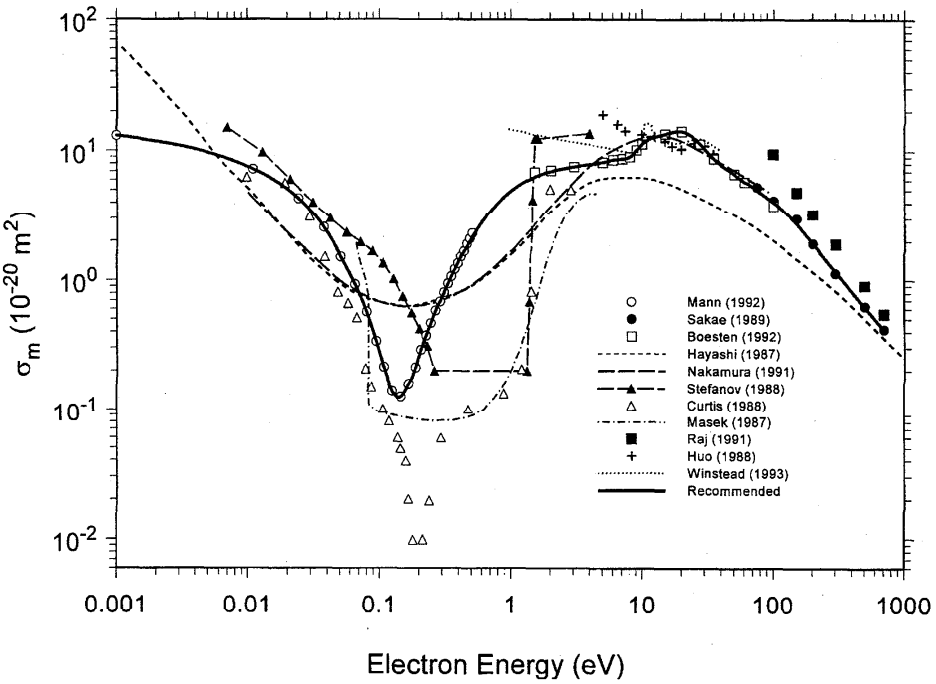

FIG. 5. Momentum transfer cross sections $\sigma_m(\epsilon)$ as a function of electron energy for CF_4. Experimentally derived (elastic): ○, Ref. 54; ●, Ref. 86; □, Ref. 31. Swarm-unfolded (effective): ----, Ref. 24; – –, Ref. 25; ▲, Ref. 82; △, Ref. 81; –.–., Ref. 84. Calculated: ■, Ref. 87; +, Ref. 61; . . . . . ., Ref. 88. Recommended: —, see Sec. 3.3 and Table 5.

energy data from the beam measurements,[54] the data of Nakamura *et al.*[25] are in reasonable agreement with the higher energy experimental values. Nakamura's cross sections are based on measurements of electron drift velocities and longitudinal electron diffusion coefficients in CF_4/Ar mixtures which were especially designed to reduce the uncertainty of the derived cross sections. Hayashi[24] determined a set of cross sections for momentum transfer and vibrational excitation such that the calculated values of the electron drift velocity w of pure CF_4, the w of mixtures of CF_4 in rare gases, and the ratio D_T/μ of the transverse electron diffusion coefficient to electron mobility using the derived cross sections, best agreed with the w data of Refs. 11, 12, and 89 for pure CF_4, the w data of Refs. 11 and 12 for mixtures of CF_4 with the rare gases, and the D_T/μ measurements of Refs. 89 and 90 for pure CF_4. Hayashi used the conventional two-term expansion approximation to the solution of the Boltzmann equation and did not consider the effects of superelastic electron scattering. Morgan[71,72] pointed out that the cross section set determined by Hayashi might have been influenced by the effect of vibrational excitation because at 300 K, 17% of the CF_4 molecules are in the ν_2 and 10% in the ν_4 vibrational states. Superelastic collisions between electrons and vibrationally excited CF_4 molecules should, therefore, be significant. Experimental measurements have indicated a rather large effect of vibrational excitation on the electron drift velocity in similar systems, for example, C_2F_6.[91] The effect of superelastic collisions on the cross sections that are derived in this manner for CF_4 (and similar molecules) needs exploration. The effect of vibrational excitation on the cross section set derived for CF_4 by Nakamura *et al.*[25] also needs to be investigated.

A Boltzmann equation analysis was also used by Stefanov *et al.*[82] who derived a cross section set based on the measurements of w by Hunter, Carter, and Christophorou[92] and on the measurements of Lakshminarasimha, Lucas, and Price[90] for the D_T/μ. Curtis *et al.*[81] reported cross sections derived from measurements they made of the characteristic energy in CF_4 using a Monte Carlo method. The results of these investigations differed substantially from those of Hayashi and Nakamura, and from the more direct measurements (see Fig. 5).

In Fig. 5 are also given the results of three calculations, one using an independent-atom model with partial waves,[87] and the other two[61,88] using the static exchange approximation. The results of these calculations agree only partially with the experimental measurements of Sakae *et al.*[86] and Boesten *et al.*[31]

The recommended data set for the elastic momentum transfer $\sigma_m(\epsilon)$ is determined from the experimental cross sections of Mann and Linder[54] below 0.5 eV (see discussion earlier in this section), and those of Sakae *et al.*[86] and Boesten *et al.*[31] above 1.5 eV. We have fitted a line through the three sets of experimental data and interpolated between data sets (0.5 eV to 1.5 eV) as shown in Fig. 5. These recommended values are listed in Table 5.

TABLE 5. Recommended elastic momentum transfer cross section, $\sigma_m(\epsilon)$.

Electron energy (eV)	$\sigma_m(\epsilon)$ (10^{-20} m^2)	Electron energy (eV)	$\sigma_m(\epsilon)$ (10^{-20} m^2)
0.001	13.03	0.8	4.01
0.0015	12.30	0.9	4.48
0.002	11.76	1	4.92
0.0025	11.30	1.5	6.26
0.003	10.92	2	6.92
0.0035	10.55	2.5	7.30
0.004	10.22	3	7.53
0.0045	9.93	3.5	7.72
0.005	9.65	4	7.89
0.006	9.14	4.5	8.04
0.007	8.67	5	8.21
0.008	8.25	6	8.55
0.009	7.85	7	8.68
0.010	7.52	8	8.96
0.015	6.15	9	10.06
0.02	5.06	10	11.23
0.025	4.16	15	13.41
0.03	3.44	20	14.10
0.035	2.82	25	12.50
0.04	2.29	30	10.38
0.045	1.90	35	8.80
0.05	1.54	40	7.80
0.06	1.10	45	7.24
0.07	0.78	50	6.66
0.08	0.55	60	5.80
0.09	0.39	70	5.28
0.10	0.26	80	4.77
0.125	0.14	90	4.37
0.15	0.13	100	4.03
0.175	0.18	150	2.74
0.2	0.27	200	1.92
0.25	0.48	250	1.46
0.3	0.76	300	1.17
0.35	1.05	350	0.97
0.4	1.39	400	0.82
0.45	1.76	450	0.71
0.5	2.13	500	0.62
0.6	2.82	600	0.50
0.7	3.45	700	0.41

3.4 Differential Elastic Electron Scattering Cross Section, $\sigma_{e,\,diff}(\epsilon)$

There are three measurements of the differential elastic electron scattering cross section $\sigma_{e,\,diff}(\epsilon)$ of CF_4 covering various ranges of incident electron energies and scattering angles. Sakae *et al.*[86] measured the $\sigma_{e,\,diff}(\epsilon)$ for CF_4 between 5° and 135°, for incident electron energies at 75, 100, 150, 200, 300, 500, and 700 eV. The experimental cross sections were extrapolated to 0° and 180° scattering angles by fitting the square of the Legendre polynomials to the measured values.[86] The uncertainty in their data was estimated to be about 10%. These results are shown in Fig. 6; the cross section $\sigma_{e,\,diff}(\epsilon)$ is seen to increase steeply at the forward angles. The second set of measurements of $\sigma_{e,\,diff}(\epsilon)$ was made by Boesten *et al.*[31] in the energy range 1.5 eV to 100 eV and for scattering angles from 15° to 130° using a crossed-beam apparatus. The relative cross section measurements were put on an absolute scale by normalization to the cross section data for He. The measured cross sections were extrapolated to 0° and 180° by phase shift fitting.[31] These cross sections are given in Table 6.

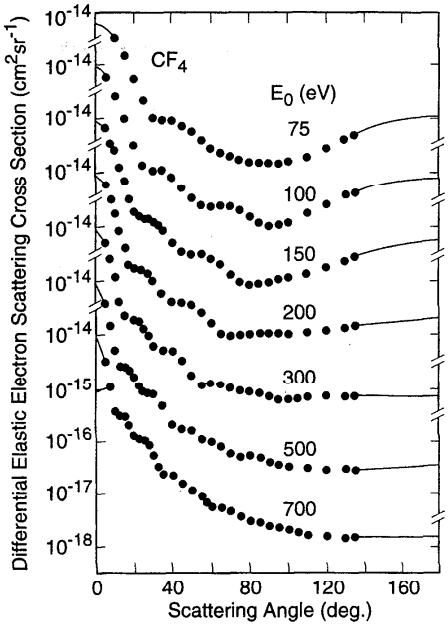

FIG. 6. Differential elastic electron scattering cross section $\sigma_{e,\,diff}(\epsilon)$ at various incident electron energies (from Ref. 86).

The third measurement of $\sigma_{e,\,diff}(\epsilon)$ was that of Mann and Linder.[54] These measurements were made at scattering angles between 10° and 105° and for electron energies from 0.5 to 20 eV. Their absolute values of $\sigma_{e,\,diff}(\epsilon)$ were obtained by integration and by normalization of the sum of the integral elastic cross section and the total cross section for inelastic electron scattering they measured at 3 eV to the total cross section of Jones[55] at this energy. The absolute uncertainty of the measurements was estimated to be 20–30%. These values are given in Table 7.

There have been five calculations of the $\sigma_{e,\,diff}(\epsilon)$ for CF_4. The first calculation was made by Raj,[87] who used an independent-atom model along with partial waves to calculate the $\sigma_{e,\,diff}(\epsilon)$ in the relatively high energy range of 100 to 700 eV. These calculated values are shown in Fig. 7 for 100, 150, 200, 300, 500, and 700 eV (open circles) in comparison with the experimental data of Sakae *et al.*[86] The second calculation was by Huo,[61] who employed the fixed-nuclei, static-exchange approximation and determined $\sigma_{e,\,dif}(\epsilon)$ in a lower energy range than Raj.[87] These results are shown in Fig. 8 for 6.5, 12.5, 17, 25, 30, and 35 eV electron energies. A comparison of the 6.5 eV cross section curve with the cross section curves at 12.5 and 17.0 eV shows that the first T_2 resonance (at about 6 eV, Table 3) affects the forward scattering more strongly than at higher energies. The cross sections at 12.5 and 17.0 eV are affected

TABLE 6. Differential elastic electron scattering cross sections, $\sigma_{e,diff}(\epsilon)$, for CF_4 in units of 10^{-16} cm^2 sr^{-1} for the indicated scattering angles θ and electron impact energies (Ref. 31). At the bottom $\sigma_{e,int}(\epsilon)$ and $\sigma_m(\epsilon)$ are listed in units of 10^{-16} cm^2.

θ (deg.)	1.5 eV	2 eV	3 eV	5 eV	6 eV	7 eV	8 eV	9 eV	10 eV	15 eV	20 eV	35 eV	50 eV	60 eV	100 eV
15	···	1.119	0.341	0.965	1.553	2.557	3.704	4.715	4.401	5.433	6.757	14.104	13.322	12.190	9.926
20	0.116	0.211	0.544	1.178	1.674	2.472	5.506	4.097	4.768	4.822	5.147	7.827	6.938	5.889	3.461
30	0.293	0.517	0.957	1.778	2.041	2.378	2.987	3.513	4.116	3.473	3.167	2.691	1.409	1.015	1.056
40	0.476	0.753	1.256	2.131	2.363	2.422	2.486	2.656	2.884	2.464	1.720	0.878	0.738	0.746	0.753
50	0.811	1.118	1.591	2.334	2.418	2.052	1.757	1.714	1.685	1.383	0.912	0.861	0.857	0.759	0.319
60	0.915	1.399	1.603	2.081	1.938	1.780	1.197	1.115	0.999	0.901	0.795	0.927	0.672	0.429	0.217
70	1.026	1.258	1.513	1.472	1.484	1.110	0.775	0.720	0.730	0.869	1.004	0.809	0.360	0.219	0.215
80	0.923	1.044	1.179	1.023	0.903	0.657	0.552	0.605	0.782	1.058	1.095	0.435	0.170	0.129	0.157
90	0.878	0.807	0.891	0.607	0.543	0.435	0.495	0.681	0.800	1.076	0.988	0.201	0.136	0.128	0.100
100	0.815	0.726	0.538	0.408	0.377	0.468	0.592	0.767	0.794	0.931	0.690	0.176	0.133	0.124	0.095
110	0.615	0.486	0.440	0.355	0.435	0.539	0.678	0.754	0.727	0.698	0.530	0.255	0.200	0.185	0.122
120	0.458	0.403	0.317	0.336	0.447	0.593	0.670	0.731	0.622	0.595	0.554	0.455	0.409	0.322	0.192
130	0.362	0.298	0.264	0.378	0.450	0.574	0.612	0.658	0.651	0.691	0.823	0.691	0.657	0.433	0.262
$\sigma_{e,int}$	7.74	8.56	10.46	12.72	13.40	13.36	13.91	15.40	16.63	16.92	17.63	16.72	14.24	13.06	9.84
σ_m	6.96	7.14	7.65	8.24	8.62	8.78	9.12	10.24	11.38	13.49	14.11	8.76	6.72	5.84	3.85

by the broad A_1 resonance at 11.7 eV and by the T_2 and E resonances near 27 eV. Because these resonances are very broad their effects on the cross sections are much weaker. The major difference between the cross sections at 25, 30, and 35 eV is found at small scattering angles (see Fig. 8b). The results of three more recent calculations[88,93,94] are discussed below (Fig. 9).

It is rather difficult to compare in detail the results of the various measurements and computations mainly because there is only a limited overlap in the two key variables: incident electron energy and scattering angle. However, three comparisons are possible and are shown in Figs. 7, 9, and 10. In Fig. 7, the calculated cross sections of Raj[87] at 100 eV and 150 eV are compared with the experimental measurements of Sakae *et al.*[86] It is seen from Fig. 7a that the calculations reproduce qualitatively the overall behavior of the experimental data, but the calculated values are much higher than the experimental data. The agreement between the measured and the calculated results improves, as expected, with increasing incident electron energy (Figs. 7b and 7c). At low energies, the values of $\sigma_{e,diff}(\epsilon)$ as calculated within the independent-atom model are larger than the measured values possibly because such factors as orbital overlap in molecules decrease the atomic contributions compared with those in the free atomic state.

In Fig. 9 are compared the experimental data of Mann and Linder[54] and Boesten *et al.*[31] with the calculated values of Huo[61] for three values of incident electron energy: 5, 10, and

TABLE 7. Differential elastic electron scattering cross section, $\sigma_{e,diff}(\epsilon)$ in units of 10^{-16} cm^2 sr^{-1} (from Ref. 54).

Energy (eV)	Scattering angle (deg)					Energy (eV)	Scattering angle (deg)				
	20	40	60	80	100		20	40	60	80	100
0.5	0.04	0.05	0.10	0.15	0.24	10.0	4.81	2.44	0.93	0.71	0.70
1.0	0.08	0.20	0.40	0.50	0.52	10.5	4.79	2.46	0.95	0.78	0.73
1.5	0.20	0.49	0.79	0.80	0.63	11.0	4.73	2.47	0.95	0.81	0.74
2.0	0.38	0.82	1.14	1.00	0.64	11.5	4.68	2.44	0.96	0.86	0.74
2.5	0.58	1.09	1.42	1.09	0.61	12.0	4.62	2.41	0.93	0.88	0.75
3.0	0.78	1.34	1.59	1.11	0.55	12.5	4.64	2.36	0.93	0.89	0.75
3.5	0.97	1.57	1.73	1.10	0.50	13.0	4.62	2.32	0.90	0.92	0.77
4.0	1.16	1.77	1.83	1.06	0.46	13.5	4.68	2.26	0.87	0.94	0.76
4.5	1.30	1.92	1.90	1.02	0.42	14.0	4.71	2.21	0.84	0.96	0.75
5.0	1.44	2.02	1.92	0.96	0.39	14.5	4.76	2.15	0.82	0.96	0.75
5.5	1.54	2.05	1.90	0.87	0.37	15.0	4.83	2.08	0.81	0.99	0.74
6.0	1.72	2.04	1.81	0.77	0.36	15.5	4.91	2.02	0.77	1.01	0.74
6.5	2.09	2.01	1.64	0.67	0.38	16.0	4.91	1.99	0.77	1.03	0.72
7.0	2.62	2.05	1.44	0.56	0.43	16.5	5.03	1.96	0.76	1.02	0.70
7.5	3.20	2.10	1.25	0.51	0.49	17.0	5.12	1.92	0.73	1.04	0.69
8.0	3.73	2.18	1.11	0.50	0.56	17.5	5.21	1.87	0.74	1.05	0.67
8.5	4.18	2.29	1.01	0.52	0.62	18.0	5.35	1.83	0.73	1.06	0.67
9.0	4.54	2.37	0.95	0.57	0.66	18.5	5.46	1.80	0.73	1.06	0.65
9.5	4.74	2.40	0.92	0.64	0.69						

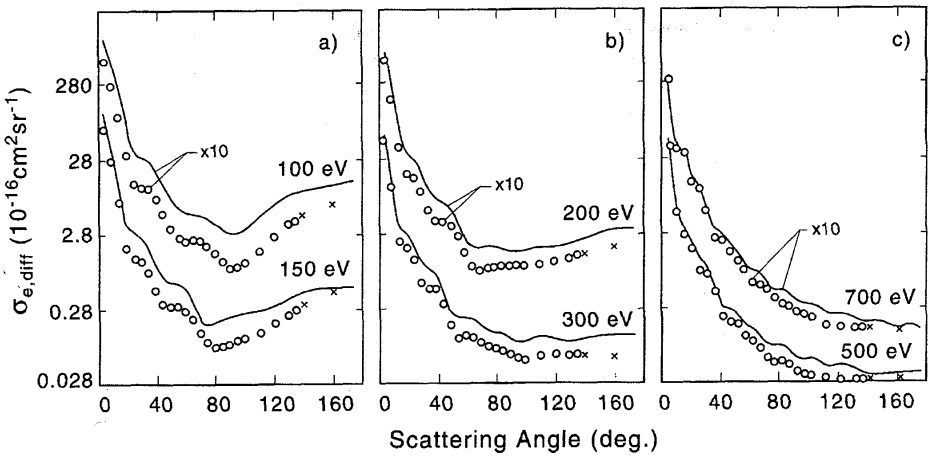

FIG. 7. Differential elastic electron scattering cross section $\sigma_{e,diff}(\epsilon)$ for CF_4 at various incident electron energies (from Ref. 87). (a) 100 eV and 150 eV, (b) 200 eV and 300 eV, (c) 500 eV and 700 eV. — calculations (Ref. 87); ○, measurements (Ref. 86); ×, extrapolated values (Ref. 86). The upper curves in each of the three figures were multiplied by 10 for the convenience of display.

15 eV. For these energies there exist data from all three sources. For energies above 10 eV, the experimental results agree well with the calculations of Huo. At 5 eV, the calculations show strong deviations from the experimental results which may be attributed to neglect of the polarization effects in the calculations. The two sets of experimental measurements[31,54] are in reasonably good agreement at all energies. Representative results on the differential electron scattering cross sections obtained for electron energies below 40 eV by the three more recent calculations,[88,93,94] are shown in Figs. 9b, 9c, and 9d, where they are compared with the results of the earlier calculations and the experimental measurements. In Figs. 9c and 9d are shown the results of the static exchange approximation of Winstead, Sun, and McKoy[88] and the results of the exact static exchange calculation of Gianturco and others[93] for 10 and 15 eV. The results of the pseudopotential calculation of Natalense *et al.*[94] for 5 and 10 eV are shown, respectively, in Figs. 9b and 9c. In general, the calculated values are in poor agreement with the measurements at the lowest energy (5 eV) for which comparisons can be made. For the higher energies (10 and 15 eV), the agreement is good for scattering angles between 30° and 130°, but outside this angle range the agreement between the calculated and the experimental data depends on the electron energy, the scattering angle, and the type of calculation.

There also exist data for $\sigma_{e,diff}(\epsilon)$ of CF_4 at 100 eV from two experiments[31,86] and one calculation,[87] which can be compared directly. As for the lower energy range (Fig. 9), the 100 eV data in Fig. 10 show agreement among the various measurements (especially at scattering angles less than 100°); the theoretical calculations, however, overestimate the magnitude of the scattering cross section although they reproduce reasonably well the angular dependence of $\sigma_{e,diff}(\epsilon)$.

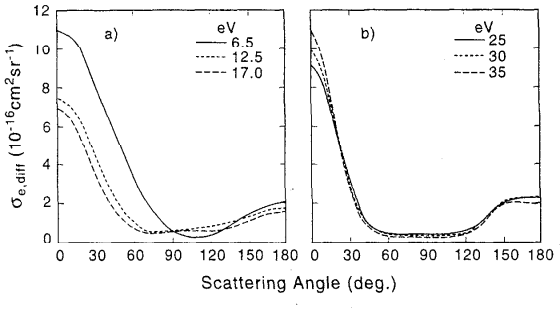

FIG. 8. Calculated differential elastic electron scattering cross sections for CF_4 (from Ref. 61). (a) Incident electron energies 6.5, 12.5, and 17.0 eV. (b) Incident electron energies 25, 30, and 35 eV.

3.5 Integral Elastic Electron Scattering Cross Section, $\sigma_{e,int}(\epsilon)$

From the differential elastic electron scattering cross sections obtained from the experiments discussed in the preceding section, Sakae *et al.*,[86] Boesten *et al.*,[31] and Mann and Linder[54] obtained values of the integral elastic cross section $\sigma_{e,int}(\epsilon)$ for electron energies above 1 eV. These cross sections are plotted in Fig. 11. Mann and Linder[54] obtained their integral elastic cross section by a simple integration procedure having weighted the cross section values they measured between 10° and 105° by $\sin\theta$ and then linearly extrapolating towards the integration limits of 0° and 180°. According to the authors, the total uncertainty is expected to be $\leq 20\%$. In order to put their data on an absolute scale, the sum of the integral elastic cross section and the total cross section for inelastic scattering was normalized to the total cross section value measured by Jones[55] at 3 eV. The observed broad enhancements in $\sigma_{e,int}(\epsilon)$ below ~20 eV are due to resonances, especially the peak at ~5 eV, which

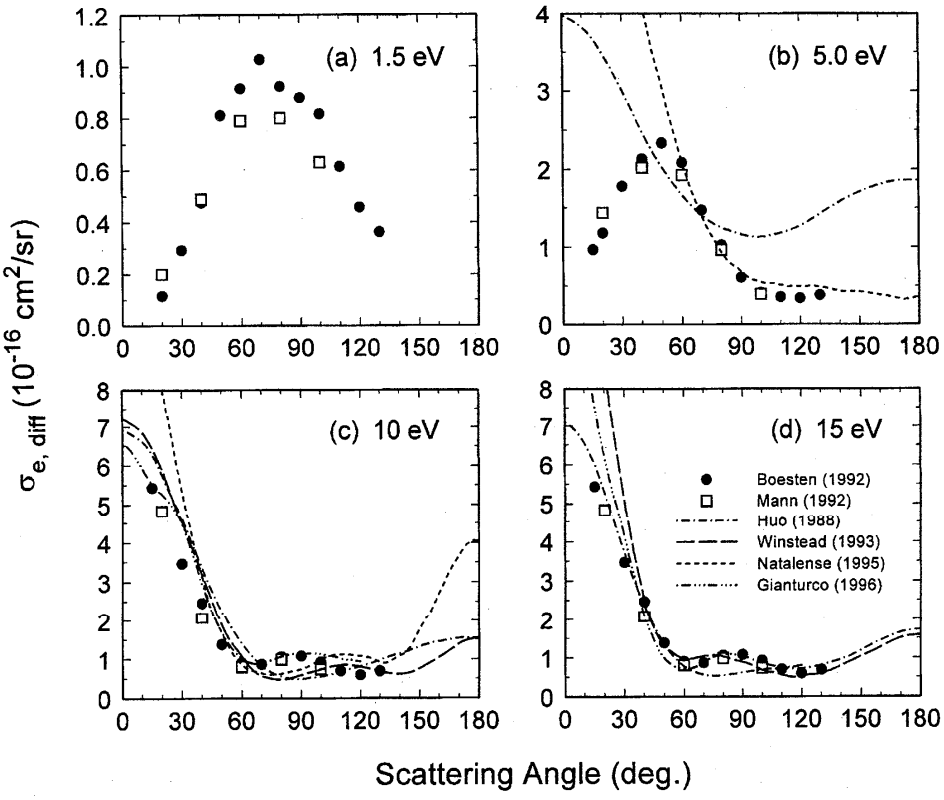

FIG. 9. Comparison of differential elastic electron scattering cross section for CF_4 at 1.5, 5, 10, and 15 eV. Experimental values: ●, Ref. 31; □, Ref. 54. Calculated values: - · - · - , Ref. 61; – –, Ref. 88; ----, Ref. 94; —···—, Ref. 93.

agrees well with the position of resonances which have been well-established by other studies (e.g., dissociative electron attachment; see discussion in Sec. 2 and Table 3). The $\sigma_{e,\,int}(\epsilon)$ data in Fig. 11 below 0.5 eV were obtained by Mann and Linder[54] using the modified effective range theory (MERT) analysis.

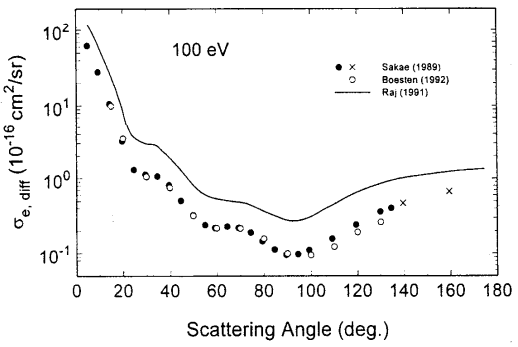

FIG. 10. Comparison of the differential elastic electron scattering cross section for CF_4 at 100 eV incident electron energy. Experimental values: ○, Ref. 31; ●, Ref. 86. Calculated values: —, Ref. 87. Extrapolated values: ×, Ref. 86.

The experimental cross sections[31,54,86] in Fig. 11 are compared with the results of five calculations.[61,87,88,93,94] The low energy result of Huo[61] indicates a structure near 6 eV, but her cross section is not in general agreement with the experimental data. Similarly, the results of the three more recent calculations[88,93,94] exhibit structure the location of which varies from calculation to calculation. The calculated values exceed the experimental ones and the overall agreement between the two is generally poor. The calculation of Raj[87] gives results which are in satisfactory agreement with the measurements of Sakae *et al.*[86] only for energies above about 500 eV.

We have fitted a line to the three sets of experimental data giving equal weight to each data set. This is shown by the solid line in Fig. 11 and represents our recommended values of $\sigma_{e,\,int}(\epsilon)$ as listed in Table 8.

3.6 Inelastic Electron Scattering Cross Section, $\sigma_{inel}(\epsilon)$

It is convenient to divide the inelastic electron scattering cross sections for CF_4 into two groups: those for vibrational excitation and those for electronic excitation.

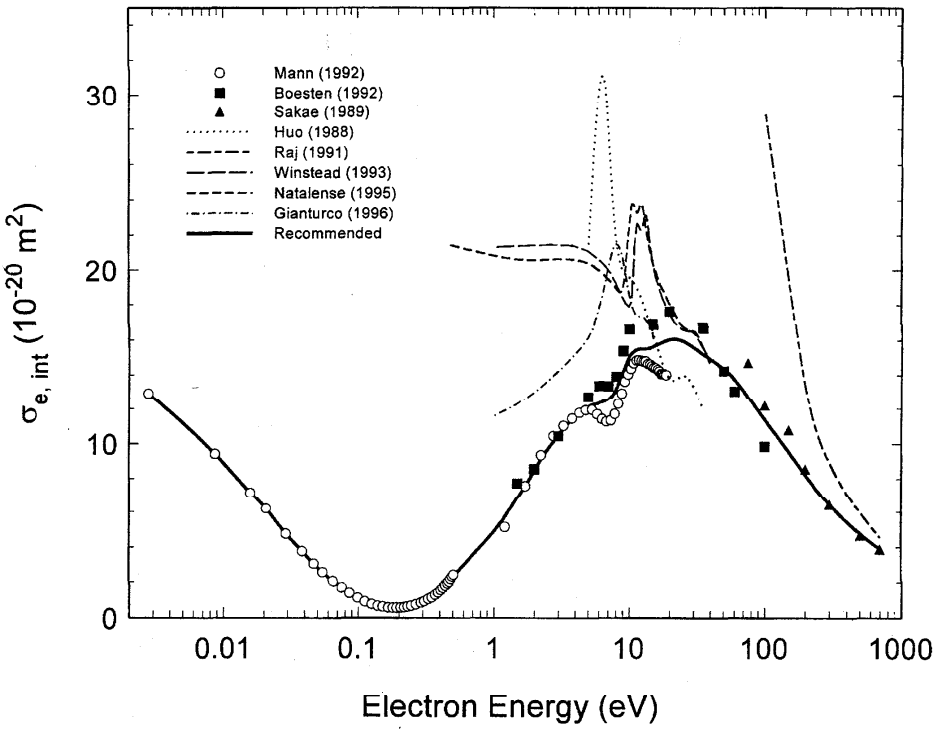

FIG. 11. Integral elastic electron scattering cross section $\sigma_{e,\,int}(\epsilon)$ for CF_4. Experimental values: ○, Ref. 54; ■, Ref. 31; ▲, Ref. 86. Calculated values: ···, Ref. 61; —·—, Ref. 87; – –, Ref. 88; -----, Ref. 94; –·–·–, Ref. 93. Recommended: —, see Sec. 3.5 and Table 8.

3.6.1 Vibrational Excitation

Information on the vibrational excitation of the CF_4 molecule comes from direct measurements using electron beam methods,[31,53] from indirect determinations via swarm-data analyses,[24,25,81,82,84] and from theory.[53,73,80]

As discussed in Sec. 2, the CF_4 molecule has four fundamental frequencies: the symmetric stretch ν_1, the symmetric bend ν_2, the asymmetric stretch ν_3, and the asymmetric bend ν_4. Vibrational excitation of the CF_4 molecule is a mixture of direct excitation and indirect excitation via resonances. In Fig. 12a is shown the energy dependence of the cross section for excitation of the asymmetric ν_3 mode obtained by Boesten *et al.*[31] at a scattering angle of 90°. The excitation cross section increases sharply for energies approaching the vibrational excitation threshold (0.157 eV) due to direct excitation of the ν_3 mode which has a large infrared (IR) activity.[31] At higher energies, the data in Fig. 12a show a strong enhancement at about 8 eV due to the T_2 resonance ($\ell=1$ partial wave) at about 6.6 eV (see Table 3), and a weak broad enhancement around 21 eV possibly due to indirect excitation via the decay of the E and T_2 resonances located in the vicinity of this energy (see Table 3). The strong direct excitation of the ν_3 mode is clearly seen in Fig. 12b where typical energy-loss spectra are shown[31] for the vibrational excitation of CF_4 at 2 eV and 8 eV. At low (20° data in Fig. 12b) scattering angles, excitation of the ν_3 mode becomes much stronger than elastic scattering; the latter decreases towards the Ramsauer–Townsend minimum. This minimum occurs at 162±25 meV,[47] i.e., it almost coincides with the threshold for excitation of the ν_3 mode. The relative weakness of the ν_4 excitation is consistent with its weak IR absorption intensity as compared to that of ν_3.[95]

Another significant electron beam study of CF_4 has been carried out by Mann and Linder[53] for electron energies ranging from about 0.5 to 12 eV. The results of these investigators are similar to those of Boesten *et al.*,[31] namely, strong inelastic scattering is observed in two distinct energy regions: one in a resonance region between 6 and 11 eV (due to the T_2 negative ion resonance) and the other in a region of direct excitation below 2 eV via the dipole moment associated with ν_3. For low scattering angle and/or low incident electron energy, the cross section for direct excitation can be much larger than the resonant cross section. Excitation of the ν_3 asymmetric stretch mode is the dominant energy loss process over the entire range of collision energies below the threshold for electronic excitation. The excitation of the ν_4 and $2\nu_3$ modes is much smaller than elastic scattering under all conditions. For the excitation behavior of other modes (including overtones and combination modes) see Refs. 31 and 53.

A comparison of measured cross sections with values calculated using the Born dipole approximation has been made by Mann and Linder[53] and is shown in Fig. 13a. For energies below 5 eV, the experimental data are roughly described by

TABLE 8. Recommended elastic integral cross sections, $\sigma_{e,int}(\epsilon)$.

Electron energy (eV)	$\sigma_{e,int}(\epsilon)$ (10^{-20} m^2)	Electron energy (eV)	$\sigma_{e,int}(\epsilon)$ (10^{-20} m^2)
0.003	12.68	2	8.48
0.0035	12.24	2.5	9.68
0.004	11.85	3	10.53
0.0045	11.50	3.5	11.13
0.005	11.19	4	11.55
0.006	10.63	4.5	11.91
0.007	10.13	5	12.14
0.008	9.68	5.5	12.28
0.009	9.27	6	12.36
0.01	8.88	6.5	12.45
0.015	7.39	7	12.58
0.02	6.35	8	13.15
0.025	5.42	9	14.17
0.03	4.68	10	15.06
0.035	4.11	12.5	15.52
0.04	3.62	15	15.65
0.045	3.21	17.5	15.90
0.05	2.85	20	16.06
0.06	2.29	25	15.94
0.07	1.87	30	15.58
0.08	1.54	35	15.21
0.09	1.29	40	14.90
0.1	1.09	45	14.63
0.125	0.76	50	14.35
0.15	0.62	60	13.74
0.175	0.55	70	13.06
0.2	0.56	80	12.43
0.25	0.68	90	11.88
0.30	0.89	100	11.39
0.35	1.18	150	9.55
0.4	1.53	200	8.22
0.45	1.91	250	7.22
0.5	2.29	300	6.47
0.6	2.96	350	5.90
0.7	3.52	400	5.46
0.8	4.02	450	5.09
0.9	4.46	500	4.78
1	4.86	600	4.29
1.5	6.87	700	3.91

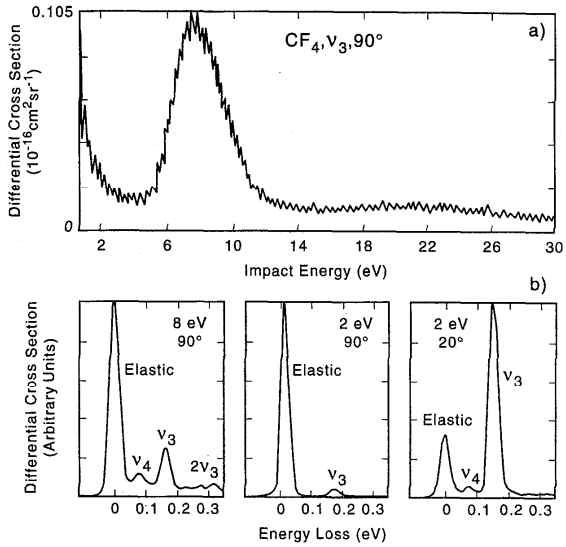

FIG. 12. (a) Differential cross section for excitation of the asymmetric stretch ν_3 mode of CF_4 as a function of electron energy for a scattering angle of 90° (from Ref. 31). (b) Electron energy-loss spectra for vibrational excitation of CF_4 at the indicated incident electron energies and scattering angles (from Ref. 31).

the Born dipole approximation. At 90°, the agreement is good up to about 5.5 eV where the resonant part of the cross section becomes visible. At 50°, the measured cross section for ν_3 between 5 and 6 eV is half of the calculated one by the Born dipole approximation. At 20°, the agreement is good for ν_3, but the measured cross section for ν_4 is larger than that obtained from the Born dipole approximation. This may be due to a contribution to the scattering cross section by higher multiple moments and/or polarization as has been observed[53,96] for modes with weak infrared (IR) activity.[31,96] In Fig. 13b is shown the enormous cross section which is obtained with the Born dipole model in the forward direction. For a scattering angle up to 30° the calculated values agree with the measurements, but for larger angles the two sets of data deviate. However, for the 7.5 eV data the difference at larger angles may be ascribed to a resonant contribution to the measured cross section.

Hayashi[24] and Nakamura[25] obtained a set of cross sections for various processes using the two-term expansion approximation to the solution of the Boltzmann transport equation but with different sets of electron transport data for pure CF_4 and for CF_4 mixtures (see original references and Sec. 3.3). Hayashi used the electron drift velocity data of Christophorou *et al.*[11,12] and Naidu and Prasad[89] which are 10–15% higher than the more recent values of Hunter, Carter, and Christophorou.[83] The vibrational cross sections $\sigma_{\nu1,3}(\epsilon)$ $[\approx\sigma_{\nu3}(\epsilon)]$, and $\sigma_{\nu2,4}(\epsilon)$ $[\approx\sigma_{\nu4}(\epsilon)]$ obtained by Hayashi for the ν_3 and ν_4 excitations, respectively, are shown by the solid lines in Figs. 14a and 14b. These and the momentum transfer cross section were chosen so as to give w and D_T/μ values that best agree with the measured w values[11,12,89] and D_T/μ values.[90] The vibrational cross sections of Nakamura for the excitation of the same modes are also shown in Figs. 14a and 14b by the short dashed lines. Nakamura obtained these cross sections using the electron drift velocities and longitudinal electron diffusion coefficients he measured in CF_4–Ar mixtures. The data of Hayashi and Nakamura differ in the threshold region and the resonant peak near 8 eV in the Nakamura cross section is absent from the Hayashi cross section function. The swarm-based cross sections,[24,25] and the swarm studies[81] at low E/N, indicated the effect of direct vibrational excitation of infrared active modes and the effect of indirect vibrational excitation via resonances at high E/N. Nakamura reported that the measured ND_L (D_L is the longitudinal electron diffusion coefficient) at high E/N necessitates a large inelastic process around 7 eV. He obtained reasonable agreement between the measured and the calculated electron transport coefficients

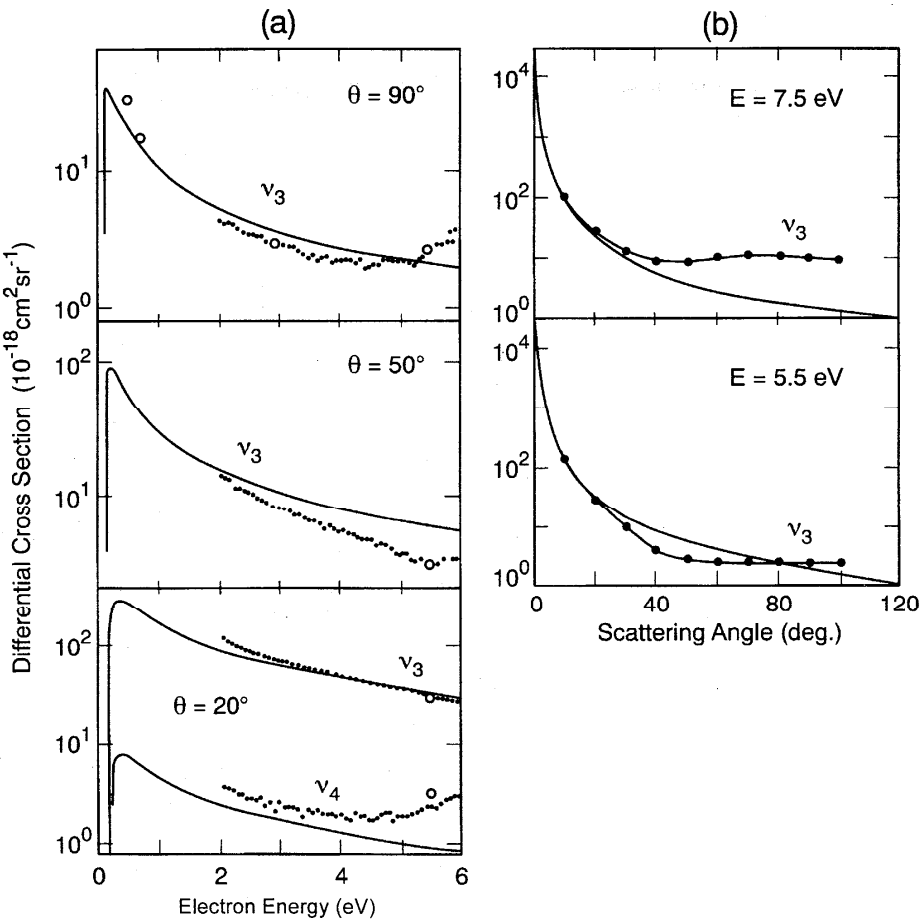

FIG. 13. (a) Differential cross sections for the ν_3 and ν_4 vibrational modes of CF_4 as a function of electron energy at 20°, 50°, and 90° scattering angles. Comparison of the experimental results of Mann and Linder (Ref. 53) with the Born dipole approximation (solid line). (b) Differential cross section for the ν_3 vibrational mode for 5.5 and 7.5 eV incident electron energies; comparison of the experimental results of Mann and Linder (Ref. 53) with the Born approximation (solid line).

by assuming a resonance peak in the vibrational excitation cross section. The magnitude of this cross section is consistent with the measurements of Jones,[55] the beam results described earlier in this section, and the positions of the negative ion resonances obtained by other methods (see Table 3).

The results of another swarm-based analysis which used a Monte Carlo simulation method[81] are compared in Figs. 14a and 14b with the results of the other two swarm-based studies.[24,25] The Monte Carlo study also shows the strong direct excitation of the IR active modes ν_3 and ν_4 at near-threshold energies, but the energy dependence of these cross sections is difficult to rationalize physically. Curtis, Walker, and Mathieson[81] also calculated the cross section for direct excitation of ν_3 and ν_4 using the Born approximation and measured IR absorption intensities; these cross sections are also shown in Figs. 14a and 14b.

Based on the reasonable agreement between the measured cross section for direct vibrational excitation and the cross sections predicted by the Born approximation, Bonham[73] calculated total vibrational excitation cross sections $\sigma_{\nu 3}$ and $\sigma_{\nu 4}$, respectively, for the ν_3 and the ν_4 modes using the Born dipole formula. These are given in Table 9. Furthermore, Bonham added $\sigma_{\nu 3}$ and $\sigma_{\nu 4}$ for the two vibrational modes which represents the total vibrational cross section, and compared it with the experimental data of $\sigma_{\text{inel, t}}(\epsilon)$ of Boesten *et al.*[31] and Mann and Linder.[53] The agreement is seen (Fig. 14c, Table 9) to be satisfactory only below about 5 eV. Above this energy, indirect electron scattering through the negative ion resonances in the 6–8 eV range (solid line in Fig. 14c) makes a large contribution to the vibrational excitation and accounts for the much larger measured cross sections compared to the values predicted by the Born approximation in this energy range.

Above 12.5 eV, the $\sigma_{\text{inel, t}}(\epsilon)$ data of Boesten *et al.* contain a contribution from electronic excitation. The difference between the measurements of Boesten *et al.* and the Born $\sigma_{\text{vib, dir, t}}(\epsilon)$ gives the cross section for indirect inelastic elec-

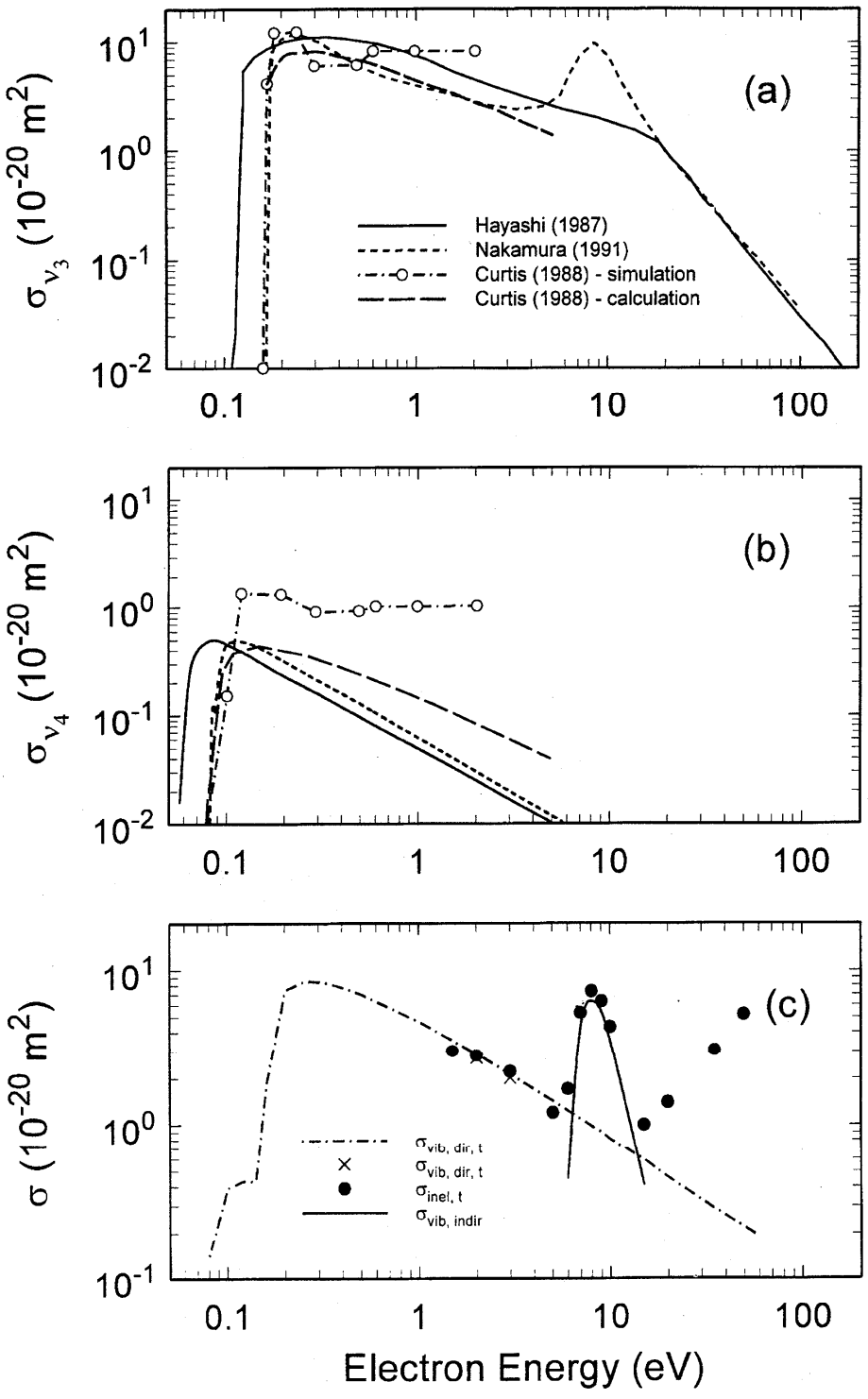

FIG. 14. (a) Vibrational excitation cross section functions $\sigma_{\nu 3}$ for the ν_3 vibrational mode deduced from electron swarm data using a Boltzmann code (—, Ref. 24; ----, Ref. 25) and a Monte Carlo simulation method (○, Ref. 81) and calculations using the Born approximation (– –, Ref. 81). (b) The same as above, but for the $\sigma_{\nu 4}$ of the ν_4 mode. (c) Total vibrational excitation cross section. - · - · - Born approximation calculation (Ref. 73) of $\sigma_{vib, dir, t} = \sigma_{\nu 3} + \sigma_{\nu 4}$. ×, measurements (Ref. 53) of $\sigma_{vib, dir, t}$. ●, measurements (Ref. 31) of $\sigma_{inel, t}$. —, indirect vibrational contribution due to resonances (see Sec. 3.6.1).

TABLE 9. Vibrational cross sections for CF_4 in units of 10^{-20} m^2.

Electron energy (eV)	$\sigma_{\nu 3}$ (Born)[a]	$\sigma_{\nu 4}$ (Born)[a]	$\sigma_{\text{vib, dir,t}} = \sigma_{\nu 3} + \sigma_{\nu 4}$	$\sigma_{\text{inel, t}} = \sigma_{\text{sc, t}} - \sigma_{\text{e, int}}$	$\sigma_{\text{inel, t}} - \sigma_{\text{vib, dir, t}} = \sigma_{\text{inel, indir, t}}$	$\sigma_{\text{vib, indir}} = \sigma_{\text{inel, indir, t}} - \sigma_{\text{a,t}}$
0.08		0.14	0.14			
0.1		0.39	0.39			
0.12		0.43	0.43			
0.14		0.43	0.43			
0.16	1.43	0.43	1.86			
0.2	7.03	0.40	7.43			
0.25	8.04	0.36	8.40			
0.275	8.11	0.35	8.46			
0.3	8.06	0.33	8.39			
0.35	7.80	0.30	8.10			
0.4	7.46	0.28	7.74			
0.5	6.77	0.24	7.01			
1	4.52	0.15	4.67			
1.5	3.43	0.11	3.54	3.0[b]		
2	2.79	0.09	2.88	2.8[b];2.7[c]		
3	2.06	0.06	2.12	2.2[b];2.0[c]		
5	1.39	0.04	1.43	1.2[b]		
6	1.20	0.04	1.24	1.7[b]	0.46	0.45
7	1.06	0.03	1.09	5.3[b]	4.21	4.19
8	0.95	0.03	0.98	7.3[b]	6.32	6.31
9	0.87	0.03	0.90	6.3[b]	5.40	5.40
10	0.79	0.02	0.81	4.3[b]	3.49	3.49
15	0.57	0.02	0.59	1.0[b]	0.41[d]	0.41
20	0.45	0.01	0.46	1.4[b]	0.94[d]	
35	0.28	0.01	0.29	3.05[b]	2.76[d]	
50	0.21	0.01	0.22	5.2[b]	4.98[d]	
60	0.18	0.01	0.19			

[a]From Ref. 73.
[b]From Ref. 31; difference between the $\sigma_{\text{sc,t}}$ of Jones (Ref. 55) and $\sigma_{\text{e,int}}$ of Boesten *et al.* (Ref. 31).
[c]From Ref. 53.
[d]Contains a contribution from inelastic scattering due to electronic excitation which increases with increasing energy above 12.5 eV.

tron scattering $\sigma_{\text{inel, indir, t}}(\epsilon)$ from the CF_4 molecule. The indirect vibrational excitation cross section $\sigma_{\text{vib, indir}}(\epsilon)$ can then be obtained by subtracting the total attachment cross section $\sigma_{\text{a, t}}(\epsilon)$ (see Sec. 6) from $\sigma_{\text{inel, indir, t}}(\epsilon)$ below 12.5 eV. This has been done in the last column of Table 9, and is shown as the solid line in Fig. 14c. Clearly, indirect vibrational excitation is the predominant inelastic electron scattering process in the energy range from about 7 eV to about 13 eV.

3.6.2 Electronic Excitation

There are no direct measurements of the cross sections for electronic excitation of the CF_4 molecule. Mann and Linder[54] determined the integral inelastic cross section (sum of cross sections for all energy loss processes) for electron scattering from CF_4 by taking the difference between the total cross section of Jones[55] and their integral elastic cross section. This cross section is presented in Fig. 15 and is in essential agreement with the data of Boesten *et al.* shown in Fig. 14c. Below the onset of electronic excitation at 12.5 eV, this cross section is due to vibrational excitation with a small contribution from dissociative electron attachment (see Sec. 6). Above this energy progressively the cross section has a larger contribution from electronic excitation (see Table 9 and Fig. 14c). It has been argued,[42] and is supported by measurements, that the total dissociation cross section for CF_4 is equal to the total electronic excitation cross section. The total electron impact dissociation cross section for CF_4

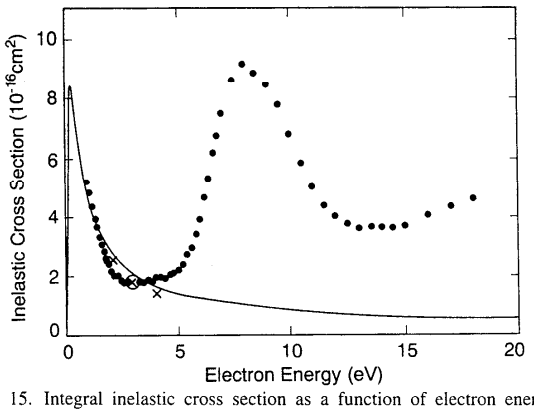

FIG. 15. Integral inelastic cross section as a function of electron energy $\sigma_{\text{inel,int}}(\epsilon)$ for CF_4. ●, difference between the total cross section of Jones (Ref. 55) and the integral elastic cross section of Mann and Linder (Ref. 53); ×, measured total vibrational excitation cross section (Ref. 53); — Born dipole approximation for vibrational excitation (Ref. 53); ⊗, normalization point.

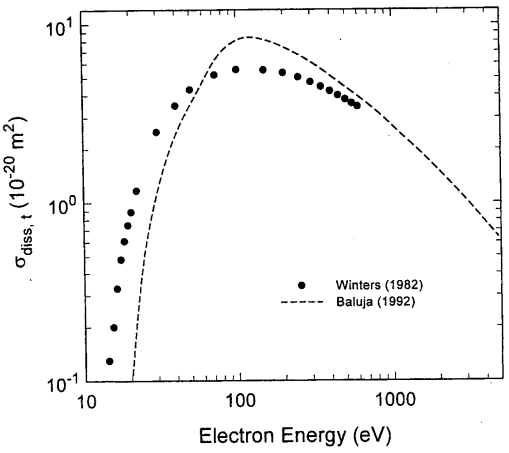

FIG. 16. Total dissociation cross section $\sigma_{diss,t}(\epsilon)$ as a function of electron energy for CF_4. ●, experimental measurements (Ref. 42); -----, calculated absorption cross section (Ref. 80).

has been measured by Winters and Inokuti[42] from threshold up to 600 eV with an overall uncertainty of ±20%. This cross section is shown in Fig. 16 and is listed in Table 10. The cross section rises from threshold to a maximum value of 5.55×10^{-20} m^2 at about 100 eV and it decreases monotonically at higher energies. The results of a recent spherical complex potential calculation[80] of the absorption cross section of CF_4 are also shown in Fig. 16 and are seen to be in reasonable agreement with the experiment over much of the energy range.

TABLE 10. Total dissociation cross section, $\sigma_{diss,t}(\epsilon)$ in units of 10^{-16} cm^2 (from Ref. 42).

Energy (eV)	$\sigma_{diss,t}(\epsilon)$
12.5	0.024[a]
13.2	0.069[a]
14.2	0.13[a]
15.2	0.20[a]
16.2	0.33[a]
17.2	0.48[a]
18.2	0.61[a]
19.2	0.75[a]
20.2	0.89[a]
22	1.17
30	2.50
40	3.50
50	4.30
72	5.20
100	5.55
150	5.51
200	5.32
250	5.02
300	4.72
350	4.45
400	4.20
450	3.98
500	3.78
550	3.60
600	3.45

[a]Obtained from Fig. 5 in Ref. 42.

An extrapolation of the measured cross sections[42] to lower energies gave an apparent threshold for dissociation of ~12.5 eV which coincides with the onset for electronic excitation. Dissociative attachment processes occur at lower energies than this energy (see Sec. 6). Dissociation into neutrals dominates near 12.5 eV, but the dissociative ionization process progressively (see Sec. 4) takes over above ~30 eV. All ionization processes apparently lead to dissociation since the CF_4^+ ion has not been observed in all but one[97] of the mass spectrometric studies. Even if some excited electronic states of CF_4^+ are stable against dissociation,[26,97] they will dissociate upon deexcitation to the ground ionic state which is unstable. The cross sections for dissociative ionization are discussed in Sec. 4 and those on dissociation into neutral fragments in Sec. 5.

If all electronically excited states of CF_4 dissociate or predissociate,[42] the total electronic excitation cross section should be equal to the total dissociation cross section. Since, moreover, at higher energies dissociative ionization dominates, the total ionization cross section should also be about equal to the total electronic excitation cross section $[\sigma_{exc,elec,t}(\epsilon)\approx\sigma_{diss,neut,t}(\epsilon)+\sigma_{i,t}(\epsilon)]$. (See Secs. 4, 5, and 9.) Model-based total electronic excitation cross sections have been reported,[24,25] but they are suspect because they are not consistent with the above relationship.

4. Electron-Impact Ionization

4.1 Total Ionization Cross Section, $\sigma_{i,t}(\epsilon)$

The total ionization cross section is defined as

$$\sigma_{i,t}(\epsilon)=\sum_{i}^{all}[q_i\sigma'_{i,partial}(\epsilon)], \quad (1)$$

where $\sigma'_{i,partial}(\epsilon)$ is the absolute partial ionization cross section including contributions from positive ion pair formation (see in the following), q_i is the number of charges on the corresponding ionic fragment, and the sum is over "all" ions produced (or, more correctly, over all ions "detected"). Many ionic fragments contribute to $\sigma_{i,t}(\epsilon)$, as can be seen from Table 11, where the threshold and translational energies for various positive ions observed in electron impact studies of CF_4 are given. Dissociative ionization is the dominant process in CF_4 at electron-impact energies above 30 eV mainly due to the reaction[98]

$$e+CF_4\rightarrow CF_3^++F+2e. \quad (2)$$

Since all excited electronic states of CF_4 and CF_4^+ are unstable, the total ionization cross section may serve as a lower limit to the total inelastic cross section.

An early discussion of electron-impact ionization of CF_4 was given by Märk.[102] Since then a number of experimental studies and calculations have been made which are reviewed in this section. Recent measurements of $\sigma_{i,t}(\epsilon)$ can

TABLE 11. Energy thresholds and excess kinetic energies of products from dissociative ionization of CF_4 by electron impact (from Ref. 69 unless otherwise stated).

Reaction products	Zero translation energy threshold (eV)	Energy threshold (eV)	Excess energy at threshold (eV)	Observed translation energy (eV)
A. Positive ion-neutral fragments				
$CF_3^+ + F$	14.7	15.9[a,b]; 16.2[c]	1.2	1.2[d]
$CF_2^+ + F_2$	19.3	22	2.7	
$CF_2^+ + 2F$	20.9		1.1	
$CF^+ + F + F_2$	22.1	27	4.9	
$CF^+ + 3F$	23.7		3.3	
$C^+ + 2F_2$	28.2	34.5	5.8	
$C^+ + F_2 + 2F$	29.8		4.7	
$C^+ + 4F$	31.4		3.1	
$F^+ + CF_3$	27.9	34.5	6.6	
$F^+ + CF_2 + F$	27.0		7.5	
$F^+ + CF + F_2$	30.3		4.2	
$F^+ + CF + 2F$	31.9		2.6	
$F^+ + C + F + F_2$	36.0		−1.5	
$F^+ + C + 3F$	37.6		−3.1	
$F_2^+ + CF_2$	23.6	35	11.4	
$F_2^+ + CF + F$	28.6		6.4	
$F_2^+ + CF_2$	32.6		2.4	
$F_3^+ + C + 2F$	34.2		0.8	
B. Doubly ionized fragments				
$CF_3^{++} + F_2$		41		
$CF_2^{++} + F_2$		42		
$CF_2^{++} + 2F$				
$CF^{++} + F + F_2$		52[e]		
$CF^{++} + 3F$				
C. Positive ion pair formation				
$CF_3^+ + F^+$	32.4	36[f]	3.6	3.9–5.0[g]
$CF_2^+ + F^+ + F$	38.1	40[f]	1.9	3–4.7[g]
$CF^+ + F^+ + F_2$	39.3	42[f]	2.7	3.6[g]
$CF^+ + F^+ + 2F$	40.9		1.1	
$C^+ + F^+ + F + F_2$	47.2	63[f]	15.8	15[g]
$C^+ + F^+ + 3F$	48.8		14.2	

[a]Average of a number of values in Refs. 43, 98, and 99 (see Ref. 69).
[b]Ref. 70.
[c]From Table 2.
[d]Ref. 98.
[e]CF^{++} has been reported in Ref. 43 to have an energy threshold of 52.1±0.5 eV.
[f]Ref. 100.
[g]Ref. 101.

be divided into three sets. The first set of measurements of absolute partial and total electron impact ionization cross sections from threshold to 180 eV was made by Stephan, Deutsch, and Märk[43] of the research group at the University of Innsbruck. These measurements have subsequently been shown[103] to be in error due to strong discrimination in the ion extraction characteristics of their equipment. The errors resulted in smaller cross section values and have been corrected by Poll *et al.*[103] The original measurements of Stephan, Deutsch, and Märk,[43] and the corrected measurements as reported by Poll *et al.*[103] are shown in Fig. 17.

The second set of measurements was by Ma, Bruce, and Bonham[98] of the research group at Indiana University. Ma, Bruce, and Bonham[98] measured the partial electron impact ionization cross section for CF_4 from threshold to 500 eV using a pulsed electron beam and a time-of-flight apparatus. They obtained the absolute value of the total ionization cross section by charge-weighted summing of all of the observed partial ionization cross sections. The uncertainty of their partial cross sections was estimated to be about 15%. These cross sections are also plotted in Fig. 17. A subsequent paper by Bruce, Ma, and Bonham[100] reported values for the "gross" ionization cross section [which is identical to what

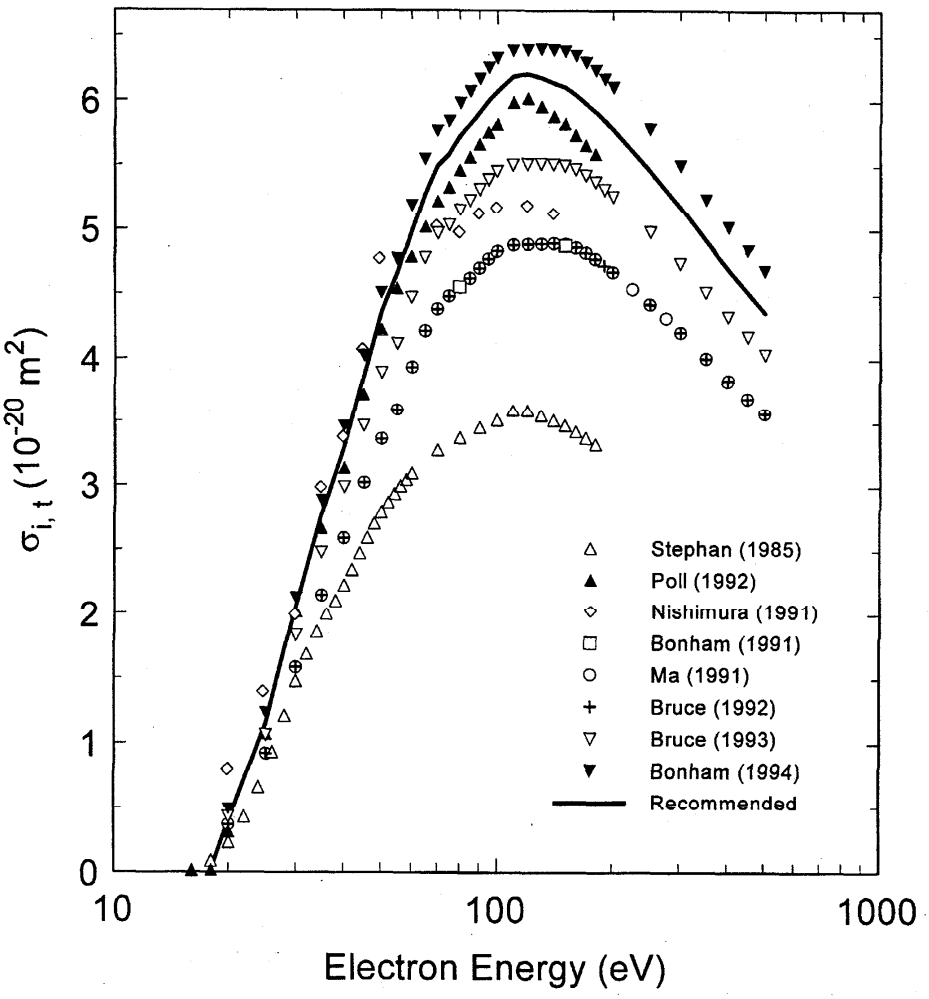

FIG. 17. Total ionization cross section $\sigma_{i,t}(\epsilon)$ as a function of electron energy for CF_4. Measured values: △, Ref. 43; ▲, Ref. 103; □, Ref. 69; ○, Ref. 98; +, Ref. 100; ▽, Ref. 104; ▼, data of Ref. 104 multiplied by 1.16 (per Bonham in Ref. 73); ◇, Ref. 106. Recommended: —, average of ▲ and ▼ (see Sec. 4.1 and Table 12).

we call here the total ionization cross section $\sigma_{i,t}(\epsilon)$], defined as

$$\sigma_{i,\,gross}(\epsilon)=\sum_{i}^{all}\left[q_i\sigma_{i,\,partial}(\epsilon)+2\sigma_{coinc,\,t}(\epsilon)\right], \quad (3)$$

where

$$\sigma_{coinc,\,t}(\epsilon)=\sum_{n=0}^{3}\left[\sigma_{CF_n^+ + F^+}(\epsilon)\right]. \quad (4)$$

The $\sigma_{CF_n^+ + F^+}(\epsilon)$ are the cross sections for the positive ion pair formation $CF_n^+ + F^+$ (for $n = 0$ to 3). The $\sigma_{i,\,partial}(\epsilon)$ of Bruce, Ma, and Bonham[100] differ from those, $\sigma'_{i,\,partial}(\epsilon)$, of Ma, Bruce, and Bonham[98] by the fact that the contribution of positive ion pair formation (see Sec. 4.3) was not considered by Ma and others. However, the total ionization cross section is not affected by positive ion pair formation and would be the same in the two measurements as can be seen by the overlapping symbols in Fig. 17. Subsequently, the data of Ma and others underwent a number of further corrections as follows. First, Bruce and Bonham[104] corrected the earlier data[98] upward by 5% to 15% to account for detection efficiency errors connected with insufficient ion impact energy on the front surface of the detector used in their equipment in the earlier measurements. The sum of the cross sections given in Table 1 of Ref. 104 can be used to determine the total ionization cross section. Second, Bonham[73,105] reported that the data of Bruce and Bonham[104] have to be revised upward by 16% due to an instrumental detection efficiency correction.[105] We introduced such a correction to the Bruce and Bonham data.[104] All of these data, and the values of $\sigma_{i,t}(\epsilon)$ for two incident electron energies obtained from Bonham and Bruce,[69] are shown in Fig. 17.

TABLE 12. Recommended total ionization cross section, $\sigma_{i,t}(\epsilon)$.

Electron energy (eV)	$\sigma_{i,t}(\epsilon)(10^{-20}$ m$^2)$
16	0.02
18	0.02
20	0.40
25	1.15
30	2.07
35	2.78
40	3.30
45	3.88
50	4.37
55	4.66
60	4.99
65	5.29
70	5.50
75	5.59
80	5.73
85	5.82
90	5.92
95	6.01
100	6.08
110	6.19
120	6.21
130	6.18
140	6.14
150	6.10
160	6.04
170	5.98
180	5.91
190	5.85
200	5.78
250	5.46
300	5.18
350	4.92
400	4.70
450	4.52
500	4.36

The third set of measurements that has not appeared in the archival literature is that of Nishimura.[106] These measurements are also shown in Fig. 17 and are seen to fall below the final set of values from the other two groups (shown in solid triangles). Interestingly, unpublished results by Rao and Srivastava[107] also indicate lower values; for example, at 100 eV, the $\sigma_{i,t}(\epsilon)$ is 5.0×10^{-20} m^2.

The agreement between the corrected[73] cross sections of Ma and others and the corrected[103] cross sections of Stephan and others for the total ionization of CF_4 is within the $\pm15\%$ uncertainty assigned to each set of the experimental data. The average of these two sets of experimental cross sections is shown in Fig. 17 by the solid line and is listed in Table 12 as the recommended set of cross sections for the $\sigma_{i,t}(\epsilon)$ of the CF_4 molecule.

The recommended cross section $\sigma_{i,t}(\epsilon)$ (Table 12) is now used to assess the results of the various calculations. A comparison between the experimental $\sigma_{i,t}(\epsilon)$ recommended by us and the results of calculations is shown in Fig. 18. Margreiter *et al.*[108] calculated the dissociative ionization cross section for singly charged species from CF_4 from threshold up to 200 eV using a semiclassical formula which is a combination of the classical binary encounter approximation, the Born–Bethe approximation, and the additivity rule. According to Margreiter and others, this calculation has the advantage that the ionization cross section can be described by a simple analytical formula which gives results in better agreement with the experimental data than the classical binary encounter approximation (i.e., the "Gryzinski formula"[109]). The results of the calculations by Margreiter *et al.*[108] are (Fig. 18) about 30% lower than the recommended values. In better agreement with the recommended cross sections are the results of the semiclassical calculation of Poll *et al.*[103] and the unpublished results of Kim[110] who used a model that combines binary encounter theory and the Bethe theory of electron impact ionization. The results obtained[108] by the "Gryzinski formula" are much higher (the peak cross section maximum is about 10×10^{-20} m^2) and are in poor agreement with the measured values.

Another source of total ionization cross sections is the "swarm-based" computations.[24,25] In these analyses, however, the ionization cross sections come from other sources, but they might be adjusted to yield electron transport, ionization, and attachment coefficients consistent with the experiment. The total ionization cross sections from analysis of swarm data reported by Hayashi[24] and by Nakamura[25] shown in Fig. 18 do not agree well with the experimental values. It is worth noting that Hayashi started with the cross section of Leiter *et al.*,[111] which is presumably the data of Stephan, Deutsch, and Märk,[43] that were found later to be in error. It is interesting to observe that Hayashi found it necessary to multiply the cross section of Leiter *et al.* by 1.1 in order to fit the experimental data on the density-normalized ionization coefficient as a function of E/N, $\alpha/N(E/N)$. No information has been given by Nakamura[25] about the source of the ionization cross section used as input in his analysis, but the results of his calculation are also in poor agreement with the recommended "experimental" cross section. In short, present theoretical calculations do not agree with each other and cannot provide a satisfactory $\sigma_{i,t}(\epsilon)$ for the CF_4 molecule.

4.2 Partial Dissociative Ionization Cross Section, $\sigma_{i,\,partial}(\epsilon)$

There are sets of measurements of partial dissociative ionization cross sections by electron impact from both the University of Innsbruck and the Indiana University groups for the following fragment ions: CF_3^+, CF_2^+, CF^+, C^+, and F^+. The first set was that of Ma, Bruce, and Bonham[98] who quoted an uncertainty of $\pm15\%$ in their measurements, and the second was that of Stephan, Deutsch, and Märk,[43] who quoted an estimated uncertainty of about $\pm10\%$. Both sets of data have subsequently been revised and are discussed below.

The original data of Ma, Bruce, and Bonham[98] [$\sigma'_{i,\,partial}(\epsilon)$, plotted as open circles in Fig. 19] have been revised [converted to $\sigma_{i,\,partial}(\epsilon)$] by Bruce, Ma, and Bonham[100] to consider the effect of positive ion pair forma-

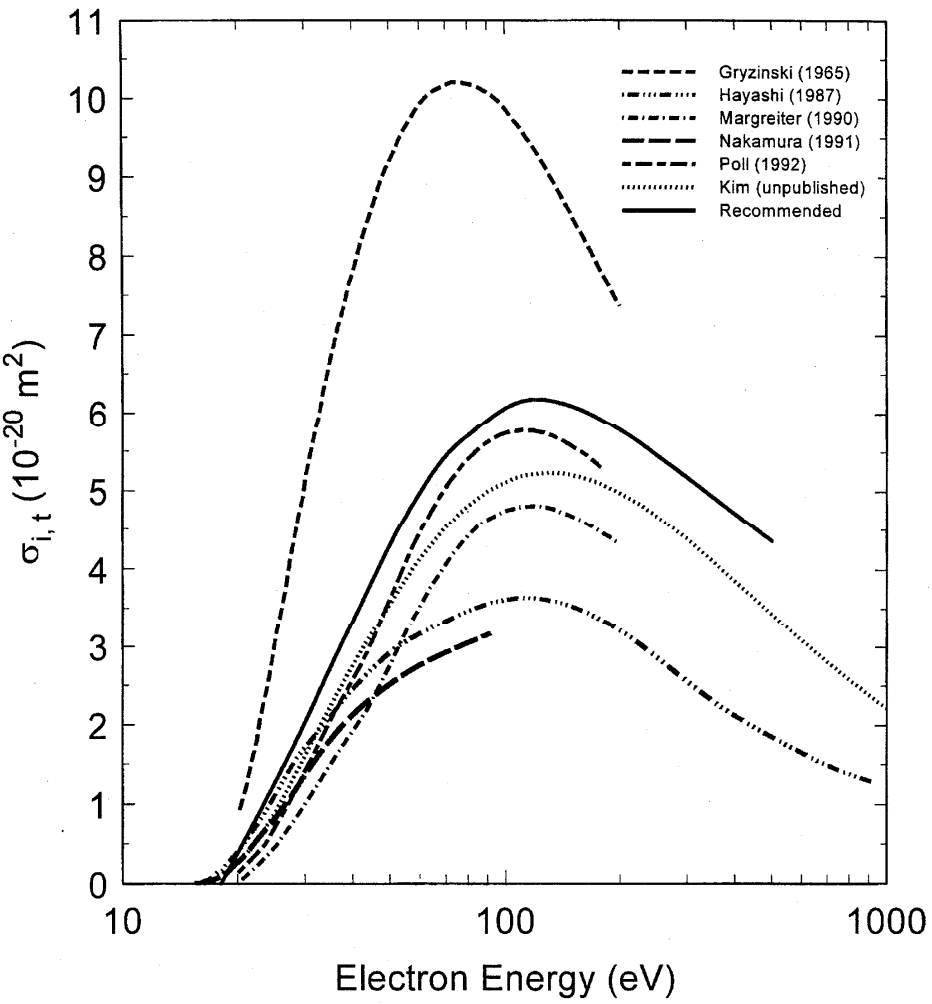

FIG. 18. Comparison of the recommended $\sigma_{i,t}(\epsilon)$ with the results of various calculations. Recommended: —, from Fig. 17, Table 12. Calculated: -----, Ref. 109; – – –, Ref. 103; - · -, Ref. 108; - · · · -, Ref. 24; – –, Ref. 25; . . . . ., Ref. 110.

tion on these cross sections. The revised data were further revised upward by Bruce and Bonham[104] to correct for detection errors due mainly to the effect of too low ion impact energy on the front surface of their detector in the earlier measurements as follows: 16% for CF_3^+, 13% for CF_2^+, 9% for CF^+, 5% for C^+, and 5% for F^+. Finally, another correction was made yet again by Bonham,[73,105] increasing their cross section values upward by 16% to account "for changes in instrumental detection efficiency." All of these cross sections are plotted in Fig. 19 and the final set is also listed in Table 13.

Similarly, we show in Fig. 19 the cross sections, $\sigma'_{i,\,partial}(\epsilon)$, of Stephan *et al.*[43] as corrected by Poll *et al.*[103] These cross sections were not corrected for positive ion pair formation. We, therefore, have made such a correction as follows: we subtracted from the Poll *et al.* cross sections the corresponding positive ion pair cross sections of Bruce, Ma, and Bonham[100] which we adjusted upward by 16% as suggested by Bonham.[73] The resultant cross sections are plotted in Fig. 19 and are listed in Table 14; they represent the final set of $\sigma_{i,\,partial}(\epsilon)$ from the University of Innsbruck group.

The cross section sets in Tables 13 and 14 represent the final corrected data from each of the two Laboratories, and they fall within the quoted combined error of the experiments. These sets have been averaged, and the values are given in Table 15; they are our recommended set of partial ionization cross sections for the CF_4 molecule producing single positive ions.

4.3 Positive Ion Pair Formation Cross Section, $\sigma_{i,\,pair}(\epsilon)$

As we have discussed in the preceding section, Bruce, Ma, and Bonham[100] corrected their previous data on the partial ionization cross sections by taking into account the contributions to the reported cross section coming from the produc-

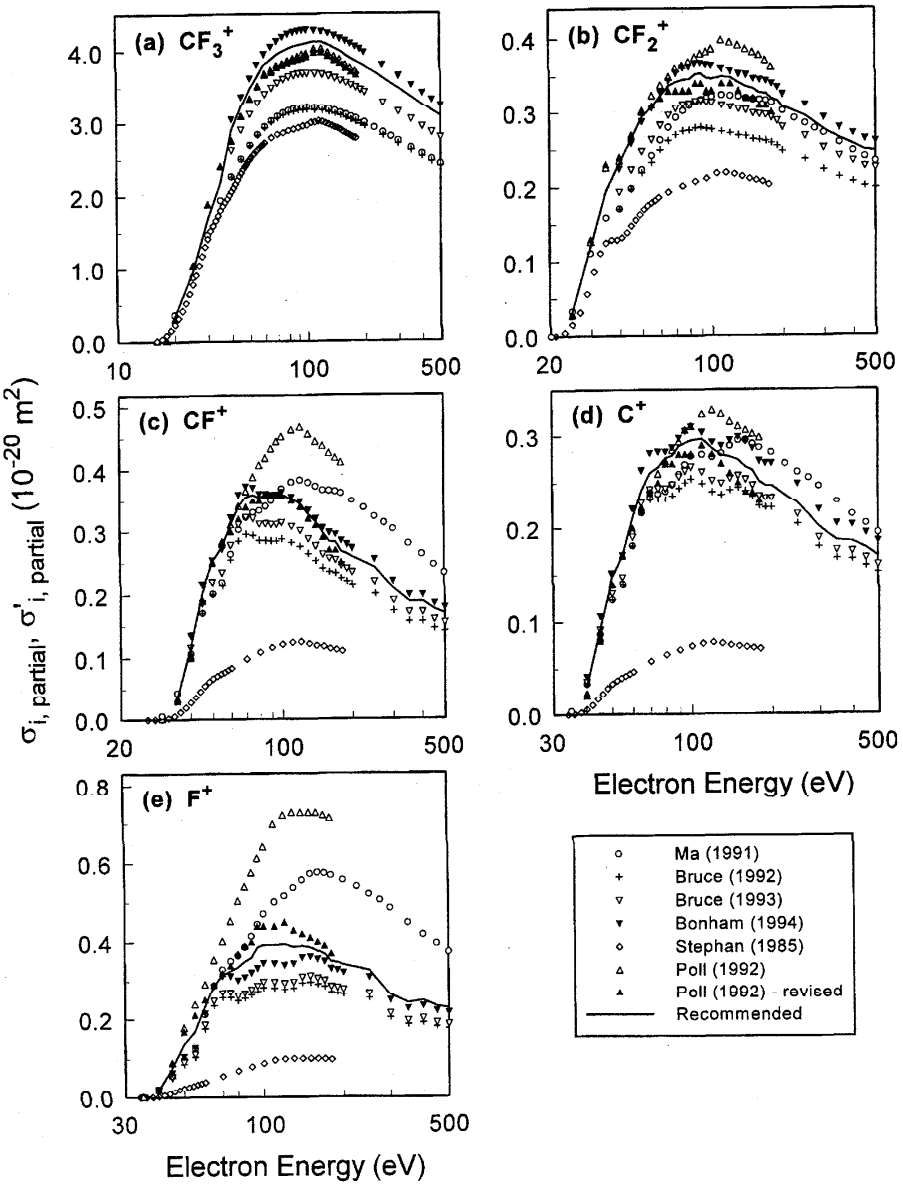

FIG. 19. Partial ionization cross section for the production of (a) CF_3^+, (b) CF_2^+, (c) CF^+, (d) C^+, and (e) F^+ by electron collision on CF_4. $\sigma'_{i,\,partial}(\epsilon)$: ◇, Ref. 43; △, Ref. 103; ○, Ref. 98. $\sigma_{i,\,partial}(\epsilon)$: +, Ref. 100; ▽, Ref. 104; ▼, Ref. 73; ▲, revised data of Ref. 103 (see text). —, average of ▼ and ▲ (see Sec. 1.2 and Table 15).

tion of two-fragment positive ions in a single electron CF_4 collision. Bruce and others used a coincidence technique that enabled simultaneous detection of two positive ions. They measured cross sections for the production of the positive pair fragment cations $C^+ + F^+$, $CF^+ + F^+$, $CF_2^+ + F^+$, and $CF_3^+ + F^+$ from threshold to 500 eV with a reported uncertainty of ±20%. These cross sections are comparable to or larger than the double-ionization cross sections (see Bruce, Ma, and Bonham[100] and Sec. 4.4), with the $CF^+ + F^+$ production having the largest cross section.

According to Bonham,[73] the data of Bruce, Ma, and Bonham[100] have to be adjusted upward by 16% to account for a change in instrumental efficiency[105] from 0.36 to 0.31. Presumably this correction is independent of the electron energy and ionic mass. We thus raised the positive ion pair formation cross section data of Bruce, Ma, and Bonham[100] by 16% and the resultant cross sections are plotted in Fig. 20 and listed in Table 16. For comparison, we have plotted in Fig. 20 for the $CF^+ + F^+$ positive ion pair formation process both the original (solid line) and the revised (solid line with

TABLE 13. Partial ionization cross sections, $\sigma_{i,\,partial}(\epsilon)$ for the production of ion (CF_3^+, CF_2^+, CF^+, C^+, and F^+) plus neutral (n) species by electron impact on CF_4 in units of 10^{-20} m^2 [data of Ma *et al.* (Ref. 98) after a series of corrections (see the text and Ref. 73)].

Energy (eV)	CF_3^++n	CF_2^++n	CF^++n	C^++n	F^++n
20	0.49				
25	1.19	0.04			
30	1.97	0.15	0.01		
35	2.61	0.21	0.06	0.04	
40	3.04	0.22	0.14	0.04	0.02
45	3.37	0.26	0.22	0.11	0.06
50	3.62	0.29	0.25	0.15	0.11
55	3.81	0.31	0.27	0.17	0.13
60	3.95	0.33	0.32	0.22	0.21
65	4.05	0.34	0.36	0.26	0.29
70	4.13	0.35	0.37	0.28	0.31
75	4.18	0.36	0.37	0.28	0.31
80	4.22	0.36	0.36	0.28	0.30
85	4.25	0.37	0.36	0.29	0.31
90	4.27	0.37	0.36	0.30	0.32
95	4.28	0.36	0.36	0.30	0.33
100	4.28	0.36	0.36	0.31	0.34
110	4.28	0.36	0.36	0.30	0.34
120	4.26	0.36	0.35	0.29	0.34
130	4.23	0.35	0.33	0.29	0.34
140	4.20	0.35	0.32	0.29	0.36
150	4.16	0.35	0.30	0.30	0.36
160	4.13	0.34	0.30	0.29	0.36
170	4.09	0.34	0.29	0.29	0.35
180	4.05	0.34	0.28	0.27	0.33
190	4.01	0.33	0.28	0.27	0.33
200	3.97	0.33	0.27	0.27	0.32
250	3.80	0.31	0.25	0.25	0.31
300	3.65	0.29	0.22	0.22	0.25
350	3.52	0.28	0.20	0.20	0.23
400	3.41	0.27	0.20	0.20	0.23
450	3.31	0.26	0.18	0.19	0.22
500	3.23	0.26	0.18	0.19	0.21

triangles) cross sections. The original data for the other double fragment cation processes were not plotted for the convenience of display.

4.4 Total Counting Ionization Cross Section, $\sigma_{i,\,t,\,count}(\epsilon)$

The total counting ionization cross section for CF_4 has been defined[98] as

$$\sigma_{i,\,t,\,count}(\epsilon)=\sum_{i}^{all}\sigma_{i,\,partial}(\epsilon). \tag{5}$$

In Eq. (5), $\sigma_{i,\,partial}(\epsilon)$ are the partial cross sections for single ionization and single ion formation. Ma, Bruce, and Bonham[98] reported $\sigma_{i,\,t,\,count}(\epsilon)$, however, which were not corrected for positive ion pair formation. Unlike the total ionization cross section, the counting cross section is affected by the positive ion pair formation process. As discussed in Sec. 4.3, Bruce, Ma, and Bonham[100] measured positive ion pair formation cross sections by a coincidence method and were able to correct the partial ionization cross sections of CF_4 for this process. Consequently, they were able to determine "true" counting cross sections for ionization using the expression

$$\sigma_{i,\,t,\,count}(\epsilon)=\sum_{i}^{all}[\sigma_{i,\,partial}(\epsilon)+\sigma_{coinc,\,t}(\epsilon)], \tag{6}$$

where $\sigma_{coinc,\,t}(\epsilon)=\Sigma_{n=0}^{3}[\sigma_{CFn^+ + F^+}(\epsilon)]$.

We have determined the $\sigma_{i,\,t,\,count}(\epsilon)$ shown in Fig. 21 and listed in Table 17 by using the partial cross sections in Table 13 and the positive ion pair formation cross sections in Table 16. The present values, which take into account all of the recent corrections due to detection efficiency, are compared in Fig. 21 with those reported by Bruce, Ma, and Bonham.[100]

4.5 Multiple Ionization Cross Section, $\sigma_{i,\,mult}(\epsilon)$

Multiple ionization cross sections have been measured[43,69,73,77,98,100,103,104,107] for only CF_3^{++} and CF_2^{++} from CF_4. No multiply charged parent ions of CF_4 have been reported. In Table 18 are listed the data of Refs. 103 and 98 (see also Refs. 73, 103, and 104) on $\sigma_{i,\,mult}(\epsilon)$ for the production of CF_3^{++} and CF_2^{++}. These two sets of data for each of these ions are plotted, respectively, in Figs. 22a and 22b. Ma, Bruce, and Bonham[98] quoted an uncertainty of $\pm 15\%$ in their values and Stephan, Deutsch, and Märk[43] of $\pm 10\%$. No correction is needed for the positive ion pair formation processes. In Table 11 are listed the threshold energies for CF_3^{++} and CF_2^{++} production; Stephan, Deutsch, and Märk[43] reported the threshold energy for another doubly charged ion, CF^{++}, to be 52.1 ± 0.5 eV. The cross sections of these two groups differ by more than the combined quoted experimental error. No explanation of this discrepancy has been advanced in the literature, but differences in the flight times of the ions in the various instruments employed may affect their respective detection efficiencies for the multiply charged ions. It is worth noting, however, that the unpublished results of Rao and Srivastava[107] are in better agreement with the measurements of Ma and others than with the measurements of Stephan and others. For instance, at 100 eV Rao and Srivastava's measured cross sections for CF_3^{++} and CF_2^{++} are, respectively, 0.024×10^{-20} m^2 and 0.075×10^{-20} m^2. Because of the significant unexplained differences in the measured cross sections, no recommended data set can be proposed.

As expected, the multiple ionization cross sections are much smaller and the energy thresholds for them are much higher than those for single ionization. The cross sections for multiple ionization are, however, comparable to those for positive pair ion fragment formation.

4.6 Dissociative Ionization Cross Section, $\sigma_{i,\,diss}(\epsilon)$

Since no parent CF_4^+ ion has been observed, the total ionization cross section $\sigma_{i,\,t}(\epsilon)$ for CF_4 is equal to the total dissociative ionization cross section $\sigma_{i,\,diss}(\epsilon)$ (see Fig. 30 later in Sec. 5.3).

TABLE 14. Partial ionization cross sections, $\sigma_{i,\,partial}(\epsilon)$, in units of 10^{-20} m^2, for the production of CF_3^+, CF_2^+, CF^+, C^+, and F^+ by electron impact on CF_4 [data of Poll *et al.* (Ref. 103) corrected by subtracting the corresponding double positive ion formation cross sections of Bruce, Ma, and Bonham (Ref. 100), themselves adjusted upwards by 1.16 (see Ref. 73 and the text)].

Energy (eV)	CF_3^+	CF_2^+	CF^+	C^+	F^+
16	0.02				
18	0.02				
20	0.31				
25	1.04	0.03			
30	1.89	0.13			
35	2.41	0.23	0.03		
40	2.76	0.24	0.10	0.02	0.02
45	3.09	0.27	0.19	0.08	0.09
50	3.34	0.30	0.25	0.14	0.17
55	3.51	0.31	0.28	0.17	0.21
60	3.67	0.32	0.30	0.20	0.25
65	3.71	0.33	0.32	0.22	0.29
70	3.77	0.33	0.34	0.24	0.32
75	3.80	0.33	0.35	0.25	0.34
80	3.83	0.33	0.35	0.27	0.37
85	3.86	0.34	0.36	0.27	0.39
90	3.88	0.34	0.36	0.28	0.40
95	3.90	0.33	0.36	0.28	0.44
100	3.92	0.33	0.36	0.28	0.44
110	3.98	0.34	0.35	0.29	0.44
120	3.98	0.34	0.34	0.28	0.45
130	3.93	0.33	0.32	0.27	0.43
140	3.87	0.32	0.31	0.26	0.42
150	3.83	0.32	0.29	0.25	0.41
160	3.76	0.31	0.27	0.24	0.40
170	3.71	0.31	0.27	0.24	0.39
180	3.67	0.30	0.25	0.23	0.37

4.7 Ionization Coefficients

4.7.1 Density Reduced Ionization Coefficient, α/N

The density reduced ionization coefficient α/N is measured as a function of E/N. It is related to the normalized electron energy distribution function $f(\epsilon,E/N)$ and the total ionization cross section $\sigma_{i,\,t}(\epsilon)$ by

$$\alpha/N(E/N)=(2/m)^{1/2}w^{-1}\int_I^\infty f(\epsilon,E/N)\epsilon^{1/2}\sigma_{i,\,t}(\epsilon)d\epsilon,$$

where I is the ionization threshold energy of the CF_4 molecule and m is the electron mass. There have been a number of room temperature measurements of α/N for CF_4. Those prior to 1975 have been summarized and discussed by Gallagher *et al.*[112] Recently there have been two measurements, one by Shimozuma, Tagashira, and Hasegawa[113] using a steady-state Townsend technique and another by Hunter, Carter, and Christophorou[114] using a pulsed Townsend technique. The results of these recent studies have been compared by Hunter and others with the earlier measurements[89,90,115–117] (see also Ref. 112) and are reproduced in Fig. 23. The data of Hunter, Carter, and Christophorou[114] were corrected for diffusion and are believed to be the most accurate. They are tabulated in Table 19 along with the uncertainties reported by the authors.

4.7.2 Effective Ionization Coefficient, $\bar{\alpha}/N=(\alpha-\eta)/N$

The effective ionization coefficient gives the difference between the density reduced ionization coefficient α/N and the density reduced electron attachment coefficient η/N (see Sec. 6.3.1). The recent measurements of Hunter, Carter, and Christophorou[114] and Datskos, Carter, and Christophorou[118] on the effective ionization coefficient for pure CF_4 as a function of E/N are presented in Fig. 24. There is general agreement between these and earlier measurements.[89,113] The fit to all the data in Fig. 24 is represented in the figure by the solid line, and is also listed in Table 20 as our recommended set of values for the effective ionization coefficient of CF_4. All data were equally weighted in the fitting process.

Measurements of the effective ionization coefficient for mixtures of CF_4 with Ar, CO_2, H_2O, and CH_4 are covered in Refs. 118 and 119.

4.7.3 Average Energy to Produce an Electron–Ion Pair, W

The average energy to produce an electron–ion pair, W, for α particles (initial energy ~5.1 MeV) has been measured for pure CF_4 and found to be 34.3 eV per ion pair.[120] The large value of this quantity for CF_4 is consistent with the high ionization onset and the large cross section for electron impact dissociation of CF_4 into neutral species (see Sec. 5).

W values for CF_4/Ar and CF_4/CH_4 mixtures for α particles have also been reported.[120]

5. Electron-Impact Dissociation Producing Neutral Species

5.1 Total Dissociation Cross Section for Neutral Species, $\sigma_{diss,\,neut,\,t}(\epsilon)$

Direct measurement of the total cross section for processes producing only neutral fragments by electron impact with CF_4 is difficult because of the problems connected with detection of low-energy neutrals. One such study by Nakano and Sugai[70] accomplished direct measurement of the electron energy dependence of the *partial* cross sections for dissociation of CF_4 into neutral CF_3, CF_2, and CF radicals, by using threshold-ionization mass spectrometry in a dual-electron beam system. Their original measurements[70] have subsequently been revised by Sugai *et al.*[121] (their data have been renormalized using the absolute cross sections for parent and dissociative ionization of CF_x radicals of Becker and co-workers[122,123]). The revised data differ substantially from the initially reported values. In the energy range 100–130 eV, the revised cross sections are lower than their initially reported values by factors of ~4, ~13, and ~16 for CF_3, CF_2, and CF, respectively. The revised data[121] are shown in Fig. 25 and are listed in Table 21.

The total neutral dissociation cross sections for CF_4 were calculated by summing the partial cross sections obtained by direct measurement.[70,121] These values represent an estimate of the total cross section for electron impact dissociation of CF_4 into the neutral fragments CF_3, CF_2, and CF, and are presented in Fig. 26 for both the original[70] (open circles) and

TABLE 15. Partial ionization cross sections, $\sigma_{i,\,partial}(\epsilon)$, in units of 10^{-20} m^2, for the production of CF_3^+, CF_2^+, CF^+, C^+, and F^+ by electron impact on CF_4: average of values listed in Tables 13 and 14. (See the text.)

Energy (eV)	CF_3^+	CF_2^+	CF^+	C^+	F^+
16	0.02				
18	0.02				
20	0.31				
25	1.04	0.03			
30	1.89	0.13			
35	2.41	0.23	0.03		
40	2.90	0.23	0.12	0.03	0.02
45	3.23	0.27	0.21	0.10	0.08
50	3.48	0.30	0.25	0.15	0.14
55	2.66	0.31	0.28	0.17	0.17
60	3.81	0.33	0.31	0.21	0.23
65	3.88	0.34	0.34	0.24	0.29
70	2.95	0.34	0.36	0.26	0.32
75	3.99	0.35	0.36	0.27	0.33
80	4.03	0.35	0.36	0.28	0.34
85	4.06	0.36	0.36	0.28	0.35
90	4.08	0.36	0.36	0.29	0.36
95	4.09	0.35	0.36	0.29	0.39
100	4.10	0.35	0.36	0.30	0.39
110	4.13	0.35	0.36	0.30	0.39
120	4.12	0.35	0.35	0.29	0.39
130	4.08	0.34	0.33	0.28	0.39
140	4.04	0.34	0.32	0.28	0.39
150	4.00	0.34	0.30	0.28	0.39
160	3.95	0.33	0.29	0.27	0.38
170	3.90	0.33	0.28	0.27	0.38
180	3.86	0.32	0.27	0.25	0.35
190	3.83	0.32	0.26	0.25	0.35
200	3.79	0.31	0.26	0.25	0.34
250	3.62	0.30	0.24	0.23	0.33
300	3.48	0.28	0.21	0.20	0.26
350	3.36	0.27	0.19	0.19	0.24
400	3.25	0.26	0.19	0.19	0.25
450	3.16	0.25	0.18	0.18	0.23
500	3.08	0.25	0.17	0.17	0.23

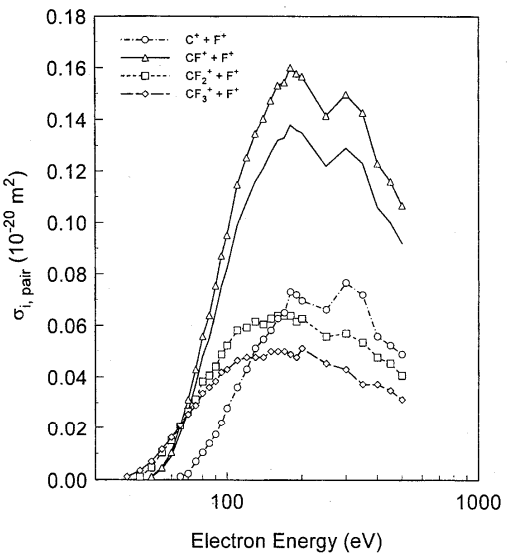

FIG. 20. Positive ion pair formation cross sections as a function of electron energy for CF_4 [data of Bruce *et al.* (Ref. 100) multiplied by 1.16 as suggested by Bonham (Ref. 73)]. ◇, $CF_3^+ + F^+$; □, $CF_2^+ + F^+$; △, $CF^+ + F^+$; ○, $C^+ + F^+$; —, original data (Ref. 100) for $CF^+ + F^+$ shown for comparison.

revised[121] (closed circles) data sets. These are compared in Fig. 26 with other total neutral dissociation cross sections obtained by indirect measurements[73,98,100] and by swarm-based calculations.[24,25] It is obvious that little agreement exists among these data.

The first indirect determination of the total dissociation cross section into neutral-neutral fragment pairs (regardless of the nature of the internal degree of excitation of the fragments) was obtained by Ma, Bruce, and Bonham[98] (open triangles) who subtracted their total ionization cross section from the total dissociation cross section of Winters and Inokuti.[42] Since in the determination of the total neutral dissociation cross section Ma and others ought to have used the total counting cross section (see Sec. 4.4) rather than the total ionization cross section, these values were revised by Bruce, Ma, and Bonham[100] to correct for double positive ion production (× symbols). However, the ionization cross sections used to derive both of these cross section sets have been subsequently revised[73,104] upward so these values for $\sigma_{diss,\,neut,\,t}(\epsilon)$ are no longer valid. In fact, the magnitude of the total counting cross section[73] now approaches (or exceeds) the magnitude of the total dissociation cross section,[42] so that the error in the difference of the two cross sections is too large for this method to be used to determine $\sigma_{diss,\,neut,\,t}(\epsilon)$ for electron energies above 30 eV. Below 30 eV, an estimate can be made for $\sigma_{diss,\,neut,\,t}(\epsilon)$ using this method, since the magnitude of the measured total dissociation cross section[42] is significantly greater than the total ionization cross section in this energy range. Bonham[73] performed this calculation, and the results are presented (solid inverted triangles) in Fig. 26. Interestingly, these data are very much greater than those measured by Sugai *et al.*[121] This discrepancy will be discussed in more detail in Sec. 5.3, but clearly more work is needed to determine these cross sections within reasonable error limits. The values for $\sigma_{diss,\,neut,\,t}(\epsilon)$ as determined by both Sugai *et al.*[121] and Bonham[73] (below 30 eV) are presented in Table 22. The most recent data of Sugai *et al.*[121] are reported as our "recommended" values in Sec. 9 since they represent the only available experimental measurements. However, they are inconsistent with the currently accepted values of $\sigma_{i,\,t}(\epsilon)$ and $\sigma_{diss,\,t}(\epsilon)$ cross sections (see Sec. 5.3).

A cross section set for $\sigma_{diss,\,neut,\,t}(\epsilon)$ derived[73] from the original data of Nakano and Sugai[70] is also shown in Fig. 26 (open inverted triangles), but this cross section set is no longer valid since the original data of Sugai and co-workers has been superceeded by their more recent analysis.[121] Also shown in Fig. 26 are the swarm-based $\sigma_{diss,\,neut,\,t}(\epsilon)$ cross sections derived by Hayashi[24] and Nakamura,[25] which significantly exceed all of the experimentally derived values.

Finally, Bruce, Ma, and Bonham[100] were able to determine

TABLE 16. Positive ion pair formation cross sections, $\sigma_{i\ pair}(\epsilon)$, in units of 10^{-20} m^2, for electron inpact dissociative ionization of CF_4 [data of Bruce, Ma, and Bonham (Ref. 100) multiplied by 1.16 as suggested in Ref. 73].

	$\sigma_{i,pair}(\epsilon)$			
Energy (eV)	$C^+ + F^+$	$CF^+ + F^+$	$CF_2^+ + F^+$	$CF_3^+ + F^+$
40				0.001
45			0.001	0.004
50		0.001	0.005	0.007
55		0.005	0.010	0.012
60		0.010	0.015	0.016
65	0.001	0.021	0.021	0.021
70	0.002	0.031	0.027	0.026
75	0.007	0.043	0.031	0.029
80	0.010	0.056	0.038	0.034
85	0.014	0.064	0.041	0.036
90	0.017	0.075	0.044	0.038
95	0.022	0.087	0.049	0.042
100	0.028	0.095	0.052	0.043
110	0.036	0.115	0.058	0.046
120	0.043	0.125	0.059	0.048
130	0.051	0.135	0.061	0.048
140	0.055	0.140	0.060	0.048
150	0.058	0.147	0.063	0.050
160	0.063	0.153	0.061	0.050
170	0.065	0.154	0.064	0.050
180	0.073	0.160	0.064	0.049
190	0.072	0.158	0.061	0.048
200	0.070	0.157	0.063	0.051
250	0.066	0.142	0.056	0.045
300	0.075	0.150	0.057	0.043
350	0.072	0.143	0.053	0.037
400	0.056	0.123	0.048	0.037
450	0.052	0.116	0.045	0.035
500	0.049	0.107	0.041	0.031

the total cross section $\sigma_{F,t}(\epsilon)$ for production of neutral fluorine by electron impact on CF_4. This cross section is listed in Table 23 and is plotted in Fig. 27. As noted by Bruce, Ma, and Bonham,[100] the cross section for the production of neutral fluorine is large (even larger than the total ionization cross section) due to the many processes that lead to the production of one or more fluorine atoms. Above ~40 eV most of the neutral fluorine results from ionization processes.

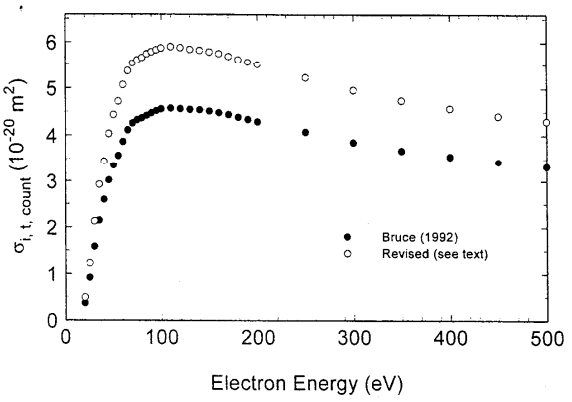

FIG. 21. Total ionization counting cross section $\sigma_{i,\,t,\,count}(\epsilon)$ as a function of electron energy for CF_4. ●, Ref. 100; ○, revised data from Table 17 (see text).

TABLE 17. Total counting ionization cross section, $\sigma_{i,t,count}(\epsilon)$, in units of 10^{-20} m^2, for CF_4 determined by taking the sum of the partial ionization cross sections in Table 13 and the sum of the double positive ion fragment cross sections in Table 16 (see the text).

Energy (eV)	$\sigma_{i,\,t,count}(\epsilon)$
20	0.49
25	1.23
30	2.13
35	2.92
40	3.44
45	4.03
50	4.43
55	4.72
60	5.07
65	5.36
70	5.53
75	5.61
80	5.66
85	5.74
90	5.79
95	5.83
100	5.87
110	5.90
120	5.88
130	5.84
140	5.82
150	5.79
160	5.75
170	5.69
180	5.62
190	5.56
200	5.51
250	5.23
300	4.96
350	4.74
400	4.57
450	4.41
500	4.30

5.2 Dissociative Excitation Cross Section, $\sigma_{diss,\,exc}(\epsilon)$

Recently, Becker[17] has discussed the formation of radiating and energetic metastable fragments following single electron impact on CF_4. A number of different processes contribute to the production of such excited and energetic fragments.[124] The study of Van der Burgt and McConkey[124] indicated the importance of two-fragment dissociation generating simultaneously excited F* and excited CF_3^+* from the process

$$e + CF_4 \rightarrow CF_4^{**} \rightarrow CF_3^{+*} + F^*. \quad (5)$$

Electron impact-induced light emission studies[17,124–126] have shown that by far the most prominent emission produced by electron impact on CF_4 is the intense continuous emission from 200 nm to 500 nm. This emission (Fig. 28) has a maximum at about 285 nm and, with the exception of

TABLE 18. Multiple ionization cross sections, $\sigma_{i,mult}(\epsilon)$, for CF_4 in units of 10^{-20} m^2.

Energy (eV)	CF_3^{++}		CF_2^{++}	
	Ref. 98	Ref. 103	Ref. 98	Ref. 103
45	0.002		0.002	
50	0.004		0.006	0.002
55	0.006	0.002	0.011	0.005
60	0.011	0.003	0.022	0.007
65	0.017	0.004	0.034	0.010
70	0.020	0.005	0.040	0.022
75	0.022	0.006	0.043	0.016
80	0.230	0.007	0.046	0.018
85	0.025	0.007	0.048	0.020
90	0.026	0.008	0.052	0.022
95	0.027	0.009	0.056	0.024
100	0.028	0.009	0.059	0.026
110	0.028	0.010	0.061	0.029
120	0.029	0.011	0.063	0.031
130	0.030	0.011	0.064	0.032
140	0.032	0.012	0.065	0.032
150	0.033	0.012	0.066	0.032
160	0.033	0.012	0.066	0.032
170	0.032	0.012	0.065	0.031
180	0.032	0.012	0.064	0.032
200	0.033		0.062	
225	0.030		0.060	
250	0.030		0.058	
275	0.027		0.055	
300	0.025		0.053	
350	0.022		0.049	
400	0.020		0.045	
450	0.019		0.042	
500	0.018		0.039	

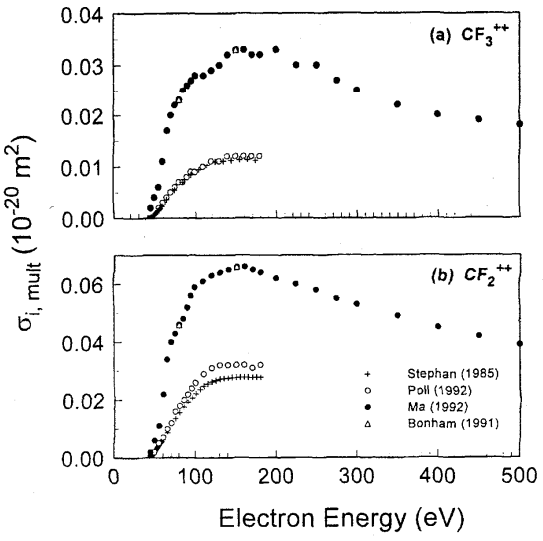

FIG. 22. Multiple ionization cross sections $\sigma_{i,\,mult}(\epsilon)$ as a function of electron energy for CF_4. +, Ref. 43; ○, Ref. 103; ●, Ref. 98; △, Ref. 69.

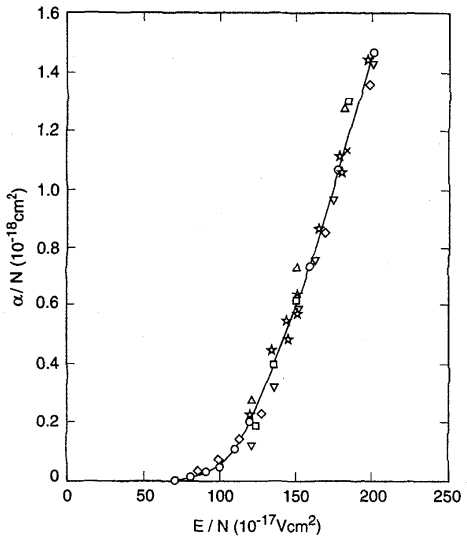

FIG. 23. Density-normalized electron-impact ionization coefficient α/N as a function of E/N for CF_4, as compiled by Hunter *et al.* (Ref. 114), ○, Ref. 114; □, Ref. 113; ◇, Ref. 115; ×, Ref. 90; △, Ref. 89; ▽, Ref. 116; ☆, Ref. 117.

a series of weak discrete emission bands in the 360–420 nm range and a shoulder at 245 nm, is essentially structureless. The source of this emission is still in question,[37,125] although Becker[17] assigned it to the CF_3^{+*} species.

Absolute cross sections for the most intense $3p \rightarrow 3s$ line emissions from atomic fluorine between 620 and 780 nm following electron impact on CF_4 in a crossed electron-gas beam apparatus have been reported by Blanks and others[127,128] and by Van Sprang, Brongersma, and de Heer.[125] These lines are emitted by atomic fluorine formed in the various excited states associated with the $1s^2 2s^2 2p^4 3p$ electronic configuration.[127–129] The measured emissions for the fluorine resonance lines are listed in Table 24. The absolute cross sections[128] are a few times 10^{-19} cm^2 at 100 eV. The energy dependence of the absolute integrated emission cross section of the FI $3p\ ^4D^0 \rightarrow 3s\ ^4P$ multiplet as a func-

TABLE 19. Density reduced electron impact ionization coefficients for CF_4 as a function of E/N [from Hunter, Carter, and Christophorou (Ref. 114)].

E/N (10^{-17} V cm^2)	α/N (10^{-18} cm^2)	Total uncertainty (10^{-18} cm^2)
80	0.11	±0.03
90	0.32	±0.05
100	0.44	±0.05
110	1.10	±0.03
120	2.08	±0.05
140	4.45	±0.05
160	7.37	±0.06
180	10.7	±0.05
200	14.7	±0.08

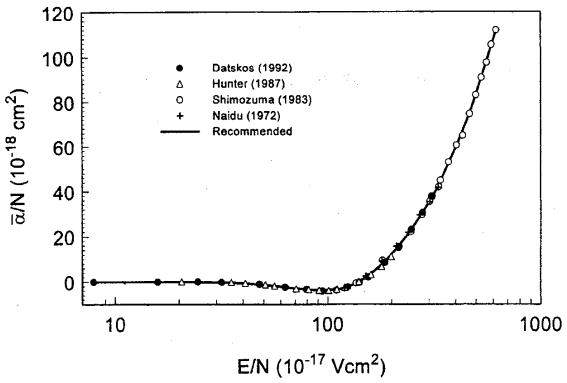

FIG. 24. Effective ionization coefficient $\bar{\alpha}/N=(\alpha-\eta)/N$ as a function of E/N for CF_4. ●, Ref. 118; △, Ref. 114; ○, Ref. 113; +, Ref. 89; —, recommended values (see Sec. 4.7.2 and Table 20).

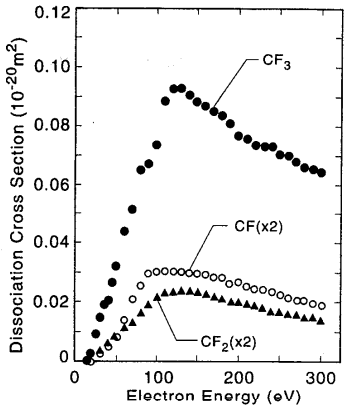

FIG. 25. Cross sections for electron impact dissociation of CF_4 into CF_3 (●); CF_2 (▲); CF (○), data of Nakano and Sugai (Ref. 70) as revised by Sugai *et al.* (Ref. 121).

tion of electron impact energy for CF_4 is shown[128] in Fig. 29. (See also Ref. 130 for emission spectra in the range 50–130 nm via dissociative excitation of CF_4 by electron impact.)

It is worth noting that a number of photoabsorption studies of CF_4 have been made using synchrotron radiation which provided complementary information on the decomposition of CF_4 and the nature of the emitting species. Thus photolytic studies have been made on the decay pathways of the excited electronic states[131] of CF_4, the emission spectra of CF_3 radicals,[132] the fluorescence cross sections, the nature of emitting species, and the possible emitting states.[133] Interestingly, Lee *et al.*[133] measured the photoabsorption and fluorescence cross sections for CF_4 and CF_3X (X=H,Cl,Br) at

TABLE 20. Recommended effective ionization coefficients $\bar{\alpha}/N$ for CF_4 as a function of E/N.

E/N (10^{-21} V m^2)	$\bar{\alpha}/N$ (10^{-18} cm^2)
8	−0.052
9	−0.056
10	−0.058
15	−0.051
20	−0.043
25	−0.143
30	−0.28
35	−0.44
40	−0.73
45	−1.09
50	−1.47
60	−2.24
70	−2.92
80	−3.47
90	−3.73
100	−3.66
110	−3.43
120	−2.68
130	−1.54
140	−0.04
150	1.61
200	12.05
250	23.49
300	35.04
350	47.23
400	59.37
450	71.39
500	83.64
600	107.45

TABLE 21. Cross sections for the production of CF_x ($x=1-3$) fragments by electron impact on CF_4 in units of 10^{-20} m^2 [data of Nakano and Sugai (Ref. 70) as revised by Sugai *et al.* (Ref. 121)].

Energy (eV)	CF_3	CF_2	CF
16	0.001		
18	0.002	0.0002	
30	0.015	0.0017	0.0012
40	0.020	0.0031	0.0025
50	0.032	0.0042	0.0042
60	0.044	0.0057	0.0069
70	0.052	0.0066	0.0105
80	0.065	0.0081	0.0128
90	0.067	0.0095	0.0148
100	0.074	0.0108	0.0152
110	0.089	0.0114	0.0152
120	0.093	0.0118	0.0152
130	0.093	0.0120	0.0152
140	0.091	0.0119	0.0150
150	0.089	0.0116	0.0148
160	0.087	0.0113	0.0147
170	0.085	0.0110	0.0143
180	0.084	0.0106	0.0141
190	0.081	0.0102	0.0132
200	0.077	0.0101	0.0134
210	0.076	0.0097	0.0127
220	0.074	0.0096	0.0123
230	0.073	0.0091	0.0122
240	0.073	0.0086	0.0119
250	0.071	0.0084	0.0114
260	0.070	0.0082	0.0108
270	0.068	0.0080	0.0105
280	0.066	0.0076	0.0105
290	0.066	0.0076	0.0100
300	0.065	0.0072	0.0097

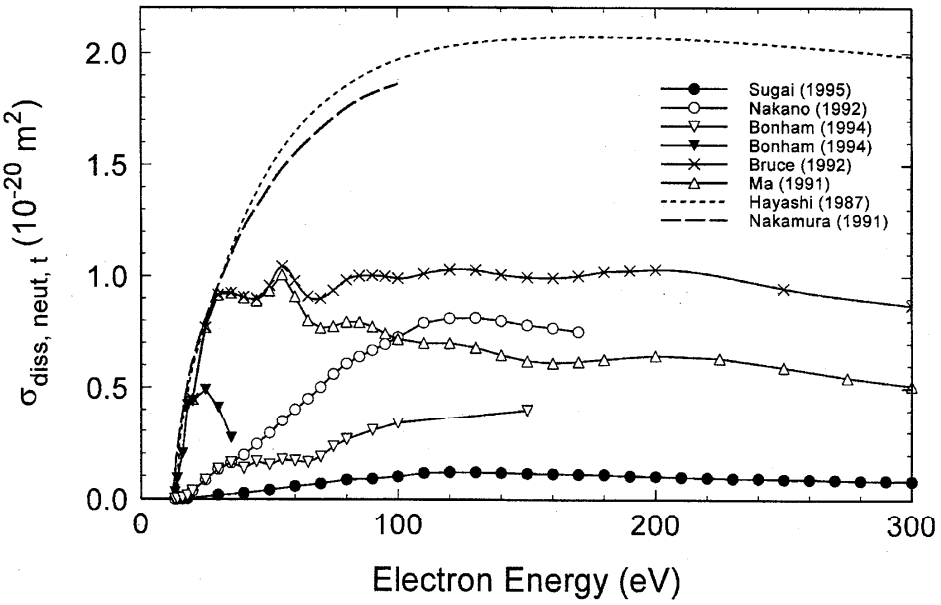

FIG. 26. Total cross section for electron impact dissociation of CF_4 into neutral–neutral pairs (△, Ref. 98; ×, Ref. 100; -----, Ref. 24; – –, Ref. 25; ▼ ef. 73), and into CF_n radicals [○, Ref. 70; ▽, measurements of Nakano and Sugai (Ref. 70) as revised by Bonham (Ref. 73); ●, measurements of Nakano and Sugai (Ref. 70) as revised by Sugai *et al.* (Ref. 121); see text].

50–106 nm using synchrotron light and identified the emitting species to be mainly the excited CF_2^*, CF_3^*, and CF_3X^{+*}, but not CF_3^{+*}. (See also Becker.[134])

Laser-induced fluorescence has been used (e.g., see Ref. 135) effectively to identify radicals and to follow their space and time distribution in high density CF_4 plasmas.

5.3 Comparison of the Total Dissociation Cross Section into Neutral Species with the Total Electron Scattering Cross Section, the Total Dissociation Cross Section, and the Total Ionization Cross Section

Since the dissociation process generating neutral fragments has a threshold of 12.5 eV,[42] which is lower than the ionization potential of CF_4 (16.2 eV, see Table 2), the neutral dissociation process should be dominant at low electron impact energies. Dissociation into neutrals dominates near threshold, while dissociation via dissociative electron attachment occurs below the dissociation threshold, and dissociative ionization (i.e., production of neutral + ion species) progressively takes over as the electron energy is increased above 16.2 eV (see Sec. 4). If indeed all excited electronic states of the CF_4 molecule dissociate or predissociate, then the total electronic excitation cross section should be equal to the total dissociation cross section $\sigma_{diss,t}(\epsilon)$, which itself is equal to the sum of $\sigma_{i,t}(\epsilon)+\sigma_{diss, neut, t}(\epsilon)$. In Fig. 30 are compared the measurements of Winters and others[41,42] on the total dissociation cross section $\sigma_{diss, t}(\epsilon)$ (Table 10), the total ionization cross section $\sigma_{i, t}(\epsilon)$ (Table 12), the total scattering cross section $\sigma_{sc, t}(\epsilon)$ (Table 4), and the Sugai *et al.*[121] total cross section for dissociation into neutrals $\sigma_{diss, neut, t}(\epsilon)$ (Table 22, Column 2). As expected, $\sigma_{diss, neut, t}(\epsilon) < \sigma_{i, t}(\epsilon) \approx \sigma_{diss, t}(\epsilon) < \sigma_{sc, t}(\epsilon)$ for energies greater than ~20 eV. As we have mentioned earlier, at low energies $\sigma_{diss, neut, t}(\epsilon)$ can be estimated by subtracting $\sigma_{i, t}(\epsilon)$ from $\sigma_{diss, t}(\epsilon)$. This determination of $\sigma_{diss, neut, t}(\epsilon)$ is shown by the dotted line in Fig. 30 and is seen to be significantly greater that the values of Sugai *et al.* This represents an important question to be answered, especially since the large difference in the cross sections occurs at electron energies of significance in glow discharges. For further discussion of dissociation processes in CF_4 and their role in plasma etching see Refs. 17, 134, and 136 (see also Bonham[73]).

6. Electron Attachment

In Sec. 2 we summarized and discussed information on the negative ion states of the CF_4 molecule as obtained from electron scattering, electron attachment, and theoretical studies. In this section we assess and discuss (i) electron beam data on cross sections for the production of specific ions by resonance and nonresonance electron attachment to CF_4, and (ii) electron swarm data on the total electron attachment cross section as a function of electron energy, electron attachment rate constants as a function of the density reduced electric field E/N and mean electron energy $\langle\epsilon\rangle$, and electron attachment rate coefficients as a function of E/N.

The negative ions that have been observed in the majority of the single-collision electron beam studies of CF_4 are the complementary ions F^- and CF_3^- (see, however, Iga *et al.*[137] and later in this section). These fragment anions are produced via two broad and overlapping resonances located be-

TABLE 22. Total electron-impact neutral dissociation cross sections for CF_4 in units of 10^{-20} m^2.

Energy (eV)	Sum of columns 2–4 in Table 21 (Ref. 121)	$\sigma_{diss,\,neut,\,t}(\epsilon)$ (Ref. 73)
13		0.03
14		0.09
16	0.001	0.20
18	0.002	0.42
20		0.44
25		0.49
30	0.018	0.41
35		0.27
40	0.026	
50	0.040	
60	0.057	
70	0.069	
80	0.086	
90	0.091	
100	0.100	
110	0.116	
120	0.120	
130	0.120	
140	0.118	
150	0.115	
160	0.113	
170	0.110	
180	0.109	
190	0.104	
200	0.101	
210	0.098	
220	0.096	
230	0.094	
240	0.094	
250	0.091	
260	0.089	
270	0.087	
280	0.084	
290	0.084	
300	0.082	

TABLE 23. Average cross section, σ_F, for the production of neutral atomic fluorine by electron impact on CF_4, in units of 10^{-20} m^2 [data of Bruce, Ma, and Bonham (Ref. 100)].

Energy (eV)	σ_F[a]
20	1.26
25	2.46
30	3.42
35	4.04
40	4.53
45	5.02
50	5.49
55	5.89
60	6.07
65	6.18
70	6.31
75	6.45
80	6.59
85	6.67
90	6.73
95	6.76
100	6.79
110	6.84
120	6.85
130	6.82
140	6.76
150	6.70
160	6.67
170	6.64
180	6.63
190	6.58
200	6.54
250	6.14
300	5.78
350	5.40
400	5.00
450	4.68
500	4.37

[a]Average of upper and lower bound cross sections; the deviations from the average values are large (see Ref. 100).

tween 4.5 and 10 eV.[50,57–60,67,138,139] The energetics and the cross sections for their production have been studied by a number of electron swarm[59,140] and electron beam measurements.[50,57–59,67,135,137,139,141]

Electron beam data, especially ion kinetic energy measurements,[49,50,60,141] have shown that the resonant electron attachment to CF_4 occurs mainly in the 6 eV to 8 eV energy range via two negative ion states: (i) Via the ground state of CF_4^- at 6.8 eV producing F^- and CF_3^- through the complementary channels

$$CF_4^- \rightarrow F^- + CF_3, \tag{6}$$

$$CF_4^- \rightarrow F + CF_3^-. \tag{7}$$

The time-of-flight measurements[49,51,60] revealed that the decomposition of CF_4^- at 6.8 eV is associated with remarkably high translational energy imparted to the products. (ii) Via

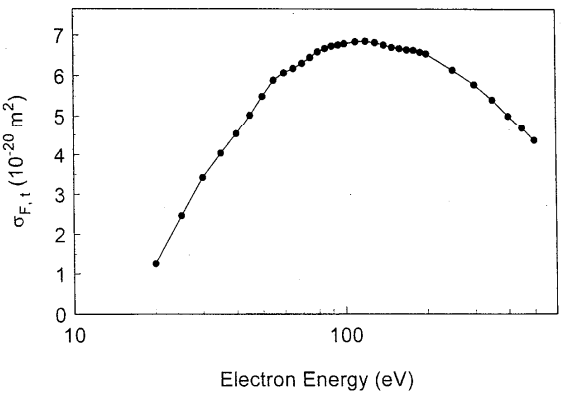

FIG. 27. Total cross section for the production of neutral atomic fluorine by electron impact on CF_4 (from Ref. 100).

TABLE 24. Absolute emission cross sections, σ_{em}, at 100 eV, for various visible FI line emissions for CF_4 [from Blanks, Tabor, and Becker (Ref. 128)].

Transition and line (nm)		σ_{em} (10^{-19} cm^2) (Ref. 128)[a]	σ_{em} (10^{-19} cm^2) (Ref. 125)[b]
	624.0	1.2	···
$^4S°\rightarrow{}^4P$	634.9	0.8	···
	641.3	0.6	···
	677.4	0.8	1.6
	679.5	0.2	···
	683.4	1.2	···
$^4D°\rightarrow{}^4P$	685.6	4.7	6.1
	687.0	0.9	···
	690.2	2.8	4.7
	691.0	0.9	···
	703.7	1.2	2.1
$^2P°\rightarrow{}^2P$	712.8	0.7	1.3
	720.2	0.4	···
$^2S°\rightarrow{}^2P$	731.1		2.0
		3.3	
	733.2		2.3
	739.9	3.9	4.1
$^4P°\rightarrow{}^4P$	746.5	0.6	1.2
	755.2		···
	757.3	1.9	···
	760.7		1.0
$^2D°\rightarrow{}^2P$	775.5	3.5	4.9
	780.0	2.1	2.0

[a]The authors quoted an uncertainty of ±20% for cross section values larger than 1×10^{-19} cm^2, and about ±25% for cross sections smaller than 1×10^{-19} cm^2. Cross sections for emissions at wavelengths longer than 750 nm have an uncertainty of ±20% (see Ref. 128).
[b]Quoted uncertainty ±10%.

the first electronically excited CF_4^{*-} state at 7.6 eV producing only F^-. This electronic state is likely a core excited resonance and may correlate with the formation of an electronically excited CF_3^* radical, viz.

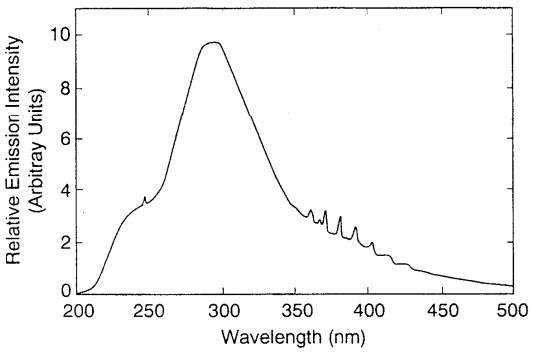

FIG. 28. Optical emission from CF_4 in the wavelength range 200–500 nm produced by collisions of 100 eV electrons with CF_4 (from Refs. 17 and 125).

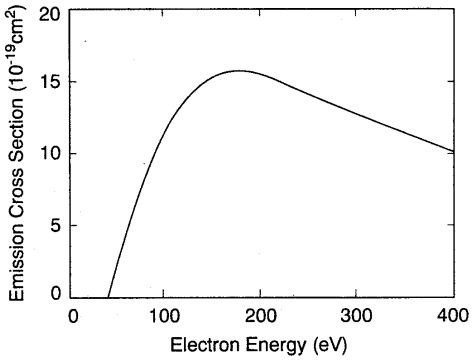

FIG. 29. Absolute integrated emission cross section of the FI $3p\,^4D^0 \rightarrow 3s^4P$ multiplet as a function of electron energy for CF_4 (from Ref. 128).

$$CF_4^{*-}\rightarrow F^- + CF_3^*. \tag{8}$$

Since F^- is produced from this reaction with only thermal kinetic energy, the CF_3^* radical must contain an amount of excess energy ranging from 4 eV at the onset of the reaction to about 8 eV at the higher energy side of the F^- resonance (the first excited electronic state[142] of CF_3 is at 5.9 eV). Thus the final channel of reaction (8) may consist of three fragments such as F^-+CF_2+F or F^-+CF+F_2. These products will be formed with little kinetic energy compared to the kinetic energy of the products formed via the ground state of CF_4^- at 6.8 eV.[49–51,60]

The energy dependence of the relative cross section for the formation of F^- and CF_3^- as given in the electron beam experiments of Illenberger and coworkers is shown in Fig. 31. The energy-dependent yield of the two complementary ions

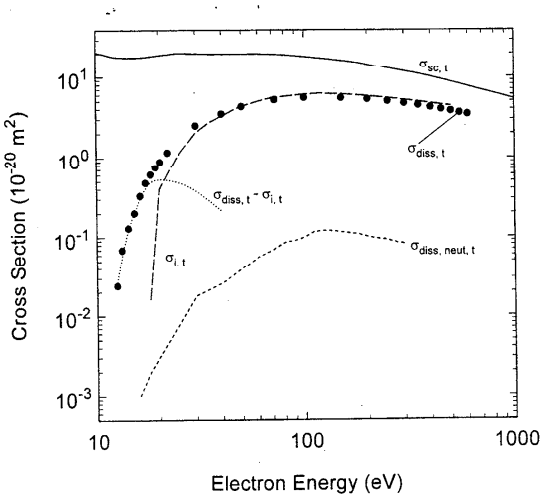

FIG. 30. Comparison of $\sigma_{sc,t}(\epsilon)$ (Table 4, —); $\sigma_{diss,t}(\epsilon)$ (Table 10, ●); $\sigma_{i,t}(\epsilon)$ (Table 11, – –); $\sigma_{diss,neutr,t}(\epsilon)$ (Table 22, ---); and $\sigma_{diss,t}(\epsilon) - \sigma_{i,t}(\epsilon)$ (. . . . .).

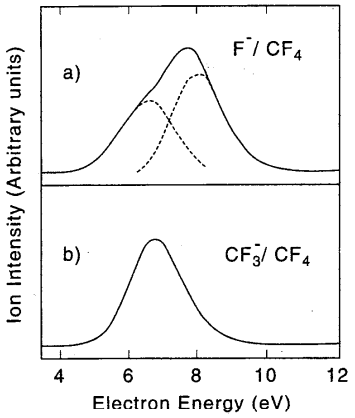

FIG. 31. Relative intensities of F^- and CF_3^- from CF_4 as a function of electron energy (from Refs. 49–51).

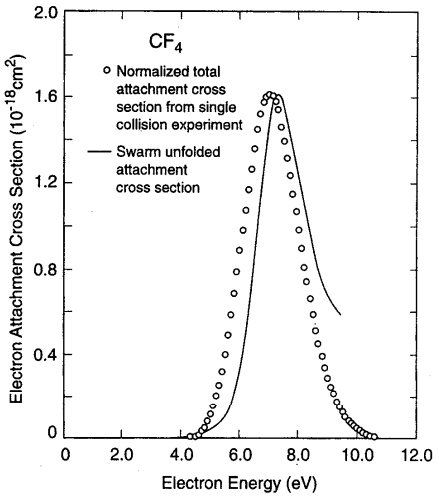

FIG. 33. Swarm-unfolded and swarm-normalized electron beam total electron attachment cross sections for CF_4 (from Ref. 59).

as measured by various investigators is shown in Fig. 32. The agreement is rather poor due partly to the different electron energy resolutions of the various experimental methods. For example, for F^- the beam experiments with lower energy resolution[57,58,139] agree among themselves and those with higher energy resolution[50,137] also tend to agree between themselves. However, this does not seem to be the case for the CF_3^- ion where the data of Iga *et al.*[137] and Lifshitz and Grajower[139] differ substantially from the rest.

There are very limited absolute measurements of the cross sections for these anions. Hunter and Christophorou[59] reported that the cross section values for the complementary anions at their respective maxima are about the same and about equal to 0.8×10^{-18} cm^2 (see further discussion in Sec. 6.1).

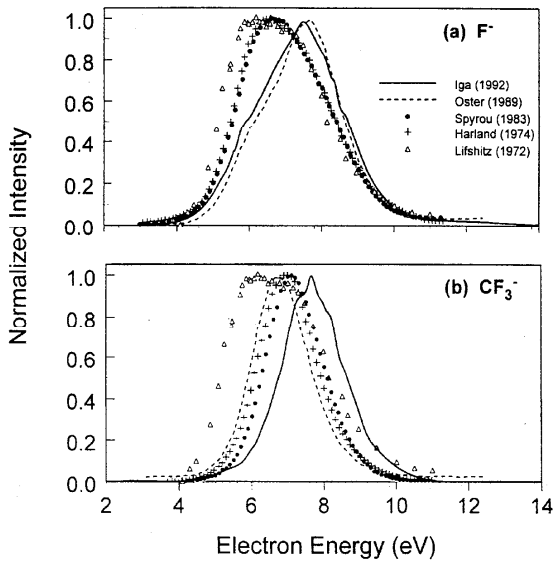

FIG. 32. Normalized intensities of CF_3^- and F^- from electron impact on CF_4 as a function of electron energy. —, Ref. 137; -----, Ref. 50: ●, Ref. 57; +, Ref. 58; △, Ref. 139.

6.1 Total Electron Attachment Cross Section, $\sigma_{a,t}(\epsilon)$

The total electron attachment cross section for the CF_4 molecule is small compared to the cross sections for electron impact dissociation and ionization of CF_4. Total electron attachment cross sections have been unfolded from electron swarm measurements[59] and are presented in Fig. 33 along with the total attachment cross section obtained by normalizing the total relative cross section measured in a single collision beam experiment to the swarm-unfolded absolute total cross section. The latter cross section (open circles in Fig. 33) is listed in Table 25. The uncertainty of these cross sections has been quoted to be ±20%. At the position of the maximum in the swarm-unfolded cross section, at 7.3 eV, the value of the total cross section[59] is 1.58×10^{-18} cm^2, which is to be compared with an earlier mass spectroscopic value[58] of 1.04×10^{-18} cm^2.

6.2 Dissociative Electron Attachment Cross Section for F^- and CF_3^-

The yields of F^- and CF_3^- in Fig. 32 can be put on an absolute scale by normalizing their respective peaks to the peak cross section value[59] of 0.8×10^{-18} cm^2. Besides these data, Iga *et al.*[137] have recently reported dissociative electron attachment cross sections for F^-, CF_3^-, and F_2^- by electron impact on CF_4 over a wide energy range that covered the resonance region below 10 eV and energies above this energy region to 50 eV where F^- and F_2^- were observed due to nonresonant processes, possibly due to negative ion-positive

TABLE 25. Total electron attachment cross section, $\sigma_{a,t}(\epsilon)$, for CF_4, in units of 10^{-18} cm^2, obtained by normalizing the total relative cross section measured in a single-collision beam experiment to the swarm-unfolded absolute total cross section [Hunter and Christophorou (Ref. 59)].

Energy (eV)	$\sigma_{a,t}(\epsilon)$ (10^{-18} cm^2)
4.31	0.004
4.60	0.012
4.79	0.048
5.00	0.108
5.18	0.202
5.38	0.317
5.56	0.486
5.77	0.681
5.94	0.881
6.15	1.07
6.34	1.26
6.52	1.44
6.73	1.57
6.91	1.61
7.14	1.58
7.32	1.46
7.52	1.31
7.72	1.14
7.93	0.977
8.10	0.802
8.33	0.656
8.51	0.506
8.75	0.389
8.93	0.284
9.13	0.213
9.35	0.146
9.52	0.099
9.76	0.069
9.96	0.043
10.20	0.022
10.40	0.009

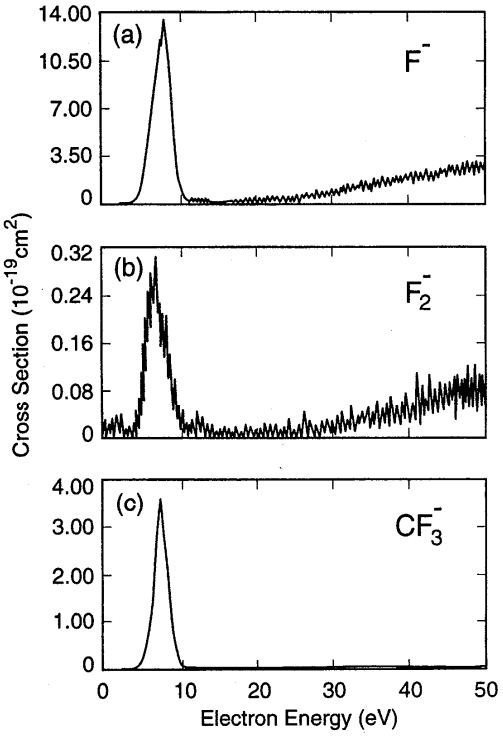

FIG. 34. Cross sections for F^-, F_2^-, and CF_3^- production by electron impact on CF_4 as a function of electron energy (from Ref. 137).

ion pair formation. These results are presented in Fig. 34. The yield of F_2^- is much lower than that of either F^- or CF_3^-. Interestingly, no CF_3^- ions were detected outside the resonance region (see Fig. 34c). The sum of the peak values of the cross sections for F^- and CF_3^- in Fig. 34, is about 1.6×10^{-18} cm^2, which is in excellent agreement with the value of Hunter and Christophorou.[59] However, in contrast to the other studies[57,58] which show the peak cross section values for F^- and CF_3^- to be about the same, the peak cross section value of Iga *et al.*[137] for the F^- as is indicated in Fig. 34 is about 3 times larger than that for the CF_3^- ion.

Production of negative ions by electron impact on CF_4 via nonresonant electron attachment processes occurs at energies above about 19 eV and is rather small.[137,143] The results of the two recent studies on the cross sections for positive ion-negative ion pair formation differ substantially. The sum of the cross sections of Iga *et al.*[137] for nonresonant production of F^- and F_2^- ranges[137,143] from 3×10^{-24} m^2 at 18.7 eV to 24×10^{-24} m^2 at 43.7 eV, while the sum of the cross sections measured by Mi *et al.*[143] for the production of F^- via a number of positive ion-negative ion pair processes [$F^-+CF_n^+$ ($n=0$–3) and F^++F^-] ranges[143] from 0.09×10^{-24} m^2 at 18.7 eV to 6.9×10^{-24} m^2 at 43.7 eV. Clearly more work is needed to quantify the cross sections for these processes. It should be noted that a negative ion mass spectrometric study of positive ion–negative ion pair formation using synchrotron radiation[144] puts the threshold for F^- production at 13.25 eV ± 0.03 eV, which is ~2 eV higher than the thermodynamic threshold of 11.3 eV for the formation of the ground state ions $F^-(^1S_g)+CF_3^+(X\ ^1A_1')$. Mitsuke *et al.*[144] concluded that the onset for the F^- production from CF_4 occurs at the adiabatic excitation energy for the Rydberg state near 13.6 eV.

6.3 Electron Attachment Coefficients and Electron Attachment Rate Constants

6.3.1 Density Reduced Electron Attachment Coefficient η/N

The density reduced electron attachment coefficient η/N is measured as a function of E/N. It is related to the total electron attachment cross section $\sigma_{a,t}(\epsilon)$ and $f(\epsilon,E/N)$ by

$$\eta/N_a(E/N)=(2/m)^{1/2}w^{-1}\int_0^\infty f(\epsilon,E/N)\epsilon^{1/2}\sigma_{a,t}(\epsilon)d\epsilon,$$

where N_a is the number density of the electron attaching gas and w is the electron drift velocity. For a unitary gas, the total number density $N=N_a$; for mixtures of an electron attaching gas in a buffer nonelectron attaching gas of density N, N is much larger than N_a. The density normalized elec-

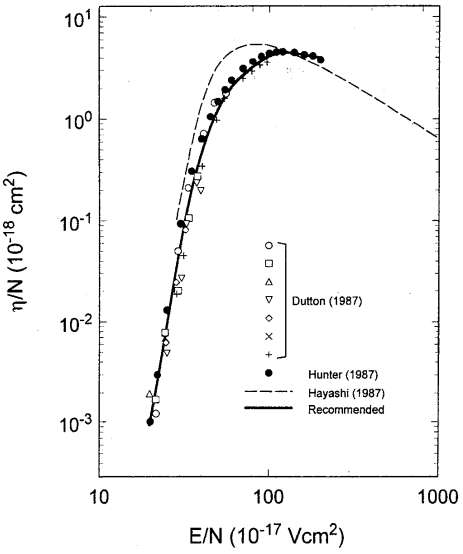

FIG. 35. Density-normalized electron attachment coefficient as a function of E/N for CF_4. ● Ref. 114; -------, Ref. 24; the rest of the symbols are the measurements of Dutton *et al.* (Ref. 140), made at various CF_4 pressures; —, recommended (see Sec. 6.3.1 and Table 26).

tron attachment coefficient for CF_4 has been measured by a number of investigators.[89,90,113–117,140] With the exception of the more recent data by Dutton *et al.*,[140] the rest of these measurements have been summarized by Hunter, Carter, and Christophorou.[114] In Fig. 35 are compared the results of Dutton *et al.*[140] with those of Hunter, Carter, and Christophorou[114] and the predicted values of Hayashi.[24] It is seen that these two latest sets of experimental data are in good agreement. It is also seen that the calculated values are generally higher than the experimental results. We have fitted the results of Dutton *et al.* and Hunter and others and the resultant values of η/N have been listed in Table 26 and represent our recommended set.

6.3.2 Total Electron Attachment Rate Constant, $k_{a,t}(E/N)$

The density reduced electron attachment coefficient $\eta/N_a(E/N)$ is related to the total electron attachment rate constant $k_{a,t}(E/N)$ by

$$k_{a,t}(E/N) = \eta/N_a(E/N) \times w(E/N).$$

The total electron attachment rate constant $k_{a,t}(E/N)$ for CF_4 has been measured[59,114] in mixtures with Ar as a function of E/N and $\langle \epsilon \rangle$. The measurements of $k_{a,t}$ of Hunter and Christophorou[59] are plotted in Fig. 36 as a function of the mean electron energy $\langle \epsilon \rangle$ and are listed in Table 27. The values of the mean electron energy were calculated[59] at each value of E/N from the known electron energy distribution functions of the buffer gas.

TABLE 26. Recommended $\eta/N(E/N)$ for CF_4.

E/N (10^{-17} V cm^2)	η/N 10^{-18} cm^{-2})
20	0.0007
22	0.003
24	0.007
26	0.018
28	0.035
30	0.069
32	0.127
34	0.12
36	0.29
38	0.40
40	0.53
42	0.72
44	0.89
46	1.05
48	1.21
50	1.38
55	1.77
60	2.14
65	2.47
70	2.78
75	3.04
80	3.26
85	3.48
90	3.69
95	3.91
100	4.07
110	4.29
120	4.40
130	4.40
140	4.33
150	4.27
160	4.21
170	4.13
180	4.04
190	3.95
200	3.86

6.3.3 Thermal Value of the Total Electron Attachment Rate Constant, $(k_{a,t})_{th}$

The value of $k_{a,t}(E/N)$, when the electron energy distribution function $f(\epsilon,E/N)$ is Maxwellian, $f_M(\epsilon,T)$, charac-

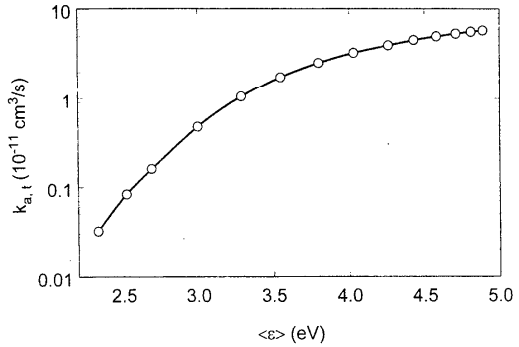

FIG. 36. Total electron attachment rate constant as a function of mean electron energy measured (Ref. 59) in mixtures of CF_4 with Ar.

TABLE 27. Total electron attachment rate constant $k_a(\langle\epsilon\rangle)$ for CF_4 in a buffer gas of Ar as a function of E/N and $\langle\epsilon\rangle$ [from Hunter and Christophorou (Ref. 59)].

$E/N(10^{-18}$ V cm$^2)$	$\langle\epsilon\rangle$ (eV)	$k_a(\langle\epsilon\rangle)$ $(10^{-11}$ cm^3 s$^{-1})$
9.32	2.33	0.032
10.97	2.52	0.083
12.4	2.69	0.16
15.5	3.00	0.48
18.6	3.29	1.05
21.7	3.55	1.76
24.9	3.80	2.53
27.9	4.03	3.28
31.1	4.26	3.97
34.2	4.43	4.54
37.3	4.58	5.00
40.4	4.71	5.35
43.5	4.81	5.62
46.6	4.89	5.80

teristic of only the gas temperature T, i.e., when $E/N \rightarrow 0$, is referred to as the total *thermal* electron attachment rate constant $(k_{a,t})_{th}$ and is given by

$$(k_{a,t})_{th} = (2/m)^{1/2} w^{-1} \int_0^\infty f_M(\epsilon, T)\, \epsilon^{1/2} \sigma_{a,t}(\epsilon)\, d\epsilon.$$

The reported values of the total thermal electron attachment rate constant are very small [$<1\times10^{-13}$ cm^3 s^{-1} (Ref. 59), $<3.1\ 10^{-13}$ cm^3 s^{-1} (Ref. 145), $<1\times10^{-16}$ cm^3 s^{-1} (Refs. 146 and 147)] and might have been affected by traces of electronegative impurities in these experiments.

6.3.4 Electron Detachment in Plasmas

It is worth pointing out that a number of interesting studies (e.g., see Refs. 148, 149, and 150) have been initiated to probe the role of electron detachment in radio-frequency plasmas in CF_4 using laser photodetachment.

7. Electron Transport

7.1 Electron Drift Velocity, w

Measurements of the electron drift velocity as a function of E/N in pure CF_4 have been made at room temperature and over a range of pressures.[11,12,83,89,119,151–155] Some of these measurements have been summarized and discussed earlier.[112,156] The most recent measurements are those of Hunter, Carter, and Christophorou,[83] who used a pulsed Townsend method. These measurements covered the largest E/N range of any other published set of measurements, from 0.03×10^{-17} to 300×10^{-17} V cm^2, and were corrected for the effects of electron attachment and ionization. The estimated maximum uncertainty above $(E/N)_{lim}$ (i.e., above the value, 140×10^{-17} V cm^2, of E/N at which $\alpha = \eta$; see Table 30 later in this section) was $\pm5\%$ and below $(E/N)_{lim}$ to decrease to $\pm2\%$ at E/N values below those corresponding to the onset for electron attachment. These are compared in

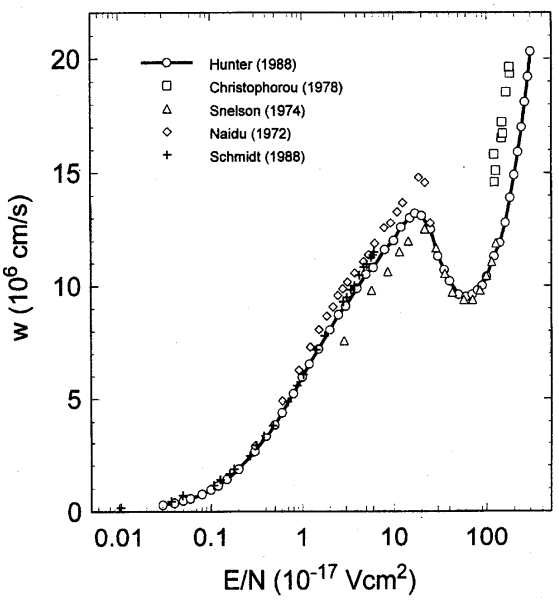

FIG. 37. Electron drift velocity as a function of E/N in CF_4. ○, Ref. 83; □, Ref. 11; △, Ref. 155; ◇, Ref. 89; +, Ref. 154; —, recommended (see Sec. 7.1 and Table 28).

Fig. 37 with other measurements.[11,89,154,155] The w data of Hunter, Carter, and Christophorou[83] are reproduced in Table 28 and are our recommended data set.

Electron drift velocities for a number of CF_4 gas mixtures have also been measured:

CF_4 in He (Refs. 11 and 13)
CF_4 in Ne (Ref. 11)
CF_4 in Ar (Refs. 11, 14, 25, 153, and 154)
CF_4 in Kr (Ref. 11)
CF_4 in Xe (Ref. 12)
CF_4 in CO_2 (Refs. 119 and 153)
CF_4 in CH_4 (Refs. 14, 119, and 152)
CF_4 in C_2H_2 (Ref. 11)
CF_4 in C_2H_6, and C_3H_8 (Ref. 14)
CF_4 in i-C_4H_{10} (Refs. 14 and 152)
CF_4 in Ar+CO_2 (Refs. 119 and 153)
CF_4 in Ar+C_2H_2 (Ref. 11)
CF_4 in Xe+C_2H_2 (Ref. 12)
CF_4 in Ar+NH_3, and Ar+H_2O (Ref. 119).

Most of the measurements on the CF_4 mixtures have been made for the purpose of identifying fast gases (i.e., gases with very large w for E/N values employed in practice) for particle detectors. An example[11] of these data on mixtures is reproduced in Fig. 38 for CF_4/Ar.

7.2 Ratios of the Transverse and Longitudinal Electron Diffusion Coefficient to Electron Mobility: D_T/μ, and D_L/μ

Measurements of D_T/μ and D_L/μ in CF_4 are rather limited. The available data[81,89,90,154] were taken at about 293 K and are summarized in Fig. 39. Curtis, Walker, and

TABLE 28. Electron drift velocity, w, in CF_4 as a function of E/N [from Hunter, Carter, and Christophorou (Ref. 83)].

E/N (10^{-17} V cm^2)	w (10^6 cm s^{-1})
0.03	0.275
0.04	0.36
0.05	0.46
0.06	0.55
0.08	0.74
0.10	0.93
0.12	1.11
0.15	1.40
0.2	1.83
0.3	2.61
0.4	3.28
0.5	3.85
0.6	4.38
0.8	5.22
1.0	5.95
1.2	6.53
1.5	7.20
2.0	8.05
2.5	8.72
3	9.10
4	9.88
5	10.5
6	10.8
8	11.6
10	12.0
12	12.6
15	13.0
17	13.2
20	13.1
25	12.5
30	11.3
35	10.7
40	10.2
50	9.6
60	9.5
70	9.6
80	9.8
90	10.0
100	10.4
120	11.3
140	11.9
160	12.8
180	13.9
200	14.9
220	15.9
240	17.0
260	18.1
280	19.2
300	20.3

Mathieson[81] quoted an uncertainty of about $\pm 5\%$ below 17 $\times 10^{-17}$ V cm^2 and 8% above this E/N value. Naidu and Prasad[89] reported that the uncertainty in their measurements varied from about $\pm 5\%$ at low E/N to about $\pm 3\%$ at high E/N. In Fig. 39 are also plotted the recent measurements of Schmidt and Polenz[154] which differ substantially from the other measurements. The solid line in Fig. 39a is a fit to the measurements of Refs. 81, 89, and 90. Values taken off the solid line are given in Table 29 as the presently recommended data on D_T/μ.

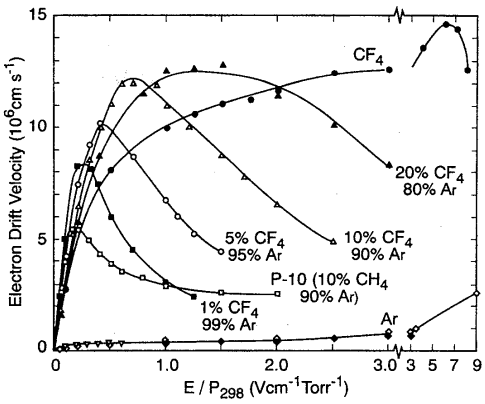

FIG. 38. Electron drift velocity as a function of E/P (T=298 K) for CF_4/Ar mixtures (reproduced from Ref. 11).

To our knowledge there is only one measurement[154] of the longitudinal electron diffusion coefficient to electron mobility ratio, D_L/μ. These data are shown in Fig. 39b and indicate lower values of D_T/μ compared to D_L/μ below about 2×10^{-17} V cm^2 and higher values of D_T/μ compared to D_L/μ above this E/N value.

7.3 Mean Electron Energy $\langle\epsilon\rangle$

Mean electron energies $\langle\epsilon\rangle$ as a function of E/N have been computed using a Boltzmann code for pure[118,119] CF_4 and for mixtures[119] of CF_4 in CO_2 and CF_4 in Ar. These data are approximate and should be used for guiding purposes only. The D_T/μ data in Fig. 39 can also be used to determine the "characteristic" (or "reduced") energy $(3/2)(D_T/\mu)$ as a function of E/N (see also Ref. 154).

7.4 $(E/N)_{lim}$

This is an interesting and useful quantity which comes naturally from the measurements of the ionization and attachment coefficients measured as a function of E/N. It is the value of the density-reduced electric field at which $(\alpha-\eta)/N=0$. This value should also be equal to the breakdown voltage of CF_4 as measured under uniform field conditions. Measured values of this quantity are given in Table 30. If we exclude the two largest values, the average of the rest of the data in Table 30 gives an $(E/N)_{lim}$ value for CF_4 equal to 140×10^{-17} V cm^2.

8. Electron Interactions with CF_4 Neutral Fragments

The studies of the interactions of low energy electrons with radicals of the CF_4 molecule are very limited. Very little, for example, is known about the electron impact ionization of CF_4 fragments, $CF_x(3>x\geq 1)$, and nothing has

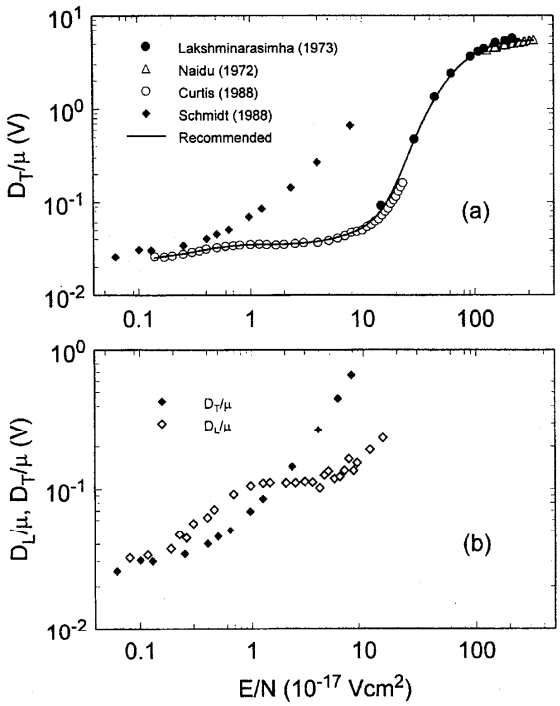

FIG. 39. (a) Ratio of the lateral electron diffusion coefficient to electron mobility as a function of E/N for CF_4. ●, Ref. 90; △, Ref. 89; ○, Ref. 81; ◆, Ref. 154; —, recommended values based on fit to the measurements of Refs. 81, 89, and 90 (see Sec. 7.2 and Table 29). (b) Comparison of $D_T/\mu(E/N)$ (◆) and $D_L/\mu(E/N)$ (◇) (data of Ref. 154).

been reported on their electron scattering and electron attachment properties. Such studies, however, are of extreme significance in many applications; especially in plasma processing uses of CF_4 gas.[17,122,135,158,159] The CF_3, CF_2, and CF radicals and their ions are the most abundant and reactive species that result from electron impact dissociation of CF_4 and are therefore important in modeling CF_4 gas discharges. The limited data are summarized and briefly discussed below.

8.1 Electron-Impact Ionization Cross Sections, $\sigma_{i,fragment}(\epsilon)$

Significant results have recently been reported[122,123,159] on electron impact ionization of the free radicals CF_3, CF_2, and CF prepared for these studies by near resonance charge transfer reactions of CF_3^+, CF_2^+, and CF^+ with various species. In Fig. 40 are plotted the absolute electron-impact ionization cross sections for the formation of the parent CF_x^+ ions from the CF_x radicals ($x=1-3$) measured[123] from threshold to 200 eV by fast neutral beam techniques (see Deutsch *et al.*[159] for calculated cross sections for the production of singly charged positive ions of these radicals). These

TABLE 29. Recommended $D_T/\mu(E/N)$ for CF_4.

E/N (10^{-17} V cm^2)	D_T/μ (V)
0.14	0.025
0.15	0.025
0.17	0.026
0.20	0.027
0.25	0.028
0.30	0.029
0.35	0.030
0.4	0.031
0.5	0.032
0.6	0.033
0.7	0.034
0.8	0.034
0.9	0.034
1	0.035
2	0.035
3	0.036
4	0.037
5	0.039
6	0.041
7	0.044
8	0.046
9	0.049
10	0.052
15	0.084
20	0.155
25	0.293
30	0.492
35	0.736
40	1.01
45	1.29
50	1.58
60	2.16
70	2.68
80	3.12
90	3.49
100	3.81
150	4.78
200	5.16
250	5.29
300	5.39

data are listed in Table 31. The reported overall uncertainties are ±15% for CF, ±16% for CF_2, and ±18% for CF_3. The cross sections above about 40 eV decrease in the order of CF, CF_2, and CF_3.

TABLE 30. $(E/N)_{lim}$ for CF_4.

$(E/N)_{lim}$ (10^{-17} V cm^2)	Reference
137	89
138	117
140	113
141	157[a]
142	118
143	115
149	116
151	8[a]

[a]Uniform field breakdown measurements; the rest of the data are the values of E/N at which $\alpha = \eta$. If we exclude the highest two values in the table, the average of the rest of the data is 140×10^{-17} V cm^2.

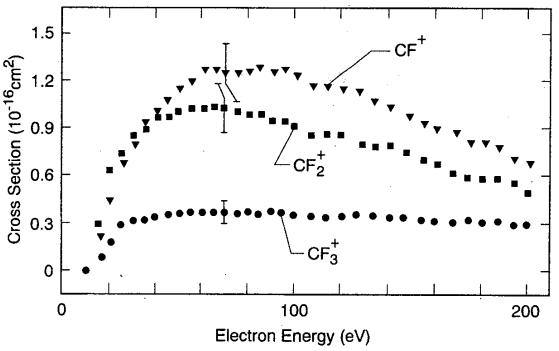

FIG. 40. Electron-impact ionization cross sections for the formation of CF_x ($x=1-3$) parent ions as a function of electron energy (Ref. 123). The total uncertainty of each cross section at 70 eV is indicated in the figure. ●, CF_3^+; ■, CF_2^+; ▼, CF^+.

8.2 Electron-Impact Dissociative Ionization Cross Sections, $\sigma_{i,diss,fragment}(\epsilon)$

Tarnovsky *et al.*[122] measured the absolute cross sections for dissociative electron-impact ionization of the CF_x ($x = 1-3$) free radicals of CF_4.

TABLE 31. Cross sections, $\sigma_{i,fragment}(\epsilon)$, for parent ionization of the fragments CF_3, CF_2, and CF by electron impact in units of 10^{-20} m^2 [from Tarnovsky and Becker (Ref. 123)].

Energy (eV)	CF_3^+	CF_2^+	CF^+
10	0.015	0.05	
11	0.029	0.09	
12	0.041	0.15	0.03
13	0.060	0.18	0.07
14	0.099	0.26	0.13
15	0.111	0.35	0.18
16	0.145	0.39	0.23
17	0.157	0.42	0.28
18	0.167	0.47	0.33
19	0.194	0.55	0.40
20	0.204	0.64	0.45
22	0.270	0.69	0.55
24	0.303	0.73	0.63
26	0.315	0.78	0.70
28	0.320	0.82	0.76
30	0.325	0.87	0.81
32	0.329	0.89	0.86
34	0.335	0.91	0.91
36	0.338	0.93	0.95
38	0.346	0.96	0.99
40	0.350	0.98	1.01
45	0.358	0.99	1.08
50	0.360	1.01	1.15
55	0.372	1.03	1.18
60	0.374	1.03	1.23
65	0.380	1.05	1.25
70	0.376	1.03	1.25
80	0.368	0.99	1.26
90	0.365	0.96	1.25
100	0.350	0.91	1.23
120	0.342	0.86	1.14
140	0.333	0.78	1.04
160	0.318	0.67	0.90
180	0.306	0.58	0.79
200	0.292	0.49	0.67

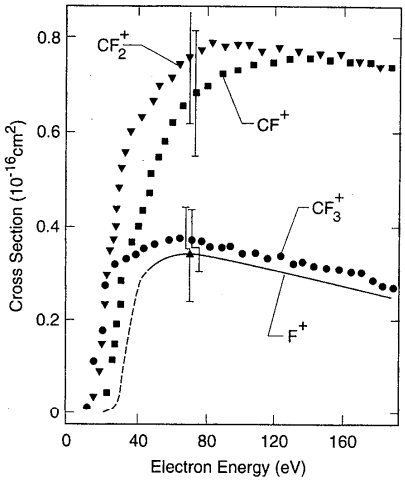

FIG. 41. Electron-impact ionization cross section for the formation of CF_3^+ parent ions, and CF_2^+ and CF^+ molecular fragment ions from CF_3 as a function of electron energy (from Ref. 122). ●, CF_3^+; ▼, CF_2^+; ■, CF^+; ▲, ---, and — represent the cross section for F^+.

CF_3:

The measurements of Tarnovsky *et al.*[122] for the production of CF_2^+ and CF^+ from the CF_3 fragment are shown in Fig. 41, and are listed in Table 32. The assigned overall uncertainty to the CF_2^+ and CF^+ cross sections is ±20%. These data agree well with the cross section values reported by Wetzel, Biaocchi, and Freund[160] [$(0.7\pm0.2)\times10^{-16}$ cm^2 for CF_2^+ and $(0.6\pm0.2)\times10^{-16}$ cm^2 for CF^+ at 70 eV]. They found that the processes of positive double ionization $CF_2^+ + F^+$ and ion pair $CF_2^+ + F^-$ play an insignificant role in the dissociative ionization of CF_3 and the fragment ions are produced with little kinetic energy.

Also shown in Fig. 41 is the cross section for the formation of F^+ (at 70 eV the magnitude of the cross section of this ion is 0.35×10^{-16} cm^2 with an estimated[122] uncertainty of ±30%), and a solid line representing the predicted[122] energy dependence of the F^+ cross section. No significant production of C^+ was observed (an upper limit of 0.1×10^{-16} cm^2 was estimated[122] for the cross section of this ion at 70 eV).

Interestingly, the cross sections for the molecular fragments (CF_2^+, CF^+ from CF_3) exceed the parent ionization cross section (CF_3^+ from CF_3). This is seen from the data[122] in Fig. 41 where the cross sections for the formation of CF_2^+ and CF^+ ions from CF_3 are compared with the cross section for the formation of the parent CF_3^+ ion. As similar in the case of CF_4, the dissociative ionization is the dominant process in CF_3. See Tarnovsky *et al.*[122] for information on threshold energies and other energetics.

CF_2:

In Fig. 42 the absolute cross section for the production of CF^+ by electron impact on CF_2 as measured by Tarnovsky *et al.*[122] is presented, and is seen to exceed that for the parent

TABLE 32. Cross sections, $\sigma_{i,\,diss,\,fragment}(\epsilon)$, for dissociative ionization of the CF_3 radical by electron impact in units of 10^{-20} m^2 [from Tarnovsky *et al.* (Ref. 122)].

Energy (eV)	CF_3^+	CF_2^+	CF^+	F^+
10	0.02			
11	0.03			
12	0.04			
13	0.06			
14	0.10			
15	0.11			
16	0.15			
17	0.16			
18	0.17	0.06		
19	0.19	0.12		
20	0.20	0.17		
22	0.27	0.25	0.04	
24	0.30	0.31	0.10	
26	0.32	0.34	0.15	
28	0.32	0.40	0.20	
30	0.33	0.49	0.26	
32	0.33	0.53	0.31	
34	0.34	0.56	0.34	
36	0.34	0.59	0.36	
38	0.35	0.61	0.37	
40	0.35	0.63	0.40	
45	0.36	0.65	0.45	
50	0.36	0.67	0.53	
55	0.37	0.71	0.58	
60	0.37	0.72	0.62	
65	0.38	0.74	0.65	
70	0.38	0.76	0.68	0.35
80	0.37	0.79	0.70	
90	0.37	0.78	0.72	
100	0.35	0.78	0.73	
120	0.34	0.78	0.75	
140	0.33	0.77	0.77	
160	0.32	0.76	0.76	
180	0.31	0.74	0.74	
200	0.29	0.73	0.72	

TABLE 33. Cross sections, $\sigma_{i,\,diss,\,fragment}(\epsilon)$, for dissociative ionization of the CF_2 radical by electron impact in units of 10^{-20} m^2 [from Tarnovsky *et al.* (Ref. 122)].

Energy (eV)	CF_2^+	CF^+	F^+
10	0.05		
11	0.09		
12	0.15		
13	0.18		
14	0.26		
15	0.35	0.04	
16	0.39	0.09	
17	0.42	0.13	
18	0.47	0.18	
19	0.55	0.20	
20	0.64	0.23	
22	0.69	0.31	
24	0.73	0.36	
26	0.78	0.40	
28	0.82	0.43	
30	0.87	0.48	
32	0.89	0.62	
34	0.91	0.74	
36	0.93	0.80	
38	0.96	0.84	
40	0.98	0.88	
45	0.99	0.97	
50	1.01	1.02	
55	1.03	1.08	
60	1.03	1.11	
65	1.05	1.16	
70	1.03	1.19	0.6
80	0.99	1.22	
90	0.96	1.25	
100	0.91	1.28	
120	0.86	1.24	
140	0.78	1.18	
160	0.67	1.12	
180	0.58	1.05	
200	0.49	0.93	

ion CF_2^+ above about 50 eV. This cross section is listed in Table 33 and has an estimated[122] overall uncertainty of $\pm 16\%$, i.e., somewhat lower than that ($\pm 20\%$) for the parent ion CF_2^+. Included in Fig. 42 is also the absolute cross section for F^+ production (0.6×10^{-16} cm^2 at 70 eV; the solid line represents the energy dependence of this ion). Tarnovsky *et al.* estimated that the F^+ cross section has a contribution of 0.4×10^{-16} cm^2 from the process $CF^+ + F^+$ and a contribution of 0.2×10^{-16} cm^2 from the F^+ single positive ion formation. The production of C^+ was reported[122] to be *small (cross section* $<0.1\times10^{-16}$ cm^2 at 70 eV).

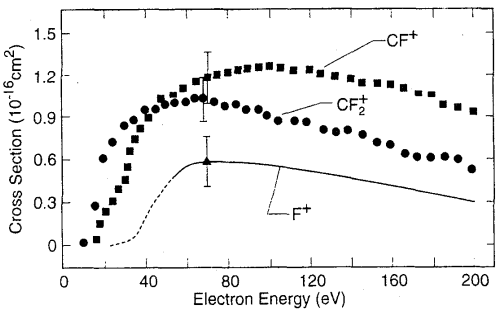

FIG. 42. Electron-impact ionization cross section for the production of CF_2^+ parent ions and of CF^+ molecular fragment ions from CF_2 as a function of electron energy (from Ref. 122). ●, CF_2^+; ■, CF^+; ▲, ---, and — represent the cross section for F^+.

It is clear from Fig. 42 that the cross section for CF^+ from CF_2 displayed two prominent onsets, a low energy one corresponding to the formation of $CF^+ + F$ and a higher energy one representing the double positive ion formation $CF_2 \rightarrow CF^+ + F^+$. The fragment ions are produced with little kinetic energy.[122]

CF:

The dissociative ionization of this radical produces weak C^+ and F^+ fragment ions. The cross sections for these two ions at 70 eV have been measured[122] to be $(0.25\pm0.1)\times10^{-16}$ cm^2 for F^+ and less than 0.1×10^{-16} cm^2 for C^+.

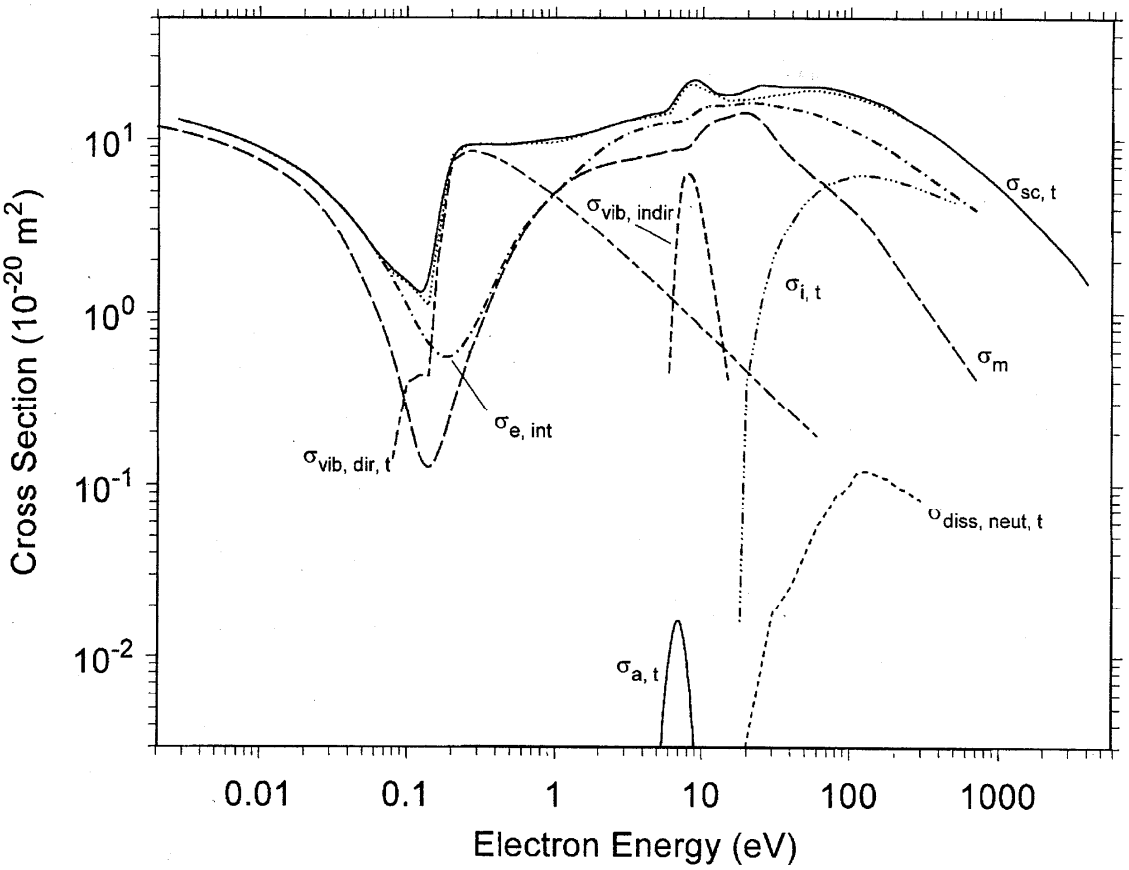

FIG. 43. Recommended electron impact cross sections for CF_4 (see the text).

9. Recommended Cross Sections and Transport Coefficients

In Fig. 43 are plotted the cross sections that were derived from several sets of data, and were designated as "recommended" in this paper. These are

- $\sigma_{sc,\,t}(\epsilon)$—Table 4, Figs. 3 and 4;
- $\sigma_m(\epsilon)$—Table 5, Fig. 5;
- $\sigma_{e,\,int}(\epsilon)$—Table 8, Fig. 11; and
- $\sigma_{i,\,t}(\epsilon)$—Table 11, Fig. 17.

For some cross sections discussed in the article there was only a limited amount of data. In these cases, for our "recommended" data set we have chosen the cross sections which we consider the best currently available in the literature. These are listed below and are also shown in Fig. 43.

- $\sigma_{vib,\,dir,\,t}(\epsilon)$—Column 4 of Table 9, Fig. 14c. This theoretical cross section is from Ref. 73. It is consistent with the limited experimental measurements and covers a larger energy range.
- $\sigma_{vib,\,indir}(\epsilon)$—Column 5 of Table 9, Fig. 14c. This cross section is derived in this article by subtracting $\sigma_{vib,\,dir,\,t}(\epsilon)+\sigma_{a,\,t}(\epsilon)$ from $\sigma_{inel,\,t}(\epsilon)$ of Boesten *et al.*[31]
- $\sigma_{diss,\,neut,\,t}(\epsilon)$—Table 22, Fig. 26. We use here the data of Sukai *et al.*[121] since they are the only independent experimental values presently available in the literature (see Sec. 5.3 regarding consistency with other recommended cross sections).
- $\sigma_{a,\,t}(\epsilon)$—Table 25, Fig. 33. This cross section is from Ref. 59 which is the only absolute measurement.

One may relate these cross sections [with the exception of $\sigma_m(\epsilon)$] by the simple equation:

$$\sigma_{sc,\,t}(\epsilon)=\sigma_{e,\,int}(\epsilon)+\sigma_{inel,\,t}(\epsilon). \tag{9}$$

Based on Eq. (9) one would expect

$$\sigma_{sc,\,t}(\epsilon)\approx\sigma_{e,\,int}(\epsilon)+\sigma_{i,\,t}(\epsilon)+\sigma_{diss,neut,\,t}(\epsilon)+\sigma_{vib,\,dir,\,t}(\epsilon)+\sigma_{vib,\,indir}(\epsilon)+\sigma_{a,\,t}(\epsilon). \tag{10}$$

Indeed, we have evaluated the right-hand side of Eq. (10) using the recommended values listed above, and have plotted the values in Fig. 43 (dotted line). The sum reproduces $\sigma_{sc,\,t}(\epsilon)$ rather well over the entire energy range from 0.001 eV to 1000 eV, with the sum being somewhat lower than $\sigma_{sc,\,t}(\epsilon)$ around 20 eV. This difference can be ascribed to (i) uncertainties in $\sigma_{e,\,int}(\epsilon)$, (ii) uncertainties in $\sigma_{diss,neut,\,t}(\epsilon)$ from 12.5 eV to 30 eV, and/or (iii) indirect vibrational excitation of CF_4 via the negative ion states that are known to exist in this energy range (see Table 3). However, the overall

observed agreement is gratifying and indicates the consistency and validity of the recommended cross sections.

In addition to the cross sections presented in Fig. 43, the recommended partial ionization cross sections for CF_4 are given in Fig. 19 and Table 15.

Our recommended data for the electron transport and the density reduced electron attachment and ionization coefficients are as follows based on the discussion in the text:

- η/N (Fig. 35, Table 26),
- α/N (Fig. 23, Table 19),
- $(\alpha-\eta)/N$ (Fig. 24, Table 20),
- w (Fig. 37, Table 28),
- D_T/μ (Fig. 39, Table 29), and
- $k_{a,t}$ (Fig. 36, Table 27).

Recommended data can be found on the World Wide Web at http:/www.eeel.nist.gov/811/refdata.

10. Conclusions

The data presented in Fig. 43 represent a comprehensive, consistent, and independently measured or determined set of electron collision cross sections for CF_4 from 0.003 eV to 1000 eV. While for many of the individual cross sections there exist published values that differ by as much as two orders of magnitude, the critical analysis of these data performed in this article has allowed the determination of a self-consistent data set whose uncertainties are expected to be between 10% and 20% for most of the cross sections. It is important to note that the recommended cross section set presented in this article (Fig. 43) is not model dependent, as other previously published cross section sets.[24,25]

While the basic knowledge that is presented in this paper on the interactions of slow electrons with CF_4 and the observed consistency among a large portion of the available data is gratifying, there exist a need for further measurements, especially on $\sigma_{diss,\,neut,\,t}(\epsilon)$ and $\sigma_{i,\,mult}(\epsilon)$. The existing values for $\sigma_{diss,\,neut,\,t}(\epsilon)$ are very uncertain, with large discrepancies between direct measurements of this cross section and values of this cross section derived from measurements of $\sigma_{i,t}(\epsilon)$ and $\sigma_{diss,\,t}(\epsilon)$. Similarly, the two measurements of $\sigma_{i,\,mult}(\epsilon)$ show no apparent agreement.

11. Acknowledgments

The authors wish to thank Dr. R. J. Van Brunt, Dr. J. W. Gallagher, Dr. J. R. Whetstone, Dr. G. W. Mallard, and Dr. D. S. Green of the National Institute of Standards and Technology for their advice and comments, Dr. R. A. Bonham of the Illinois Institute of Technology for providing valuable literature, and Dr. M. Kushner of the University of Illinois for valuable discussions. This work has been supported in part by the U.S. Air Force Wright Laboratory under Contract No. F33615-96-C-2600 with the University of Tennessee.

12. References

[1] M. J. Kushner, J. Appl. Phys. **53**, 2923 (1982).
[2] G. S. Oehrlein, Phys. Today **39**, 26 (October 1986).
[3] D. M. Manos and D. L. Flamm, *Plasma Etching* (Academic, Boston, 1989).
[4] L. E. Kline and M. J. Kushner, Crit. Rev. Solid State Mater. Sci. **16**, 1 (1989).
[5] L. G. Christophorou, S. R. Hunter, J. G. Carter, and R. A. Mathis, Appl. Phys. Lett. **41**, 147 (1982).
[6] S. R. Hunter, J. G. Carter, and L. G. Christophorou, J. Appl. Phys. **58**, 3001 (1985).
[7] P. Bletzinger, in Proceedings of the 4th IEEE Pulsed Power Conference, Albuquerque, New Mexico, June, 1983, p. 37.
[8] R. E. Wootton, S. J. Dale, and N. J. Zimmerman, in *Gaseous Dielectrics II*, L. G. Christophorou (Ed.) (Pergamon, New York, 1980), p. 137.
[9] D. R. James, L. G. Christophorou, and R. A. Mathis, in *Gaseous Dielectrics II*, L. G. Christophorou (Ed.) (Pergamom, New York, 1980), p. 115.
[10] J. Berg and E. Kuffel, in Proceedings of the Ninth International Symposium on High Voltage Engineering, August, 1995, Graz, Austria, p. 2252.
[11] L. G. Christophorou, D. L. McCorkle, D. V. Maxey, and J. G. Carter, Nucl. Instrum. Methods **163**, 141 (1979).
[12] L. G. Christophorou, D. V. Maxey, D. L. McCorkle, and J. G. Carter, Nucl. Instrum. Methods **171**, 491 (1980).
[13] M. K. Kopp, K. H. Valentine, L. G. Christophorou, and J. G. Carter, Nucl. Instrum. Methods **201**, 395 (1982).
[14] Y. Yamashita, H. Kurashige, M. M. Morii, T. T. Nakamura, N. Nomura, N. Sasao, K. Shibata, Y. Fukushima, Y. Ikegami, H. Kobayashi, and T. Taniguchi, Nucl. Instrum. Methods Phys. Res. A **317**, 213 (1992).
[15] J. B. Gerardo and J. T. Verdeyen, *Low-Temperature Plasma Physics: Its Importance and Potential in Technology and Commerce*, Sandia National Laboratory Report No. SAND 87-1875 (1987).
[16] G. Ecker and K. U. Riemann, Exp. Tech. Phys. **35**, 119 (1987).
[17] K. H. Becker, in *Electron Collisions with Molecules, Clusters, and Surfaces*, H. Ehrhardt and L. A. Morgan (Eds.) (Plenum, New York, 1994), pp. 127–140.
[18] Intergovernmental Panel on Climate Change (IPCC), The 1994 Report of the Scientific Assessment Working Group of IPCC.
[19] V. Ramanathan, L. Callis, R. Cess, J. Hansen, I. Isaksen, W. Kuhn, A. Lacis, F. Luther, J. Mahlman, R. Reck, and M. Schlesinger, Rev. Geophys. **25**, 1441 (1987).
[20] R. S. Stolarski and R. D. Rundel, Geophys. Res. Lett. **2**, 443 (1975).
[21] R. A. Morris, T. M. Miller, A. A. Viggiano, J. F. Paulson, S. Solomon, and G. Reid, J. Geophys. Res. **100**, 1287 (1995).
[22] L. G. Christophorou, *Atomic and Molecular Radiation Physics* (Wiley-Interscience, New York, 1971).
[23] L. G. Christophorou (Ed.), *Electron Molecule Interactions and Their Applications* (Academic, Orlando, Florida, 1984), Vol. 1.
[24] M. Hayashi, in *Swarm Studies and Inelastic Electron-Molecule Collisions*, L. C. Pitchford, B. V. McKoy, A. Chutjian, and S. Trajmar (Eds.) (Spinger, New York, 1987), pp. 167–187.
[25] Y. Nakamura, in *Gaseous Electronics and Their Applications*, R. W. Crompton, M. Hayashi, D. E. Boyd, and T. Makabe (Eds.) (KTK Scientific, Tokyo, Japan, 1991), pp.178–200.
[26] C. R. Brundle, M. B. Robin, and H. Basch, J. Chem. Phys. **53**, 2196 (1970).
[27] J. A. Beran and L. Kevan, J. Phys. Chem. **73**, 3860 (1969).
[28] K. Kuroki, D. Spence, and M. A. Dillon, J. Chem. Phys. **96**, 6318 (1992).
[29] J. A. Stephens, D. Dill, and J. L. Dehmer, J. Chem. Phys. **84**, 3638 (1986).
[30] M. B. Robin, *Higher Excited States of Polyatomic Molecules* (Academic, New York, 1974), Vol. I, pp. 178–191.
[31] L. Boesten, H. Tanaka, A. Kobayashi, M. A. Dillon, and M. Kimura, J. Phys. B **25**, 1607 (1992).
[32] G. C. King and J. W. McConkey, J. Phys. B **11**, 1861 (1978).
[33] W. R. Harshbarger, M. B. Robin, and E. N. Lassettre, J. Electron Spectrosc. Relat. Phenom. **1**, 319 (1972/73).
[34] T. A. Carlson, A. Fahlman, W. A. Svensson, M. O. Krause, T. A. Whitley, F. A. Grimm, M. N. Piancastelli, and J. W. Taylor, J. Chem. Phys. **81**, 3828 (1984).
[35] I. Iga, M. C. A. Lopes, and J. U. Galdino, in *Abstracts of Scientific Papers*, J. B. A. Mitchell, J. W. McConkey, and C. E. Brion (Eds), 19th Interna-

tional Conference on the Physics of Electronic and Atomic Collisions, Whistler, British Columbia, Canada, July, 1995 (Univ. of Western Ontario, London, Ontario, 1995), p. 435.
[36]G. R. Cook and B. K. Ching, J. Chem. Phys. **43**, 1794 (1965).
[37]L. C. Lee, X. Wang, and M. Suto, J. Chem. Phys. **85**, 6294 (1986).
[38]G. J. Verhaart, W. J. van der Hart, and H. H. Brongersma, Chem. Phys. **34**, 161 (1978).
[39]L. C. Lee, E. Phillips, and D. L. Judge, J. Chem. Phys. **67**, 1237 (1977).
[40]R. E. Rebbert and P. Ausloos, J. Res. Natl. Bur. Stand. Sect. A **75**, 481 (1971).
[41]H. F. Winters, in *Swarm Studies and Inelastic Electron-Molecule Collisions*, L. C. Pitchford, B. V. McKoy, A. Chutjian, and S. Trajmar (Eds.) (Springer, New York, 1987), pp. 347–350.
[42]H. F. Winters and M. Inokuti, Phys. Rev. A **25**, 1420 (1982).
[43]K. Stephan, H. Deutsch, and T. D. Märk, J. Chem. Phys. **83**, 5712 (1985).
[44]B. Brehm, R. Frey, A. Küstler, and J. H. D. Eland, Int. J. Mass Spectrom. Ion Phys. **13**, 251 (1974).
[45]L. M. Sverdlov, M. A. Kovner, and E. P. Krainov, *Vibrational Spectra of Polyatomic Molecules* (Wiley, New York, 1974).
[46]N. V. Mantzaris, A. Boudouris, and E. Gogolides, J. Appl. Phys. **77**, 6169 (1995).
[47]D. Field, J. P. Ziesel, P. M. Guyon, and T. R. Govers, J. Phys. B **17**, 4565 (1984).
[48]M. G. Curtis and I. C. Walker, J. Chem. Soc. Faraday Trans. II **85**, 659 (1989).
[49]E. Illenberger, Chem. Phys. Lett. **80**, 153 (1981).
[50]T. Oster, A. Kühn, and E. Illenberger, Int. J. Mass Spectrom. Ion Processes **89**, 1 (1989).
[51]E. Illenberger, in *Linking the Gaseous and Condensed Phases of Matter*, L. G. Christophorou, E. Illenberger, and W. F. Schmidt (Eds.) (Plenum, New York, 1994), pp. 49–72.
[52]Y. Le Coat, J.-P. Ziesel, and J.-P. Guillotin, J. Phys. B **27**, 965 (1994).
[53]A. Mann and F. Linder, J. Phys. B **25**, 545 (1992).
[54]A. Mann and F. Linder, J. Phys. B **25**, 533 (1992).
[55]R. K. Jones, J. Chem. Phys. **84**, 813 (1986).
[56]C. Szmytkowski, A. M. Krzysztofowicz, P. Janicki, and L. Rosenthal, Chem. Phys. Lett. **199**, 191 (1992).
[57]S. M. Spyrou, I. Sauers, and L. G. Christophorou, J. Chem. Phys. **78**, 7200 (1983).
[58]H. P. W. Harland and J. L. Franklin, J. Chem. Phys. **61**, 1621 (1974).
[59]S. R. Hunter and L. G. Christophorou, J. Chem. Phys. **80**, 6150 (1984).
[60]R. Hashemi, A. Kühn, and E. Illenberger, Int. J. Mass Spectrom. Ion Processes **100**, 753 (1990).
[61]W. M. Huo, Phys. Rev. A **38**, 3303 (1988).
[62]J. A. Tossell and J. W. Davenport, J. Chem. Phys. **80**, 813 (1984); Erratum **83**, 4824 (1985).
[63]H. J. T. Preston and J. J. Kaufman, Chem. Phys. Lett. **50**, 157 (1977).
[64]M. J. S. Dewar and H. S. Pzepa, J. Am. Chem. Soc. **100**, 784 (1978).
[65]A. A. Christodoulides, D. L. McCorkle, and L. G. Christophorou, in *Electron Molecule Interactions and Their Applications*, L. G. Christophorou (Ed.) (Academic, New York, 1984), Vol. 2, Chap. 6.
[66]J. Lotter, A. Kühn, and E. Illenberger, Chem. Phys. Lett. **157**, 171 (1989).
[67]J. Lotter and E. Illenberger, J. Phys. Chem. **94**, 8951 (1990).
[68]H. M. Rosenstock, K. Draxl, B. W. Steiner, and J. T. Herron, J. Phys. Chem. Ref. Data **6**, Suppl. No. 1 (1977).
[69]R. A. Bonham and M. R. Bruce, in *Proceedings of the Joint Symposium on Electron and Ion Swarms and Low Energy Electron Scattering*, Gold Coast, Australia, July, 1991, pp. 5–8.
[70]T. Nakano and H. Sugai, Jpn. J. Appl. Phys. **31**, 2919 (1992).
[71]W. L. Morgan, JILA Data Center Report No. 34, June 1 (1991).
[72]W. L. Morgan, Plasma Chem. Plasma Proc. **12**, 477 (1992).
[73]R. A. Bonham, Jpn. J. Appl. Phys. **33**, 4157 (1994).
[74]A. Zecca, G. P. Karwasz, and R. S. Brusa, Phys. Rev. A **46**, 3877 (1992).
[75]H.-X. Wan, Ph.D. dissertation, University of Maryland, 1990.
[76]O. Sueoka, in *Atomic Physics with Positrons*, J. W. Humberston and E. A. G. Armour (Eds.) (Plenum, New York, 1987), pp. 41–54.
[77]S. Mori, Y. Katayama, and O. Sueoka, At. Coll. Res. Japan Progr. Rept. **11**, 19 (1985).
[78]O. Sueoka and S. Mori, J. Phys. Soc. Jpn. **53**, 2491 (1984); J. Phys. B **19**, 4035 (1986).
[79]Y. Jiang, J. Sun, and L. Wan, Phys. Rev. A **52**, 398 (1995).
[80]K. L. Baluja, A. Jain, V. Di Martino, and F. A. Gianturco, Europhys. Lett. **17**, 139 (1992).
[81]M. G. Curtis, I. C. Walker, and K. J. Mathieson, J. Phys. D **21**, 1271 (1988).
[82]B. Stefanov, N. Popkirova, and L. Zarkova, J. Phys. B **21**, 3989 (1988).
[83]S. R. Hunter, J. G. Carter, and L. G. Christophorou, Phys. Rev. A **38**, 58 (1988).
[84]K. Masek, L. Laska, R. D' Agostino, and F. Cramarossa, Contrib. Plasma Phys. **27**, 15 (1987).
[85]R. Tice and D. Kivelson, J. Chem. Phys. **46**, 4743 (1967).
[86]T. Sakae, S. Sumiyoshi, E. Murakami, Y. Matsumoto, K. Ishibashi, and A. Katase, J. Phys. B **22**, 1385 (1989).
[87]D. Raj, J. Phys. B **24**, L431 (1991).
[88]C. Winstead, Q. Sun, and V. McKoy, J. Chem. Phys. **98**, 1105 (1993).
[89]M. S. Naidu and A. N. Prasad, J. Phys. D **5**, 983 (1972).
[90]C. S. Lakshminarasimha, J. Lucas, and D. A. Price, Proc. IEE **120**, 1044 (1973).
[91]L. G. Christophorou, P. G. Datskos, and J. G. Carter, Chem. Phys. Lett. **186**, 11 (1991).
[92]S. R. Hunter, J. G. Carter, and L. G. Christophorou, J. Appl. Phys. **58**, 3001 (1985)
[93]F. A. Gianturco, R. R. Lucchese, and N. Sanna, J. Chem. Phys. **104**, 6482 (1996); see also F. A. Gianturco, R. R. Lucchese, and N. Sanna, *ibid.* **100**, 6464 (1994).
[94]A. P. P. Natalense, M. H. F. Bettega, L. G. Ferreira, and M. A. P. Lima, Phys. Rev. A **52**, R1 (1995).
[95]W. G. Golden, C. Marcott, and J. Overend, J. Chem. Phys. **68**, 2081 (1978).
[96]Y. Itikawa, J. Phys. Soc. Jpn. **36**, 1127 (1974).
[97]M. Schmidt, R. Seefeldt, and H. Deutsch, Int. J. Mass Spectrom. Ion Processes **93**, 141 (1989).
[98]C. Ma, M. R. Bruce, and R. A. Bonham, Phys. Rev. A **44**, 2921 (1991); Erratum **45**, 6932 (1992).
[99]W. Zhang, G. Cooper, T. Ibuki, and C. E. Brion, Chem. Phys. **137**, 391 (1989).
[100]M. R. Bruce, C. Ma, and R. A. Bonham, Chem. Phys. Lett. **190**, 285 (1992).
[101]K. Codling, L. J. Frasinski, P. A. Heatherly, M. Stankiewicz, and F. P. Larkins, J. Phys. B **24**, 951 (1991).
[102]T. D. Märk, in *Electron Molecule Interactions and Their Applications*, L. G. Christophorou (Ed.) (Academic, Orlando, Florida, 1984), Vol. 1, Ch. 3.
[103]H. U. Poll, C. Winkler, D. Margreiter, V. Grill, and T. D. Märk, Int. J. Mass Spectrom. Ion Processes **112**, 1 (1992).
[104]M. R. Bruce and R.A. Bonham, Intern. J. Mass Spectrom. Ion Processes **123**, 97 (1993).
[105]M. R. Bruce and R. A. Bonham, J. Mol. Structure **352/353**, 235 (1995).
[106]H. Nishimura, in *Proceeding of the 8th Symposium Plasma Processing*, Nagoya, Japan, 1991, K. Tachibana (Ed.), pp. 333–336.
[107]M. V. V. S. Rao and S. K. Srivastava, private communication, 1996, and to be published.
[108]D. Margreiter, H. Deutsch, M. Schmidt, and T. D. Märk, Int. J. Mass Spectrom. Ion Processes **100**, 157 (1990).
[109]M. Gryzinski, Phys. Rev. A **138**, 305 (1965).
[110]Y.-K. Kim, private communication, 1996. For the method used see Y.-K. Kim and M. E. Rudd, Phys. Rev. A **50**, 3954 (1994); W. Hwang, Y.-K. Kim, and M. E. Rudd, J. Chem. Phys. **104**, 2956 (1996).
[111]K. Leiter, K. Stephan, H. Deutsch, and T. D. Märk, in Proceedings of the Symposium on Atomic and Surface Physics, 1984.
[112]J. W. Gallagher, E. C. Beaty, J. Dutton, and L. C. Pitchford, J. Phys. Chem. Ref. Data **12**, 109 (1983).
[113]M. Shimozuma, H. Tagashira, and H. Hasegawa, J. Phys. D **16**, 971 (1983).
[114]S. R. Hunter, J. G. Carter, and L. G. Christophorou, J. Chem. Phys. **86**, 693 (1987).
[115]C. S. Lakshminarasimha, J. Lucas, and R. A. Snelson, Proc. IEE **122**, 1162 (1975).
[116]I. M. Bortnik and A. A. Panov, Sov. Phys. Tech. Phys. **16**, 571 (1971).
[117]S. E. Bozin and C. C. Goodyear, J. Phys. D **1**, 327 (1968).
[118]P. G. Datskos, J. G. Carter, and L. G. Christophorou, J. Appl. Phys. **71**, 15 (1992).

[119] L. G. Christophorou, P. G. Datskos, and J. G. Carter, Nucl. Instrum. Methods Phys. Res. A **309**, 160 (1991).
[120] G. F. Reinking, L. G. Christophorou, and S. R. Hunter, J. Appl. Phys. **60**, 499 (1986).
[121] H. Sugai, H. Toyoda, T. Nakano, and M. Goto, Contrib. Plasma Phys. **35**, 415 (1995).
[122] V. Tarnovsky, P. Kurunczi, D. Rogozhnikov, and K. Becker, Int. J. Mass Spectrom. Ion Processes **128**, 181 (1993).
[123] V. Tarnovsky and K. Becker, J. Chem. Phys. **98**, 7868 (1993).
[124] P. J. Van der Burgt and J. W. McConkey, J. Phys. B **24**, 4821 (1991).
[125] H. A. van Sprang, H. H. Brongersma, and F. J. de Heer, Chem. Phys. **35**, 51 (1978).
[126] U. Müller, T. Bubel, G. Schulz, A. Sevilla, J. Dike, and K. Becker, Z. Phys. D **24**, 131 (1992).
[127] K. A. Blanks and K. Becker, J. Phys. B **20**, 6157 (1987).
[128] K. A. Blanks, A. E. Tabor, and K. Becker, J. Chem. Phys. **86**, 4871 (1987).
[129] M. B. Roque, R. B. Siegel, K. E. Martus, V. Tarnovsky, and K. Becker, J. Chem. Phys. **94**, 341 (1991).
[130] S. Wang, J. L. Forand, and J. W. McConkey, Can. J. Phys. **67**, 699 (1989).
[131] I. R. Lambert, S. M. Mason, and R. P. Tuckett, J. Chem. Phys. **89**, 2683 (1988).
[132] M. Suto, N. Washida, H. Akimoto, and M. Nakamura, J. Chem. Phys. **78**, 1019 (1983).
[133] L. C. Lee, J. L. Han, C. Ye, and M. Suto, J. Chem. Phys. **92,** 133 (1990).
[134] K. H. Becker, Comments At. Mol. Phys. **30**, 261 (1994).
[135] C. Suzuki and K. Kadota, Appl. Phys. Lett. **67**, 2569 (1995).
[136] H. F. Winters, J. W. Coburn, and E. Kay, J. Appl. Phys. **48**, 4973 (1977).
[137] I. Iga, M. V. V. S. Rao, S. K. Srivastava, and J. C. Nogueira, Z. Phys. D **24**, 111 (1992).
[138] E. Illenberger, Chem. Phys. Lett. **80**, 153 (1981).
[139] C. Lifshitz and R. Grajower, Int. J. Mass Spectrom. Ion Processes **10**, 25 (1972/1973).
[140] J. Dutton, A. Goodings, A. K. Lucas, and A. W. Williams, J. Phys. D **20**, 1322 (1987).
[141] K. A. G. MacNeil and J. C. J. Thynne, Int. J. Mass Spectrom. Ion Phys. **3**, 455 (1975).
[142] J. W. Hastie and J. L. Margrave, J. Phys. Chem. **73**, 1105 (1969).
[143] L. Mi, C. R. Sporleder, and R. A. Bonham, Chem. Phys. Lett. **251**, 252 (1996).
[144] K. Mitsuke, S. Suzuki, T. Imamura, and I. Koyano, J. Chem. Phys. **95**, 2398 (1991).
[145] F. J. Davis, R. N. Compton, and D. R. Nelson, J. Chem. Phys. **59**, 2324 (1973).
[146] R. W. Fesssenden and K. M. Bansal, J. Chem. Phys. **53**, 3468 (1970).
[147] R. Schumacher, H.-R. Sprünken, A. A. Christodoulides, and R. N. Schindler, J. Phys. Chem. **82**, 2248 (1978).
[148] J. L. Jauberteau, G. J. Meeusen, M. Haverlag, G. M. W. Kroesen, and F. J. de Hoog, J. Phys. D **24**, 261 (1991).
[149] A. Kono, M. Haverlag, G. M. W. Kroesen, and F. J. de Hoog, J. Appl. Phys. **70**, 2939 (1991).
[150] E. Gogolides, M. Stathakopoulos, and A. Boudouris, J. Phys. D **27**, 1878 (1994).
[151] N. Gee and G. R. Freeman, J. Chem. Phys. **95**, 102 (1991).
[152] J. Va'vra, P. Coyle, J. Kadyk, and J. Wise, Nucl. Instrum. Methods Phys. Res. A **324**, 113 (1993).
[153] O. Kiselev, O. Prokofiev, and A. Vorobyov, GEM Report No. TN-93-417 (1993).
[154] B. Schmidt and Polenz, Nucl. Instrum. Methods Phys. Res. A **273**, 488 (1988).
[155] R. A. Snelson, Ph. D. thesis, University of Liverpool, 1974.
[156] S. R. Hunter and L. G. Christophorou, in *Electron Molecule Interactions and Their Applications*, L. G. Christophorou (Ed.) (Academic, Orlando, Florida, 1984), Vol. 2, Ch. 3.
[157] D. R. James, L. G. Christophorou, and R. A. Mathis, in *Gaseous Dielectrics II*, L. G. Christophorou (Ed.) (Pergamon, New York, 1980), p. 115.
[158] L. G. Christophorou, R. J. Van Brunt, and J. K. Olthoff, "Fundamental Processes in Gas Discharges," in *Proceedings of the Eleventh International Conference on Gas Discharges and Their Apllications*, Chuo University, Tokyo, Japan, Sept., 1995, Vol. 1, pp. I536–I548.
[159] H. Deutsch, T. D. Märk, V. Tarnovsky, K. Becker, C. Cornelissen, L. Cespiva, and V. Bonacic-Koutecky, Int. J. Mass Spectrom. Ion Processes **137**, 77 (1994).
[160] R. C. Wetzel, F. A. Biaocchi, and R. S. Freund, Bull. Am. Phys. Soc. **30**, 147 (1985).